



Universität für Bodenkultur Wien

Department für Integrative Biologie und Biodiversitätsforschung
und Department für Materialwissenschaften und Prozesstechnik

Institut für Botanik und Institut für Holztechnologie und
Nachwachsende Rohstoffe

Advisor/Advisors: Assoc. Prof. Dipl.-Ing. Dr. Sabine Rosner

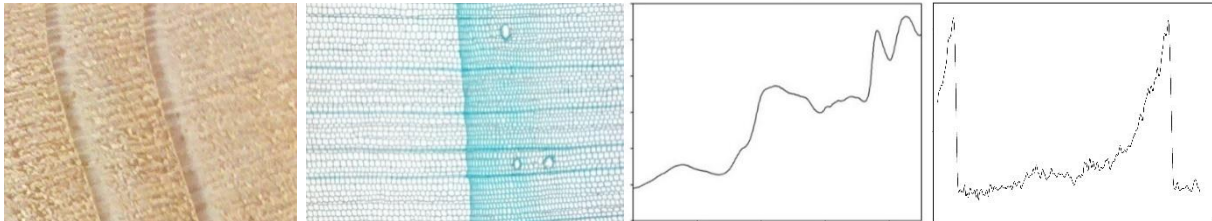
NOVEL APPROACHES TO ESTIMATE HYDRAULIC VULNERABILITY OF NORWAY SPRUCE SAPWOOD

Dissertation
for obtaining a doctorate degree
at the University of Natural Resources and Applied Life Sciences
Vienna

Submitted by
Saskia Luss MSc BEd

Vienna, Februar 2020

NOVEL APPROACHES TO ESTIMATE HYDRAULIC VULNERABILITY OF NORWAY SPRUCE SAPWOOD



What do this dissertation and a tree have in common?

- Each season brings its own challenges
 - Droughts must be overcome
 - Stability must be proven
 - You have to have thick periderm
- It takes some time for a splendid tree to grow from a seed, and finally
- You can collect many year rings with experience behind all the strains

Saskia Luss

Acknowledgements

Many people have accompanied and supported me on this path, and I would like to thank them.

My very special thanks go to my supervisor Assoc. Prof. Dipl.-Ing. Dr. Sabine Rosner for her great support and friendship. Without her, this work would not have been possible. I am very fortunate to have had a supervisor like her and I will always remember her wonderful cooperation. I'll keep the time with you, Sabine, in good memory. It is not self-evident that someone has such a support as I had it and for that I am infinitely grateful to you. You always had an open ear and shared your knowledge with me. I consider myself lucky that I had the opportunity to be your PhD student. Thank you so much for your time and support.

I would also like to say a huge thank you to Mr. Sven-Olof Lundqvist. Through his input he has brought me to where I stand today and I am very grateful to him for that. It is not a matter of course that project partners get involved in this way and I do not see his support as a matter of course. As a PhD student you can count yourself lucky if you are allowed to work with someone like Sven-Olof.

Assoc. Prof. Dr.rer.nat. Notburga Gierlinger, thank you for the chance to be a part of Trees for future. I would like to thank Ao. Univ. Prof. Mag. Dr. Barbara Hinterstoisser, Univ. Prof. Mag. rer. nat. Dr. rer. nat. Peter Hietz and Dipl. Ing. Dr. Manfred Schwanninger, who offered me the framework conditions to carry out my work. I would also like to thank the co-authors of the joint publications for their cooperation.

I would also like to thank my colleagues Dipl.-Ing Kristina Plenk, Dr. rer. nat. Katharina Schwanda, Mag. Susanne Scheffknecht, Karin Fohringer, Dipl.-Biol. Dr. rer. nat. Steffen Hameister, Dipl. Ing. Nora Stoeckl, Dr. rer. nat. Ena Smidt, Ing. Robert Stingl and Dipl.-Ing. Dr. nat. techn. Johannes Tintner, Dipl.-Ing. Dr. rer. nat Katharina Böhm, , Assoc. Prof. Dipl.-Ing. Dr. Johannes Konnerth for their exchange of ideas and help. In addition to the people mentioned, I would also like to thank all my colleagues who contributed to the excellent working atmosphere and helped enable me to remember my dissertation time fondly.

I would also like to thank all my colleagues in the Trees4future project. The research has received funding from the European Union's Seventh Framework Programme for research, technological development, and demonstration under grant agreement n° 284181, the Swedish strategic research program Bio4Energy, and the European Union's Horizon 2020 research and innovation program under the Marie Skłodowska-Curie grant agreement no 645654 (Topwood).

Last but not least I would like to thank my family for their support. I would especially like to thank my husband, Alexander, who gave me the necessary support and space to finish this work. My son, who enriches my life and who had a long nap so that I could write my thesis during this time.

And I thank my weaker inner self who sometimes didn't believe that this work would come to an end.

Abstract

Climate change and the associated effects of drought stress on Norway spruce (*Picea abies* (L.) Karst.) are on focus of much debate in recent decades. Thereby, classical methods for the efficient characterization of the hydraulic properties of trees have often been discussed. Classical methods are destructive, take a lot of time and they are prone to errors.

In search for an alternative to classical methods to determine hydraulic vulnerability (P_{50}) of sapwood in Norway spruce, several approaches were tested. The following criteria were used in the selection of methods: (I) non-destructive, (II) efficient, (III) easy to assess, (IV) using well established techniques, and (V) limited sample preparation needed. Two methods that met these criteria are Fourier transform near-infrared (FT-NIR) spectroscopy and the calculation of hydraulic traits from SilviScan measurements.

After an introduction, the thesis includes two articles presenting research on these two methods, followed by general conclusions.

The first article deals with FT-NIR spectroscopy, a method established in many fields of research, often used due to its speed and user-friendliness. FT-NIR spectroscopy combined with partial least squares regression (PLS-R) models were used to predict the parameters P_{50} (applied air pressure causing 50% loss of hydraulic conductivity) and RWL_{50} (applied air pressure causing 50% relative water loss). It was found that spectra recorded from the axial wood surface provided better results than spectra from the radial surface for P_{50} ($r = 0.81$) and for RWL_{50} ($r = 0.88$).

The second article deals with use of a SilviScan instrument to determine wood density (WD) and anatomical parameters of the wood in order to find efficient proxies for P_{50} . It was confirmed that WD is one of the best proxies available for P_{50} ($r = -0.64$), but it does not necessarily reflect the mechanism behind cavitation resistance. New approaches based on the anatomical data from the instrument, such as the introduction of dynamic aspects of conductivity loss through the analysis of 5% steps in the cumulated hydraulic conductivity (K), provided even stronger correlations ($r = -0.72$). The correlations of P_{50} with averages for earlywood (EW), transitional wood (TW), and latewood (LW) were lower than with the averages of the sample, both for WD ($r = -0.60$ for WD_{EW} , $r = -0.56$ for WD_{TW} , $r = -0.23$ for WD_{LW}) and for all anatomical characteristics investigated, reflecting that the proportions of the three parts play an important role.

In summary, both methods, FT-NIR and SilviScan, have many advantages compared to classical methods. They are more efficient and, first of all, the original sampling can be performed without harvesting the tree. At this stage, it is not possible to judge objectively which method is the better one, as it will depend on the research question. In terms of sample preparation, FT-NIR spectroscopy can be more efficient. However, prediction models developed for one type of wood may need to be updated or new developed for application on other types of wood. For SilviScan, sample preparation can be more time-consuming despite use of dedicated machines, but it provides anatomical and physical information directly from the samples. Both methods represent interesting alternatives to the classical methods.

Zusammenfassung

Der Klimawandel und die damit verbundenen Auswirkungen von Trockenstress auf Fichten (*Picea abies* (L.) Karst.) sind in den letzten Jahrzehnten immer mehr ins Zentrum vieler Diskussionen gerückt. Dabei sind klassische Methoden zur effizienten Charakterisierung der hydraulischen Eigenschaften von Bäumen häufig diskutiert worden. Klassischen Methoden wird nachgesagt, dass sie nicht zerstörungsfrei sind, viel Zeit in Anspruch nehmen und die Fehlerwahrscheinlichkeit relativ hoch ist. Ziel dieser Studie war es, das Potenzial alternativer, effizienterer Methoden zur Bestimmung der hydraulischen Verwundbarkeit (P_{50}) zu testen, um klassische Methoden zu ersetzen. Bei der Auswahl der Methoden wurden folgende Kriterien herangezogen: (I) zerstörungsfrei, (II) effizient, (III) einfach zu beurteilen, (IV) etablierte Techniken und (V) begrenzte Probenaufbereitung erforderlich. Zwei Methoden, die diese Kriterien erfüllten, sind die Fourier-Transform-Nahinfrarot-(FT-NIR)-Spektroskopie und die Berechnung von hydraulischen Eigenschaften aus SilviScan-Messungen.

Nach der Einleitung werden in dieser Arbeit zwei Publikationen präsentiert, die die oben beschriebenen Methoden darstellen, gefolgt von einer allgemeinen Schlussfolgerung.

Der erste Artikel beschäftigt sich mit der FT-NIR-Spektroskopie, einer in vielen Bereichen der Wissenschaft etablierten Methode, die aufgrund ihrer Schnelligkeit und Benutzerfreundlichkeit häufig eingesetzt wird. Die FT-NIR-Spektroskopie in Kombination mit PLS-R-Modellen (Partial Least Squares Regression) wurde zur Vorhersage der Parameter P_{50} (Überdruck, der 50% Verlust der hydraulischen Leitfähigkeit verursacht) und RWL_{50} (Überdruck verursacht 50% relativen Wasserverlust) verwendet. Es wurde festgestellt, dass die von der axialen Holzoberfläche aufgenommenen Spektren bessere Ergebnisse lieferten als die Spektren von der radialen Oberfläche für P_{50} ($r = 0,81$) und für RWL_{50} ($r = 0,88$).

Der zweite Artikel beschäftigt sich mit der Verwendung eines SilviScan-Instruments zur Bestimmung der Holzdicke (WD) und anatomischer Parameter des Holzes, um effiziente Vertreter (Proxies) für P_{50} zu finden. Es wurde bestätigt, dass WD einer der besten Proxies für P_{50} ($r = -0,64$) ist, aber die Korrelation spiegelt nicht unbedingt den Mechanismus hinter dem Kavitationswiderstand wider. Neue Ansätze, die auf den anatomischen Daten des Instruments basieren, wie die Einführung dynamischer Aspekte des Leitfähigkeitsverlustes durch die Analyse von 5%-Schritten der kumulierten hydraulischen Leitfähigkeit (K), lieferten noch stärkere Korrelationen ($r = -0,72$). Die Korrelationen von P_{50} mit den Durchschnittswerten für Frühholz (EW), Übergangsholz (TW) und Spätholz (LW) waren niedriger als mit den Durchschnittswerten der Stichprobe, sowohl für WD ($r = -0,60$ für WD_{EW} , $r = -0,56$ für WD_{TW} , $r = -0,23$ für WD_{LW}) als auch für alle untersuchten anatomischen Parameter, was zeigt, dass die Anteile der drei Teile eine wichtige Rolle spielen.

Zusammenfassend lässt sich sagen, dass beide Methoden (FT-NIR und SilviScan) viele Vorteile gegenüber klassischen Methoden aufweisen. Sie sind effizienter und vor allem kann die Probenahme durchgeführt werden, ohne den Baum fällen zu müssen. Zum jetzigen Zeitpunkt ist es nicht möglich, objektiv zu beurteilen, welche Methode die bessere ist, da dies von der Forschungsfrage abhängt. In Bezug auf die Probenvorbereitung kann die FT-NIR-Spektroskopie effizienter sein. Allerdings müssen die für eine Holzart entwickelten Vorhersagemodelle möglicherweise für eine andere Holzart aktualisiert oder neu entwickelt werden. Für SilviScan kann die Probenvorbereitung trotz Einsatz spezieller Maschinen zeitaufwändiger sein, liefert aber anatomische und physikalische Informationen direkt aus den Proben. Demnach stellen beide Methoden interessante Alternativen zu den klassischen Methoden dar.

Table of Content

1.	GENERAL INTRODUCTION	8
1.1	NORWAY SPRUCE – AN ECONOMICALLY IMPORTANT BUT ENDANGERED SPECIES	9
1.2	HYDRAULIC FUNCTIONS WITHIN THE TREE TRUNK OF NORWAY SPRUCE	9
1.3	CLASSICAL METHODS TO DETERMINE HYDRAULIC VULNERABILITY USING VULNERABILITY CURVES (VCs)	12
1.3.1	THE AIR INJECTION METHOD.....	12
1.3.2	CALCULATION OF HYDRAULIC PARAMETERS AND VULNERABILITY CURVES	15
1.4	DEMANDS FOR MORE EFFICIENT ALTERNATIVE METHODS	17
1.4.1	CRITERIA FOR SELECTION OF ALTERNATIVE METHODS TO BE INVESTIGATED	18
1.4.2	SHORT METHOD OVERVIEW	19
1.5	NOVEL APPROACHES.....	19
1.5.1	PREPARATION OF SAMPLES TO BE COMPARED	19
1.5.2	FT-NIR SPECTRA AND PREDICTION MODELS	20
1.5.2	HIGH RESOLUTION MEASUREMENTS OF WOOD DENSITY AND ANATOMY WITH SILVISCAN	24
1.5.3	REJECTED METHODS	28
1.6	THESIS OUTLINE	31
2.	HYDRAULIC TRAITS OF NORWAY SPRUCE SAPWOOD ESTIMATED BY FOURIER TRANSFORM NEAR-INFRARED SPECTROSCOPY (FT-NIR)	32
3.	WITHIN-RING VARIABILITY OF WOOD STRUCTURE AND ITS RELATIONSHIP TO DROUGHT SENSITIVITY IN NORWAY SPRUCE TRUNKS	40
4.	GENERAL CONCLUSIONS	64
5.	REFERENCES	67
6.	TABLE OF FIGURES.....	74
7.	CURRICULUM VITAE	75

1. General Introduction

1.1 Norway spruce – an economically important but endangered species

Norway spruce (*Picea abies* (L.) Karst.) (Figure 1) is a fast growing, large, evergreen, shallow-rooted conifer species. It can grow in many adverse soil conditions and grows in different types of sites (Skrøppa 2003). In addition, the spruce can be found at altitudes ranging from sea level to about 2,300 m (Skrøppa 2003; Farjon 2017). It becomes between 20 and 45 m high, and the trunk's diameter of old trees can become between 1 and 1.5 m (Schmidt-Vogt et al. 1986; Skrøppa 2003).

Originally, the spruce was mainly found in north-eastern and northern Europe. Today it is widespread to temperate forests all over the world, and it is the most common tree in Austria. Approximately 48% of Austria's total area is covered with forest, i.e. 4 million hectares of 8.4 million hectares. Conifers cover 63.5% of this area, with 50.7% spruce. (Schadauer et al. 2015).

Norway spruce is an important high-quality wood tree in Europe. Its long fibers makes it important for the pulp and paper industry. The wood is also used as construction wood, for furniture, and selected wood even for musical instruments (e.g. for the soundboards of pianos, guitars, and violins). It is a popular Christmas tree in Europe (Farjon 2017). Furthermore it has high ecological importance as a key species in Europe (Strasburger et al. 1983; Skrøppa 2003).

Coniferous species, such as Norway spruce, are one of the most endangered plant groups in terms of forest dieback due to drought (Solberg 2004; Bréda and Badeau 2008; Sargent et al. 2012; Klein et al. 2018; Rosner et al. 2018, 2019b). During the past years, drought and heat waves have been frequently observed (Allen et al. 2010; Sargent et al. 2012), and, as a consequence of climate change, it is predicted that more extreme and frequent drought and heat waves will occur (Schär et al. 2004; IPCC 2012, 2014). The physiological mechanisms behind dieback due to drought sensitivity are not yet well understood (McDowell et al. 2008; Hentschel et al. 2014). Facing global change (IPCC 2014), the development of fast and easy to use screening methods to predict drought sensitivity of conifer species and trees may allow the selection of more suitable individuals for propagation (Rosner 2013; Rosner et al. 2019a, 2019b).



Figure 1: *Picea abies*, Illustration by Koehler 1887

1.2 Hydraulic functions within the tree trunk of Norway spruce

Through the development of a water transport system to the xylem, conifers have become well adapted to their environment (Tyree et al. 1994; Schopfer Peter; Brennicke Axel 2010; McElrone et al. 2013). Plants need water for the photosynthesis in the leaves. In plants living

on land, the force achieving the transport of water from the soil to the leaves is created by loss of water through transpiration. Water always moves from a region with a high water potential (Ψ) to a region with a low water potential, in this case from the soil with a potential close to zero, to the air surrounding the leaves with large negative water potential. Loss of water through transpiration can however also put the trees at risk on drought.

To briefly summarize the theory of water transport: Plants take up the water from the soil via the root system, a complex network of individual roots (Cochard 2014). As trees get older, the roots form a periderm very similar to that of the trunk of the tree. It is very important for trees to be able to absorb large amounts of water despite this periderm formation and the associated reduction in the permeability of older roots (Chung and Kramer 1975; Macfall et al. 1990; McElrone et al. 2013), as the woody roots in some forests can make up a high proportion of the root surface (up to 99%) (Kramer and Bullock 1966). The water absorbed by the roots must pass through several cell layers before it reaches the specialized water transport tissue, the xylem. These cell layers have an important function because they act as a filter system in the root. They have a much higher resistance to water flow than the xylem, in which the water is transported in more open tubes. In conifers, the water in the xylem is transported over long distances in these conductive elements, the tracheids. In contrast to conifers, angiosperms have specialised conducting elements, the vessels. The drive for the water transport is provided by the evaporation of water vapor through the leaves. This creates a transpiration suction in the plant. This process is generally referred to as the cohesion tension mechanism (C-T) (Böhm 1893; Tyree and Zimmermann 2002; McElrone et al. 2013). For adequate function, the water column created from roots to leaves as a result of the suction may not break off, which is ensured by the strong cohesion forces between the water molecules amongst each other and to the cell walls of the xylem tubes (Linder and Knodel 2012). From the xylem, the water then passes through the petiole and into the leaves (McElrone et al. 2013). Figure 2 roughly shows the water path through the tree.

Interruptions of the water columns, such as cavitation when bubbles of air are released in the water-conducting system resulting in embolism, can severely affect the hydraulic efficiency (Tyree and Sperry 1989; Tyree and Zimmermann 2002). Vulnerability to air emboli formation in the xylem sap is one key aspect to understanding the survival or mortality of plants (McDowell et al. 2008; Mayr et al. 2014; Klein et al. 2018; Hammond et al. 2019). From the moment plants left the sea and settled on land, they had to cope with water shortages. Despite good adaptation to their environment, under special circumstances, there is a risk of air bubbles entering their water-conducting system (McDowell et al. 2008; Vergeynst 2015).

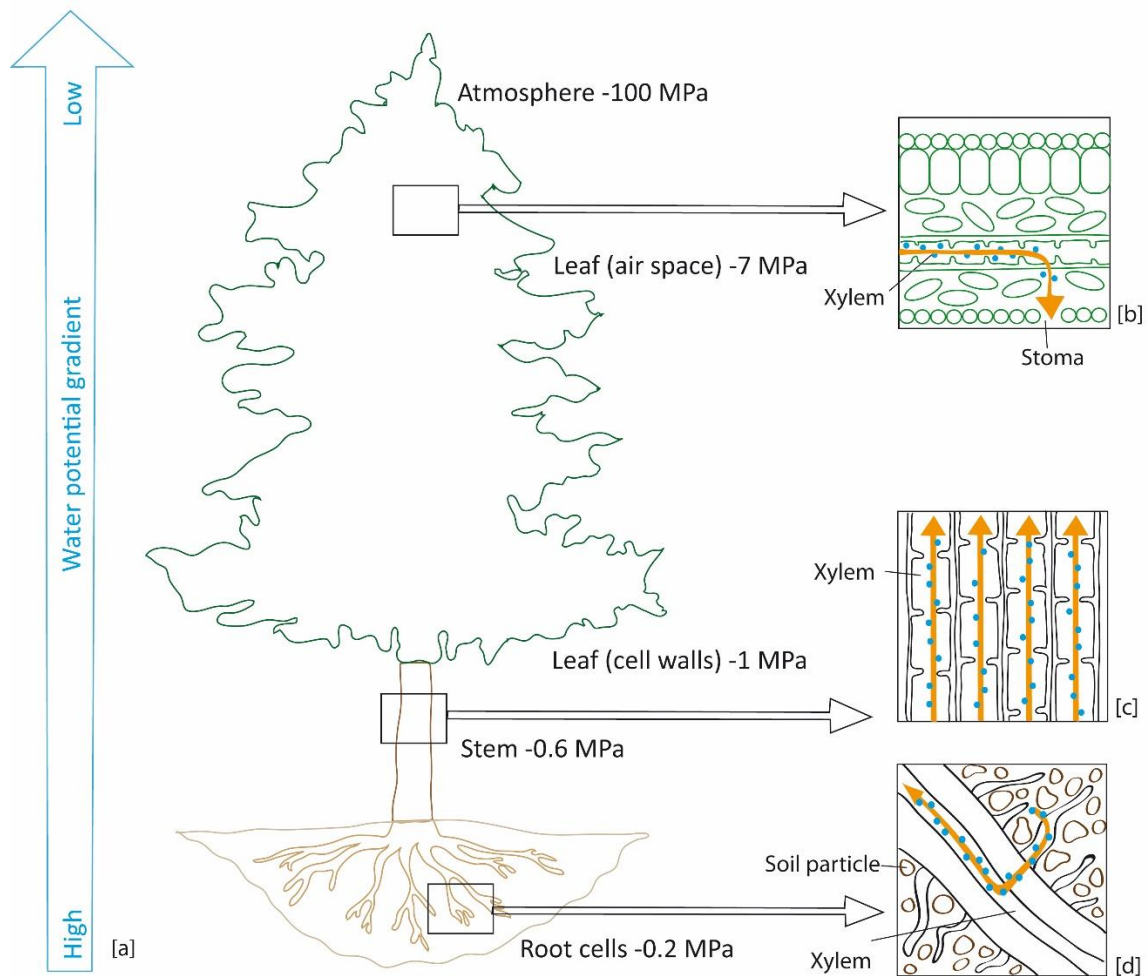


Figure 2: [a] Schema of the water potential in conifers according to McElrone et al. 2013; [b] transpiration draws water from the leaf; [c] cohesion and adhesion draws water up the xylem; [d] negative water potential draws water into the roots. Blue circles show the water molecules.

Norway spruce trees are designed to survive in northern regions (Solberg 2004) and at the alpine timberline (Mayr et al. 2002). They are exposed to drought stress and to freeze-thaw stress during winter (Mayr et al. 2014). Sectorial radial architecture, in which almost completely isolated hydraulic pathways to particular stem and crown regions are present, can be a possible survival strategy under harsh environmental conditions in the timberline (Larson et al. 1993, 1994). However, an embolism dysfunction induced by drought stress is not always permanent. Indeed, it is possible that trees can recover from drought stress by refilling tracheids with water within days or by the next growth season. There are several studies currently dealing with the topic of refilling (Mayr et al. 2014; Klein et al. 2018). But it is also possible that permanent damage occurs (Tyree and Zimmermann 2002). Economic losses due to top dieback after heat and drought waves could be due to a weak adaptation of Norway spruce to the environmental conditions in the lowlands (Solberg 2004; Rosner et al. 2014).

There is a need to get more information about hydraulic vulnerability. In the next chapter "Classical methods to determine hydraulic vulnerability using vulnerability curves (VCs)" (Page 12), different classical methods under laboratory conditions are described and an example is given, before more efficient alternative methods are described in the chapter "Novel approaches" (Page 19).

1.3 Classical methods to determine hydraulic vulnerability using vulnerability curves (VCs)

There are different techniques for estimating water potential and for measuring hydraulic conductivity loss in order to construct vulnerability curves (VCs) (Page 15). Cochard et al. (2013) provided a good overview of the different methods and previous publications. They concluded that almost 96% of all VCs are produced by four methods: the bench-top dehydration method "gold standard", the air injection method, centrifugation, and the cavitron (also a centrifuge method). The proportion of VCs obtained with centrifugation and air injection technology has increased significantly in recent years compared to the classic bench dehydration method. This can be explained by the fact that the centrifuge and air injection techniques are faster and consume less plant material (Cochard et al. 2013). Martin-StPaul et al. (2014) compared the three methods (bench-top dehydration, cavitron, and air injection method) and concluded that the cavitron and air injection methods deliver reliable results for conifer species but should be used with caution for long vessel species. The next subchapter concentrates on the air injection method, which in this thesis has been used as the reference method for determining hydraulic vulnerability in Norway spruce trees, towards which the more efficient proxies have been compared.

1.3.1 The air injection method

The air injection technique applies pressure to water conducting plant material, thereby mimicking decrease in water potential and its effects on water transport. In the case of this thesis, the plant materials were small specimens of wood. More details on the plant material used can be found in Chapters 2 and 3 (Material and Methods, Page 34 and 44) and in Rosner et al. 2008. Figure 3 gives a brief overview of the samples used and how they were produced. The specimens (wood micro-beams) from sapwood used for the measurements had dimensions of 6 mm (radial) × 6 mm (tangential) × 120 mm (axial).

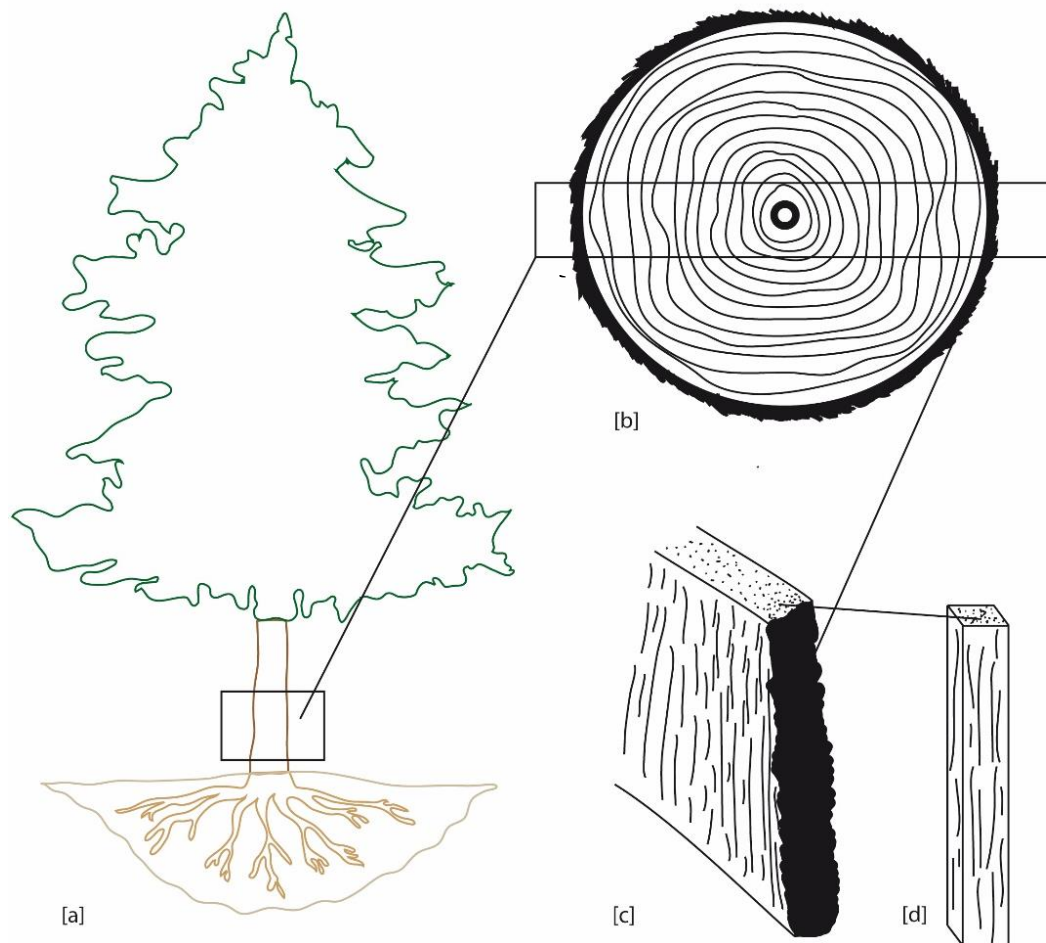


Figure 3: Schema of sampling and sample preparation according to Rosner *et al.*, 2008. [a to b] Wood boles, 20 – 30 cm in length, were taken from the main trunk of Norway spruce trees after felling; [b to c] “Plank-like” longitudinal samples were produced along a diameter at the centre of the boles by splitting along the grain [c to d]. These samples were debarked and small beams were split along the grain from their sapwood. Thereafter, these were planed on a sliding microtome; small beams of sapwood with a size of 6 mm × 6 mm × 120 mm (radial × tangential × axial), were used for the measurements

Before the first flow measurement, the samples were completely saturated in H₂O (Figure 4b). A modified Sperry-Apparatus (designed by Mayr, 2002, Figure 4a) was used for the flow measurements. The small beams were sealed into a hydraulic system in which water was forced to move through the specimen in the longitudinal tracheid direction at constant pressure between the ends of the sample, while the flow rate was determined (Sperry *et al.* 1988). The modified Sperry apparatus has the advantage that parallel arranged measuring channels allow the analysis of several samples. Overall, handling has also been simplified and routine work made possible (Mayr 2002).

After the determination of the saturated weight and the flow measurement at full saturation, cavitation was mimicked through the application during specified time (1 minute) of an air overpressure (P) to the sides of the small wooden beams in a double ended pressure collar, followed by a repeated measurement of the flow through the now partly embolized wood of the micro beam. During air injection, the two ends of the wood beam protrude from the double-ended pressure collar (PMS Instrument Company, Corvallis, Oregon) (4c and Figure 5). The collar is pressurized stepwise (0.5 MPa) with compressed air.

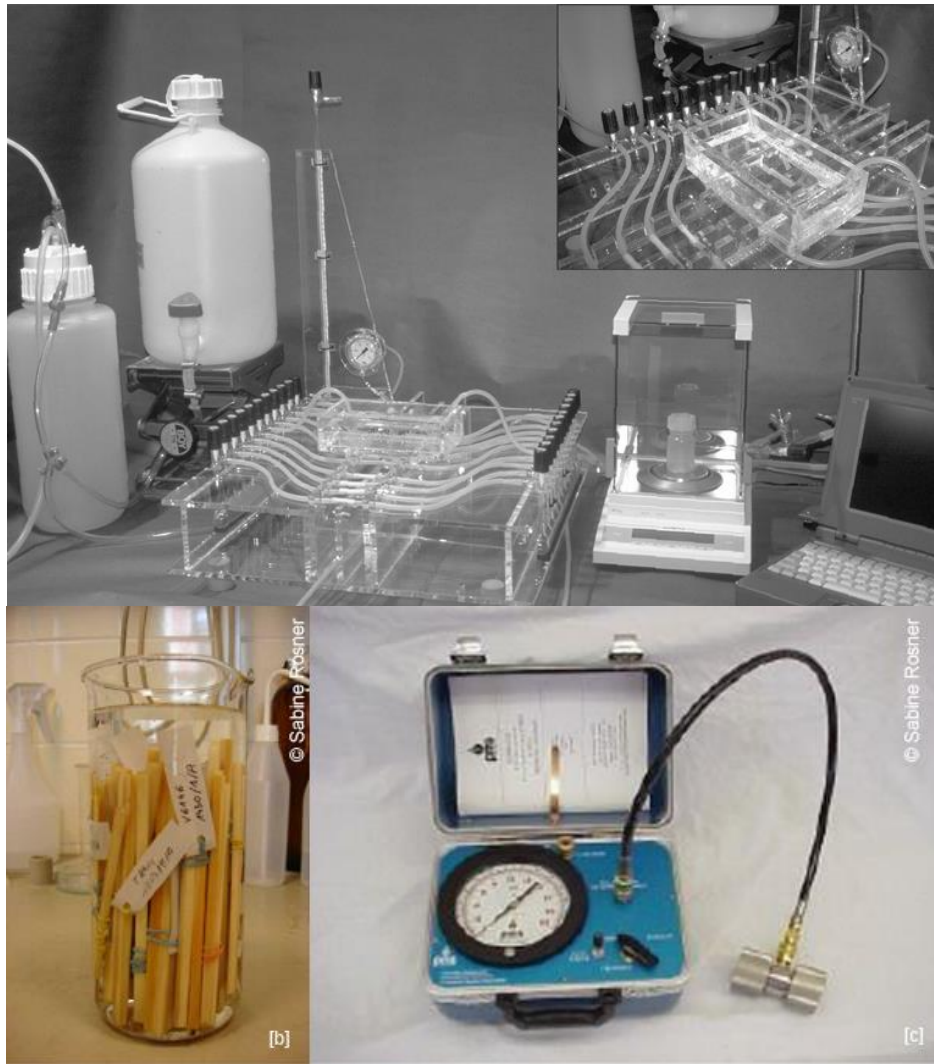


Figure 4: [a] Modified Sperry equipment designed by Mayr 2002 for repeated flow measurement; [b] fully saturated wood beams; [c] PMS instrument

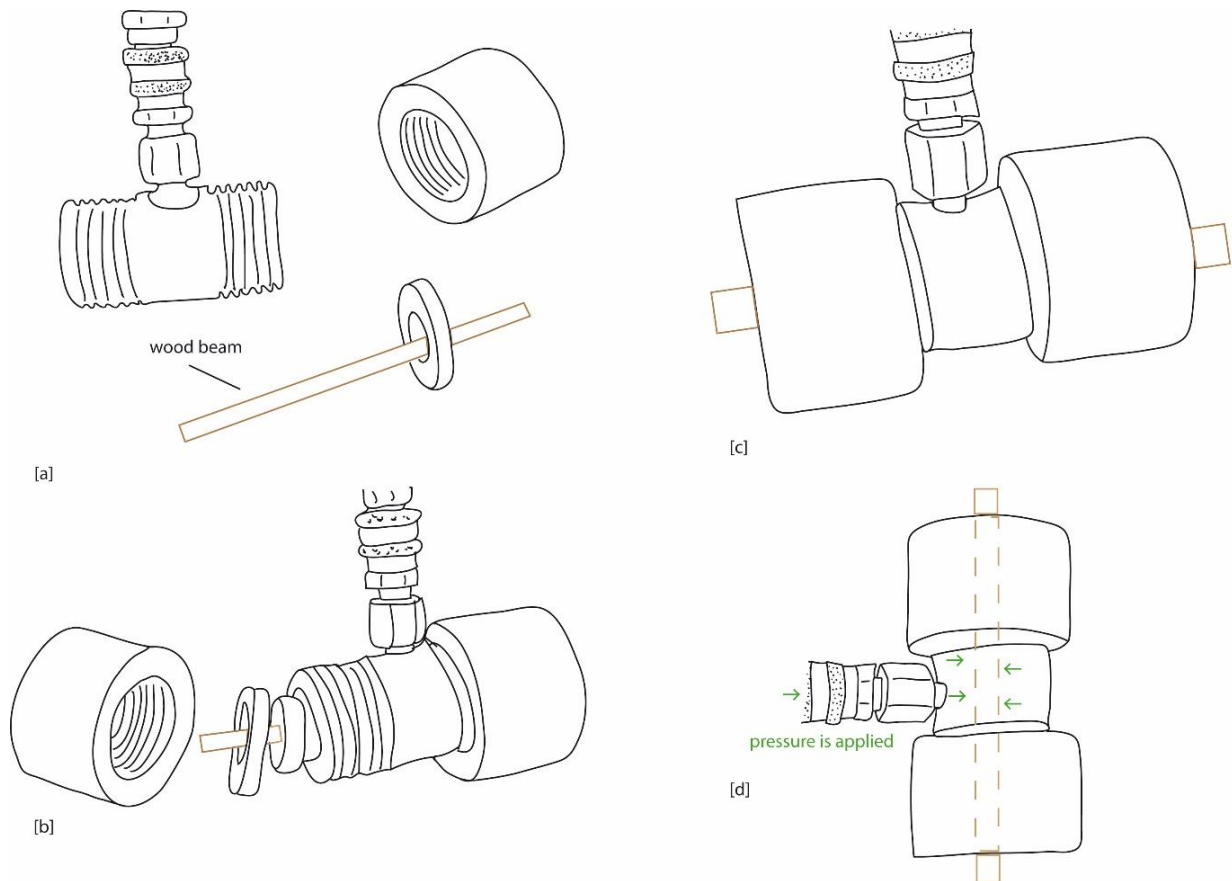


Figure 5: PMS instrument and [a and b] how the small wood beams (brown scheme) have to be fixed in the double ended pressure collar. [c] Closed pressure collar; [d] Pressure is applied (green arrows)

1.3.2 Calculation of hydraulic parameters and vulnerability curves

For a better understanding of how the parameters of interest (P_{50} and RWL_{50}) were obtained, the approach with wooden beams is now briefly described.

To calculate P_{50} (applied air pressure causing 50% loss of hydraulic conductivity) and RWL_{50} (applied air pressure causing 50% relative water loss), the fresh mass and flow through the small wood beams have to be determined, after stepwise application of air pressure (0.5 MPa) in a double ended pressure collar. The weight at full saturation and the first flow measurement performed also at full saturation serve as reference values for calculating the relative moisture loss and the loss of hydraulic conductivity after the sequential application of positive pressure in the double ended pressure collar. The results of the measurements are water release curves and vulnerability curves (VCs) for assessment of vulnerability to cavitation.

A VC is a two-dimensional graph that shows how the conductivity loss in a woody tissue varies with water potential (Cochard et al. 2013). The most widely used hydraulic vulnerability parameter is P_{50} , defined as the change in water potential that causes a 50% loss in hydraulic conductivity in sapwood (Choat et al. 2012).

The sapwood area specific hydraulic conductivity (k_s) is defined as:

$$k_s = F \times L \times A_s^{-1} \times \Delta P^{-1} \text{ (m}^2\text{s}^{-1}\text{MPa}^{-1}\text{)}$$

where F is the volume flow rate ($\text{m}^3 \text{ s}^{-1}$), L is the length of the segment (m), A_s is the cross-sectional sapwood sample area (m^2) and ΔP is the pressure difference between the ends of the segment (MPa).

The percent loss of conductivity PLC is calculated as

$$\text{PLC (\%)} = 100 - \left(\left(\frac{k_s \text{ after pressure}}{k_s \text{ max}} \right) \times 100 \right)$$

where $k_s \text{ after pressure}$ is the hydraulic conductivity measured stepwise, $k_s \text{ max}$ is the hydraulic conductivity at full saturation.

By stepwise increasing the exterior pressure mimicking decreases in the water potential, measuring the corresponding hydraulic conductivity and calculating the PLC for each pressure application, the effects of increasing deficit of water can be simulated by constructing a VC from the individual values (Figure 6). After fitting a sigmoid function, parameters of interest, e.g. the P_{50} , can be calculated (Pammenter and Vander Willigen 1998).

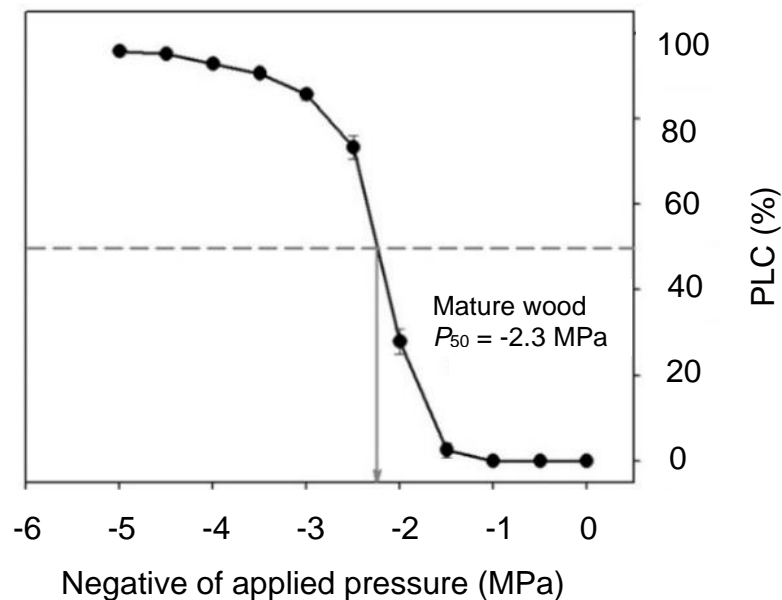


Figure 6: Example of a vulnerability curve showing how the percent loss of conductivity is related to the negative of the applied pressure, starting from pressure 0 MPa to the right, moving leftward to more negative water potentials.

Additional information about the hydraulic performance of sapwood can be obtained from the relative water loss (RWL) resulting from the overpressure, described with RWL_{50} , the pressure resulting in 50% water loss (Hietz et al. 2008; Rosner et al. 2008). RWL_{50} has been reported to be strongly related to basic density (Rosner et al. 2008), and it is supposed to give important information on the water storage capacity (i.e. capacitance) (Cochard et al. 2013). The following equation was used to calculate RWL:

$$RWL (\%) = \left(1 - \frac{\text{actual fresh mass} - \text{dry mass}}{\text{saturated mass} - \text{dry mass}} \right) \times 100$$

RWL_{50} is determined in the same way as P_{50} (Figure 7), but by fitting a cubic rather than a sigmoidal curve (Rosner et al. 2008).

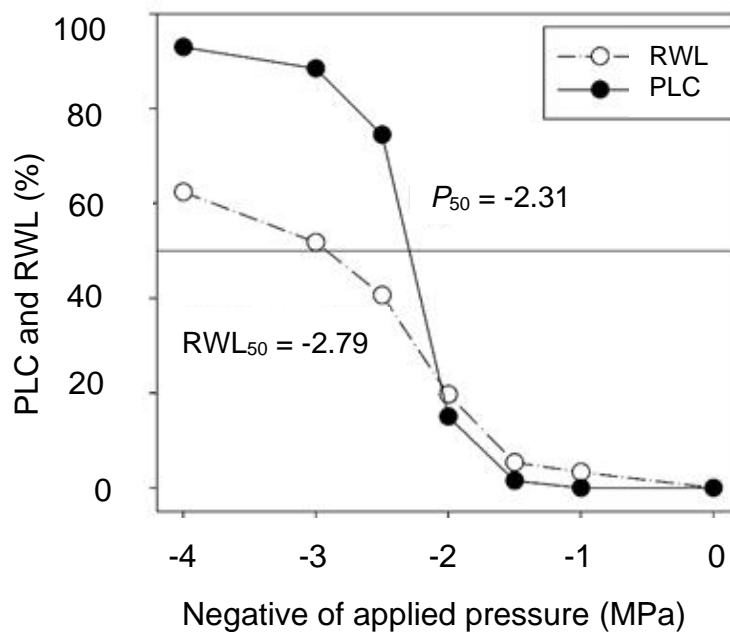


Figure 7: Example of a vulnerability curve for the determination of P_{50} and RWL_{50} . The relationship between RWL and the negative of the applied pressure was thereafter fitted by means of a cubic curve and RWL_{50} was calculated (Rosner et al. 2008).

1.4 Demands for more efficient alternative methods

The classical methods to determine hydraulic traits like P_{50} , also the air injection method described above, have some disadvantages. They are destructive, delicate, very labour intensive, provide data from small samples only, which sometimes can be problematic for representability, and the measurements take a lot of time. Moreover, they are prone to errors. Therefore, there is a need for more efficient alternative methods.

In our time of increasing risks for drought damages, and due to these disadvantages of the classical methods, there is an increasing need for more rapid and cost efficient methods for hydraulic analysis (Cochard et al. 2013), which would allow the determination of vulnerability to drought on larger numbers of samples for better statistics and representativity, in order to

improve our knowledge about processes behind vulnerability and help select more suitable individuals for propagation (Rosner et al. 2014). There are already a few approaches tested in search for alternatives to classical methods to determine hydraulic vulnerability of conifer wood (e.g. Luss, et al., 2015; Rosner, 2017; Luss et al., 2019; Rosner, et al., 2019a; Rosner, et al., 2019b). In this thesis, selected alternatives have been compared and validated towards classical reference measurements.

1.4.1 Criteria for selection of alternative methods to be investigated

The following criteria were set up for selection of alternative methods to evaluate. They should be:

- non-destructive
- efficient
- easy to assess
- based on established techniques
- need limited sample preparation

Definition of criteria:

Non-destructive: Non-destructive can be understood in two ways; most important, the survival and health of the tree, which should have supreme priority, secondly, for the sample. The second aspect is often also very important, especially when different methods are to be compared. In this thesis non-destructive means that neither the tree needs to be harvested (wood cores) nor the sample is damaged.

Efficient: The method should allow processing of large quantities efficiently regarding time and cost.

Easy to assess: Their use should be easy and the evaluation of the results should be possible without much technical know-how. This is especially relevant for a next step of application, after the method development has been completed.

Based on established techniques: Already well-established techniques in this or other fields should be used. These techniques are also applicable for the samples of this study. In addition, the techniques or devices should be accessible to a wider audience.

Limited sample preparation needed: Ideally, the samples could be used for the measurements without complex preparation work, once the method development has been completed.

1.4.2 Short Method overview

Two methods, both fulfilling the criteria above, were thoroughly tested:

1. Fourier transform near-infrared (FT-NIR) spectroscopy, see Page 20 and with further detail in Chapter 2, Page 32.
2. Use of wood density and anatomic information from measurements with SilviScan, see Page 24 and with further details in Chapter 3, Page 40.

Two other methods were also looked upon, despite their not meeting the above criteria:

3. Mechanical testing (compression in radial direction)
4. Pit anatomy

Since the initial results with the latter methods also did not look very promising, these studies were not pursued further, but they are still briefly presented in the chapter "Rejected methods" (Page 28).

1.5 Novel approaches

This chapter first describes the samples used, the two methods that met all criteria set up for selection of alternative methods, then briefly the two rejected methods.

1.5.1 Preparation of samples to be compared

For the "new approaches" it was necessary to do some further sample preparation with the samples previously analysed with the classical air injection method as basis for comparison and validation. This implicated some extra steps which would not be needed using routine measurements.

After the previous flow tests and the determination of the dry mass, the specimens had been stored at -18°C until the start of the measurements with the alternative methods. Therefore, the wooden beams had to be reconditioned.

A total of 1,126 smaller samples were produced from the 147 original specimens prepared for the classical measurements, representing 59 trees. From 2-4 of the original wood specimens per tree (Figure 8, left part), 5-11 shorter specimens were sawn from the middle part, each with a size of $6\text{ mm} \times 6\text{ mm} \times 6\text{ mm}$ (Figure 8, right part), leaving two end pieces, kept for future measurements. All these samples were used for FT-NIR and the rejected methods. For the SilviScan measurements, one sample from each tree was used, a total of 59 cubes.

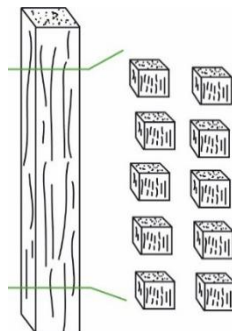


Figure 8: Sample preparation. Buzzsawn pieces

1.5.2 FT-NIR spectra and prediction models

In about 1800, NIR energy was discovered by Herschel as the first region of the electromagnetic spectrum after the visible region (Hindle 2001). In terms of transmitted or reflected spectra, near infrared (NIR) (Figure 9) is in a wavelength range from 800 to 2,500 nm (wavenumber range 12,500 to 4,000 cm^{-1}). Almost 100 years after this discovery of the NIR region, the development of the Michelson interferometer is often referred to as the beginning of Fourier transform spectroscopy (FT).

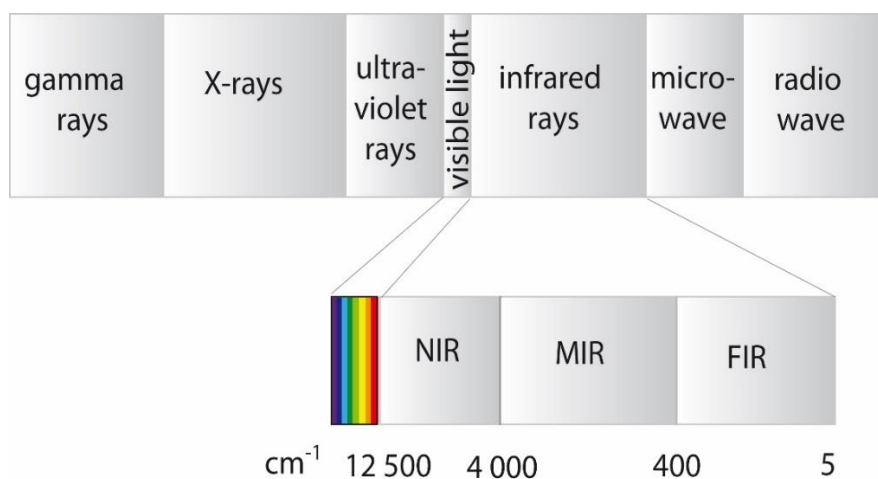


Figure 9: Electromagnetic spectra with focus on Infrared rays (IR)

FT-NIR spectroscopy was developed to overcome the limitation of the dispersive NIR instruments. The dispersion instrument uses a prism or a movable grid to separate the individual frequencies emitted by the near-infrared source. A detector is then used to measure the amount of energy that has passed through the sample at each frequency. This process takes time. Therefore, to shorten the analysis time, a method was needed that measures all infrared frequencies at the same time. The development of an FT-NIR spectrometer makes it possible to generate a unique type of signal, a so-called interferogram. In an interferogram all infrared frequencies are "encoded." The measurements of the signals are very fast, since several scans can be performed per second. A following Fourier transformation then transforms, or "decodes" the interferogram into a spectrum of intensity versus frequency or wavenumber (Doshi 1998; Lipták 2006; Smith 2011).

Only with the advent of minicomputers was it possible for FT-IR spectroscopy to dominate IR identification. At that time, however, chemometric techniques were still very slow. This is because chemometrics require many spectra. An FT-IR spectrum has thousands of data points compared to a disperse spectrum, which has only hundreds of spectral data points. The development of even more powerful computers increased the interest in chemometrics for Fourier transform spectrometers and led to the growth of the FT-NIR spectrophotometer industry. Today, many companies manufacture FT-NIR spectrophotometers to take advantage of the NIR region. (Hindle 2001).

FT-NIR is a non-destructive method that records the interaction of infrared light with matter (Smith 1999). Non-destructive shall in this context be understood as that the method does not destroy the prepared sample. In the FT-NIR range, radiation is absorbed by various chemical

bonds (e.g. C-H, N-H, S-H, C=O, and O-H). Each type of bond has a frequency and wavenumber signature and the number of bonds of each type interacting with the radiations influence the spectrum recorded. Therefore, FT-NIR spectra contains information about the organic composition of a wood sample (Foley et al. 1998; Owen-Reece et al. 1999; Viscarra Rossel et al. 2006; Nicolai et al. 2007; Shenk et al. 2008).

However, a FT-NIR spectrum (Figure 10) does not only carry information about the chemical (molecular absorption) properties of the sample. It is also influenced by its physical properties due to reflection and scattering effects on the radiation (Blanco and Villarroya 2002; Foley et al. 1998; Shenk et al. 2008). For good results, variations in reflection and scattering on the surface and from within the samples have to be controlled on sample preparation, not to confuse interpretation. But this sensitivity to reflection and scattering may also offer possibilities to obtain information about physical properties not related to chemistry. Further, measurements with NIR spectroscopy are indirect measurement relying on use of models to estimate the properties from the spectra, models which must be developed with use of adequate sets of reference data. Various types of pre-treatments of spectra are normally performed before modelling and estimations.

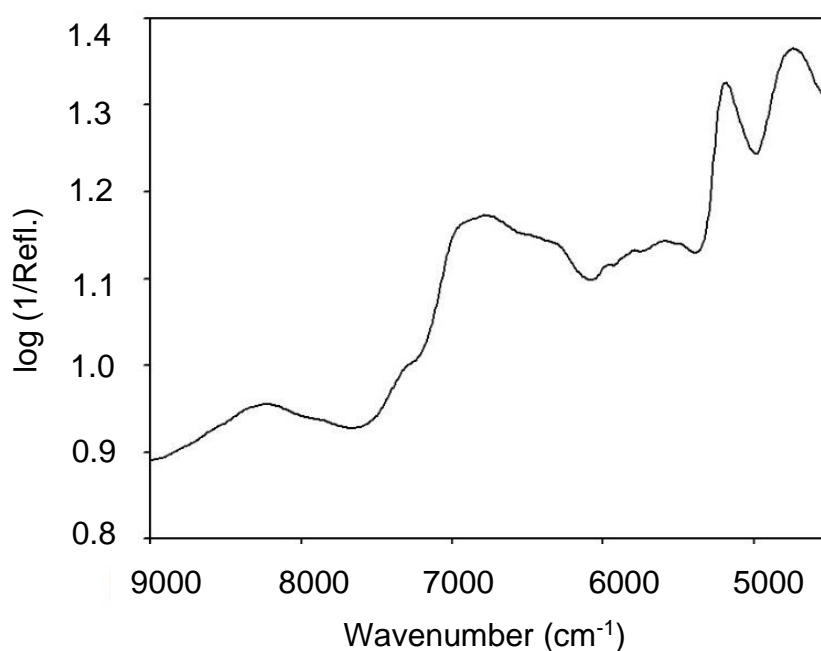


Figure 10: Example of a spectrum. A spectrum can be compared with a fingerprint. Due to the unique combination of atoms of each different material, it is not possible for another compound to show the exact same near infrared spectrum.

To obtain the information about the properties, multivariate statistical models such as partial least squares regression (PLS-R) are used. There, the relationship between the spectral FT-NIR absorption and the chemical components are described or the properties of the reference methods are compared. With PLS-R models, many validation and evaluation steps are necessary to ensure a reliable model. The fully developed PLS-R model can then be used to predict the physical or chemical properties of new samples of similar origin. From these new samples, only the FT-NIR spectra need to be collected (Foley et al. 1998; Workman Jr. 2008).

As mentioned, FT-NIR spectroscopy has quickly developed into a fast and non-destructive analysis method for many physical and chemical properties of woody materials (Smith 1999; Workman Jr. 1999; Schimleck et al. 2000; So et al. 2004; Tsuchikawa 2007; Leblon et al. 2013; Tsuchikawa and Schwanninger 2013). NIRs show a great potential in all facets of material assessment and have been mainly used for measurements of organic material (Tsuchikawa and Schwanninger 2013).

There are two principle ways to collect NIR spectra: Spectra of radiation returning from the sample, reflection mode, and spectra of radiation passing through the sample, transmission mode. Compared to diffuse reflection spectroscopy, transmission measurements normally require more sample preparation (Schwanninger et al. 2011). Another important aspect is that water show very strong absorption in the NIR range, meaning that unwanted variations in humidity may be an issue.

For the FT-NIR measurements in this thesis, diffuse reflection mode has been used. Before the measurements started, the surface properties between the samples were equalised, as roughness can influence the NIR spectra (Cooper et al. 2011). The radial sides of the small wooden cubes were already planed, as the wooden beams for the hydraulic measurements were made on a sliding microtome. The axial surfaces were carefully sanded after the sawing, and then cleaned with compressed air. Then, the wood samples were stored at 21°C and 60% relative humidity for more than seven days to guarantee a uniform wood moisture content of approximately 11% for acquisition of FT-NIR spectra, in order to avoid influence from different moisture contents. A total of 4,505 spectra of the axial ($n = 2,252$) and radial ($n = 2,252$) surface of each solid wood sample were collected in this thesis.

In addition, two measurement methods were tested, using different FT-NIR devices. In the first test series, the wood samples were measured directly with a fiber optic probe (Figure 11 a and b).

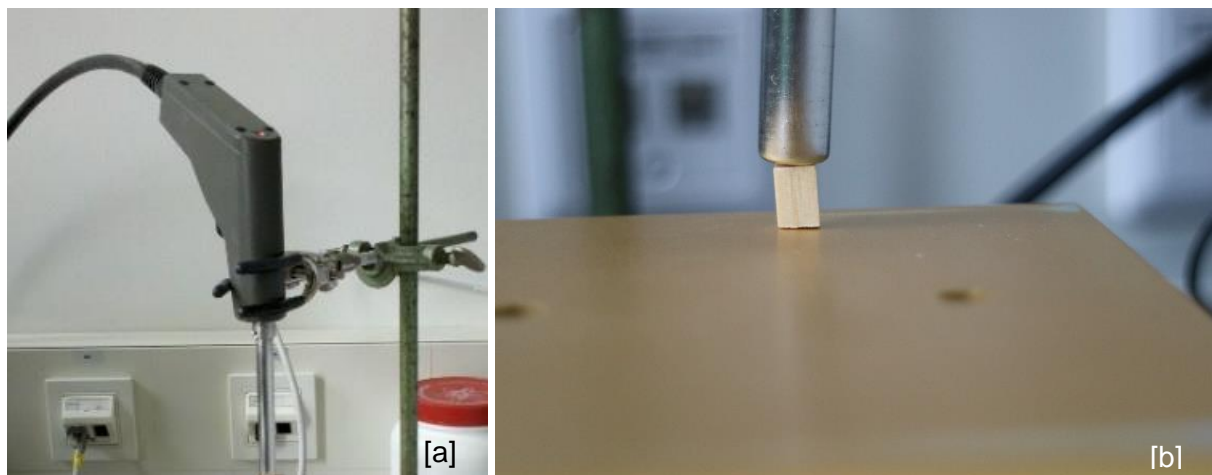


Figure 11: [a] FT-NIR fiber optic; [b] detail of the fiber optic with an example of a wood sample

The measurement with the probe had in this case some disadvantages related to the size of the measurement window of the probe used compared to the sizes of the samples, resulting in that parts of the sample could not be measured. It was also difficult to place the probe in parallel to the sample surface. For this reason, a second series of tests with the Integrating Sphere of a Multi Purpose Analyser (MPA, Brucker Optics) (Figure 12 a and b) was performed.

Since no disadvantages affecting the results were detected during this test, this was the preferred measuring method.

To be thorough, it should be mentioned that the Multi-Purpose Analyser (MPA, Bruker Optics) has a modular design with units offering also other possibilities for sample measurement: Sample compartment, fiber optic module, integrating sphere and transmission unit.



Figure 12: [a] MPA; [b] Sample on an integrating sphere

For this thesis, spectra from $12,000$ to $3,600\text{ cm}^{-1}$ were acquired from the whole surface in diffuse reflection, with zero filling two (i.e. spectrum size is doubled), 16 cm^{-1} spectral resolution, and 50 scans per spectrum. For data analysis, the spectra of each specimen and tree were averaged, resulting in 59 spectra per radial and axial surface, respectively.

In order to enable multivariate calibration and validation after the measurements, the software OPUS QUANT 2 (Bruker, Germany) was used. This software is based on the common algorithm Partial Least Squares (PLS). The method development is not time-consuming because the setup of this software includes useful diagrams, statistics, and tools such as the removal of redundant samples, the automatic selection of test kits, and an optimization tool to find the parameters for the potentially best model (Bruker Optik GmbH 2012). In order to find the best model to predict P_{50} or RWL_{50} , the entire spectrum was first analyzed before focusing on certain wavenumber regions for band assignment, such as lignin and cellulose (Schwanninger et al. 2011; Luss et al. 2015). This focus on lignin and cellulose was because these two chemical properties could be related to wood density (Leblon et al. 2013; Tsuchikawa and Schwanninger 2013; Luss et al. 2015). More information about the FT-NIR results can be found in Chapter 2 (Page 32).

FT-NIR spectroscopy has many advantages because it is an easy to use, measuring speed is very fast, non-destructive method. The sample preparation in the lab and the handling of the equipment is simple and there is a good reproducibility (Schwanninger et al. 2011). In practice, the tools are very helpful, but it is necessary to manually find the best model. There are many ways to find the "best" model. The first evaluations with software, samples, and sample pre-treatment can therefore take a little longer than expected. After some time, the time factor can be optimized due to the experience with modelling.

1.5.2 High resolution measurements of wood density and anatomy with SilviScan

The anatomy of the xylem is obviously of fundamental importance for its hydraulic properties. Conductivity is strongly related to the size of the conduit, power 4. Thus, the lumen size distribution must be very important for the hydraulic properties. The lumen size is defined by the radial width, tangential width and wall thickness of the tracheid, which are also major determinants of the local wood density and mechanical properties of the xylem. Therefore, the focus of this part of the work was placed on the study of relationships between wood anatomy, wood density, conductivity and drought susceptibility, including anatomical variations between and within annual rings. The potential of this approach got further attention after Dalla-Salda et al. (2014) showed that cavitation in Douglas-fir is related also to wood density fluctuations within the rings. Influences of such differences is a major topic in the analyses of this thesis. In the subsequent statistical evaluation, the influence of earlywood, transition wood, and latewood in rings was examined more closely.

In the early 1990s, Dr. Rob Evans and his team at CSIRO, Melbourne, Australia, developed an instrument called SilviScan for efficient, high resolution assessment of spatial variations in wood density and cross-sectional dimensions of tracheids (Evans 1994; Defo 2008). These measurements are achieved through the integration of video microscopy and X-ray transmission measurements performed on samples automatically translated with a motorized stage. In the late 1990s, an upgraded version was developed as part of an Australian research program on hardwoods, including new routines for instance for characterization of vessels (Chen and Evans 2010; Lundqvist et al. 2010). This new version also included the integration of X-ray diffraction for measurement of microfibril angle and wood stiffness (Evans 2006). Some years later, CSIRO developed with support from STFI (now RISE), Stockholm, Sweden, a third restructured version, in which automated microscopy, X-ray transmission and diffraction measurements are performed in parallel on separate units, integrated via a server, for increased throughput. The three existing instruments are located in Melbourne, Stockholm, and Vancouver.

Figure 13 illustrates the three measurement units and how they are integrated: an image analyzer for measurements of fiber cross-sections, an X-ray densitometer for measuring wood density, and an X-ray diffractometer for analyzing the structure of the fiber and wall. One of the physical installations is shown in Figure 14:

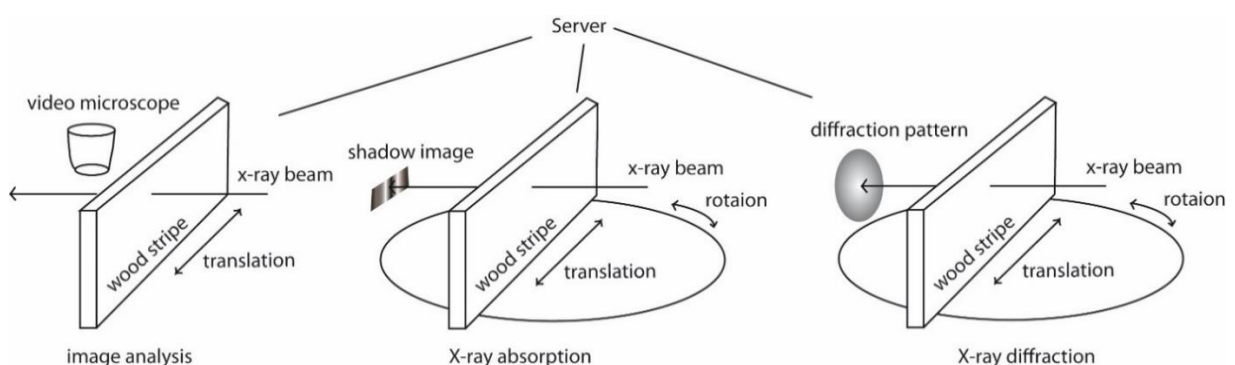


Figure 13: Illustration of the three measurement units of the current SilviScan instruments and how they are integrated. Referring to Robert Evans illustrations



Figure 14: The three measurement units of SilviScan-3. Left to right: the densitometer (density variation), cell scanner (tree ring orientations and cross-sectional cell dimensions) and diffractometer (microfibril angle, wood stiffness), which are integrated via a server. [Photo: ©Rob Evans, CSIRO]

SilviScan has been used since the mid 1990-ies for scientific and commercial activities related to both softwood and hardwood species and in a wide span of areas, including tree improvement, climate effects, forestry, forest product, sawn products, pulp and paper research. It has become a well-established method of measuring that has been used in many projects (Evans 1994; Evans et al. 1995; Downes et al. 2000; Buksnowitz et al. 2008; Lundqvist et al. 2010, 2018; Schimleck et al. 2010, 2019; Knapic et al. 2018). Examples from research on different softwoods are Lindström et al. 1998; Downes et al. 2002; Lundgren 2004; Kostianen et al. 2009; Fries et al. 2014; Piispanen et al. 2014 and on modelling properties of Norway spruce Wilhelmsson et al. 2002; Lundqvist et al. 2005; Franceschini et al. 2012; Auty et al. 2013.

The sample preparation and measurements are performed in a lab with conditioned atmosphere for stable moisture content in the samples. Prior to measurements, radially oriented sample strips of cross-section 2 mm x 7 mm and the length of interest, often from pith to bark, are produced and the top surface polished for microscopy with efficient high precision equipment, see Figure 15a. Such strips can be produced from various sources, such as stem boles as in Figure 3, increment cores or planks. The next step is to determine gravimetrically the average wood density of each sample strip from its mass (by scale) and its extensions. (This is later used to automatically calibrate the density measurement, as the X-ray attenuation constant of wood can vary.) Other types of sample strips may be produced for special measurements. An example of that within the work of this thesis is shown in Figure 15b, where a large number of specimens previously analysed for P_{50} have been glued to each other and onto a support prior to being processed into a sample strip analogous to the one in Figure 15a for analysis with SilviScan.



Figure 15: Example of a samples for measurements on SilviScan: [a] typical sample strip from pith to bark, polished at the top for measurements of cross-sectional tracheid dimensions (Lundqvist and Olsson, 2007); [b] 6 mm x 6 mm pieces from specimens analysed for P₅₀, glued onto a support, prior to its processing with SilviScan's precision equipment into a sample similar to [a], to be followed by high resolution measurement of variations in wood density and cross-sectional tracheid dimensions from edge to edge of each specimen, as well as averages for all their annual rings and their parts of earlywood, transition wood and latewood.

After the gravimetric measurement of wood density, the sample strip is mounted into a holder, normally together with more samples filling up the holder. They then stay there when the holder is moved between the units for different measurements, while data from the individual samples are integrated via the server in a common database. First, a microscopy image of the full length of the sample strip is recorded, from which the cross-sectional dimensions of the fibres are determined with image analysis. At the same time, the angles of all annual rings are determined, and used when measuring on the two other units for successive rotary adjustments of the sample holder to align the ring structure in parallel with the X-ray beams. By this, sharper information on properties of the rings and their parts of earlywood, transition wood and latewood is obtained. Next, the density variations are recorded, with such alignment of the ring structure. Local wood density is also exploited for high quality data on fibre wall thickness according to Scallan and Green (1974). The synchronized data in the database are then used to provide property information as averages for consecutive radial intervals of width 50 μm . Finally, if of interest for the study, also radial sequences of X-ray diffractograms are recorded, from which the radial variations in microfibril angle are determined, and also in wood stiffness by combining diffractogram and density information.

To summarize, these measurements provide data on radial variations of the following properties:

- Wood density
- Widths in radial and tangential direction and wall thickness of tracheids in softwoods and fibres in hardwoods
- Numbers and widths of vessels in hardwoods
- Microfibril angle (MFA)
- Wood stiffness (estimated acoustic MOE)

Based on these data, for trees with annual growth seasons, the annual rings and their compartments of earlywood (EW), transition wood (TW) and latewood (LW) can be identified, more about that below, and averages for rings and their parts calculated. It is also possible to derive information on further properties and features of wood. Examples of information used in work behind this thesis are:

- Widths of annual rings and their parts of earlywood, transition wood and latewood
- Proportions of EW, TW and LW
- Estimated hydraulic conductivity
- New proxies for P_{50} , see Chapter 3 (Page 40)

As influences of within ring fluctuations in tracheid anatomy and wood density are important parts of the thesis, some more words about how these are dealt with: The fundament is the high-resolution data from edge to edge of each individual specimen, from which averages are calculated for the specimens. It is however also interesting to discuss average properties of rings and their parts. Traditionally, growth rings have been divided into two compartments: earlywood and latewood. The most common definition was introduced by Mork (1928). Previous work has however indicated that xylem close to the interface between these two compartments plays an important role as a last resort of conductance on severe drought and should be given special attention (Dalla-Salda et al. 2014). Therefore, we have used the “20-80 density” definition, illustrated in Figure 16. This definition based on within ring density variations introduces a third ring compartment, transition wood, describing the transition phase between pronounced earlywood and latewood, and which is under strong influence from within year weather variations. The definition is further described and motivated in Lundqvist et al. (2018). The method was first introduced by Olsson et al. (1998), and has since been established and used in many publications addressing various aspects of wood related research (Kostiainen et al. 2009; Franceschini et al. 2012; Chen et al. 2014; Hong et al. 2015; Lundqvist et al. 2018).

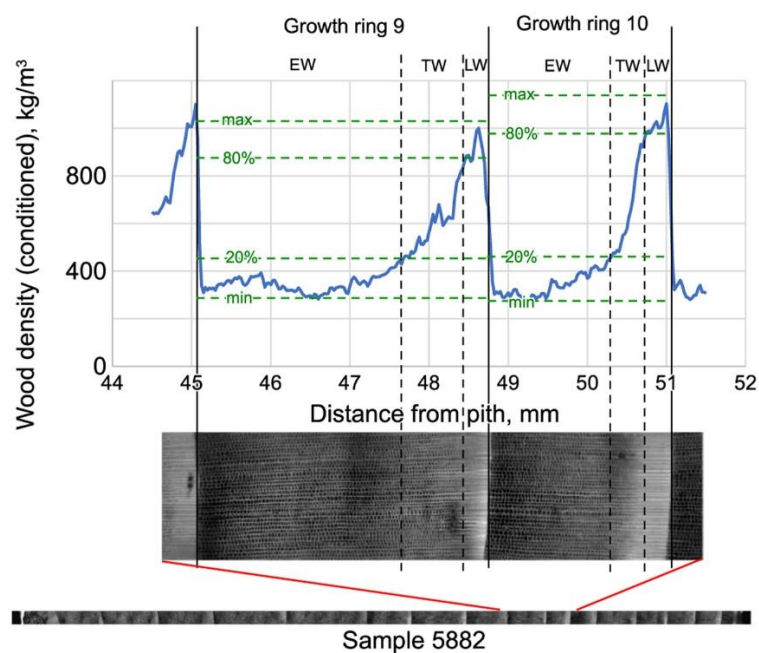


Figure 16: X-ray densitometric images and illustration of density thresholds for earlywood, transition wood and latewood. [Image and Illustration: Lundqvist et al., 2018]

When the interfaces between the rings and these compartments have been identified, property averages are calculated for all rings and their compartments, as well as their proportions of EW, TW and LW. After the measurements with SilviScan and generation of additional data according to above, the data are evaluated using statistical programs. More information about the evaluations based on the SilviScan results can be found in Chapter 3 (Page 40).

1.5.3 Rejected methods

As in many studies, different methods were tested in this thesis. However, not all methods proved to be suitable, which had different causes. This chapter outlines two methods tested in the search for alternatives to determine hydraulic vulnerability. Both were rejected on the basis of the criteria described in Chapter “1.4.1 Criteria for selection of alternative methods to be investigated” (Page 18). No data and results are presented here. The focus is on presenting the basic idea and a short description of the methods.

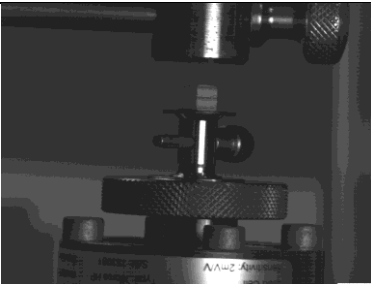
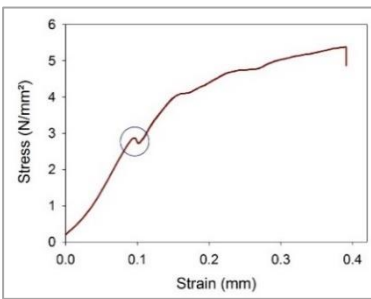
Mechanical Parameters

Rosner and Karlsson (2011) found the peak force calculated from stress/strain curves for radial compression was strongly related to $(t/b)^2$. Moreover, Luss et al. (2019) detected significant correlations between $(t/b)^2$ and P_{50} .

The aim of the mechanical testings was to relate the peak force of a stress/strain curve of compression perpendicular to the grain directly to P_{50} , in order to test the potential of biomechanical testing as a proxy for P_{50} . Hardly any literature deals with this problem as mechanical testing of wood in this direction (perpendicular to the grain) is not quite common (Müller et al. 2003). The combination of hydraulic/biophysical testing (Figure 17) was introduced by Rosner and Karlsson (2011) and has not been performed by anybody else so far.

The first results of the correlations of the parameters from the mechanical testing were promising (data not shown). However, this method had to be rejected because it did not meet the criteria described on Page 18. The mechanical testing is a destructive method since measuring the peak force of radial compression deforms the samples. Because of this deformation, further analyses on the sample are not possible. A small overview of the parameters, methods and key data is summarized in Table 1.

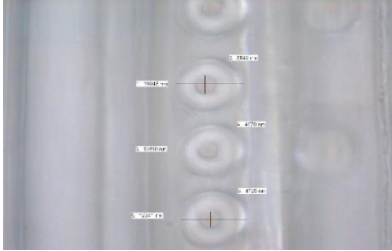
Table 1 Short overview about the mechanical testing

Parameters of interest	Mechanical parameter Radial compression strength perpendicular to the grain
Used equipment	Hardware Zwick/Roell Z020 (Figure 17) Software testXpert® II
Picture of the equipment during the measurement	 <p>Figure 17: Norway spruce sample during the measurements with the Zwick/Roell Z020</p>
Generic measurement output	<p>Stress/strain curve for radial compression perpendicular to the grain (Figure 18) shows a typical pattern in Norway spruce wood</p>  <p>Figure 18: Course of the stress/strain curve for radial compression perpendicular to the grain: The blue circle marks the position for acquisition of the parameter “peak force, radial compression” (σ).</p>
Advantage	<ul style="list-style-type: none"> – Fast – Well established equipment
Disadvantage	<ul style="list-style-type: none"> – Destructive – Not efficient

Pit anatomy

A few studies have already dealt with the topic of bordered pits and hydraulic efficiency (Hacke et al. 2001; Pittermann and Sperry 2006; Bouche et al. 2014). Hydraulic vulnerability should depend on the characteristics of the bordered pits, thus it is assumed that the relationship between P_{50} with wood density and/or tracheid anatomy is indirect. Rosner et al. (2007) found no relationship between pit traits (D_a , D_m , PP) and P_{50} , but strong relationships between specific hydraulic conductivity at full saturation and pit aperture diameter (D_a) and pit aperture percentage (PP). Bouche et al. (2014) found a rather weak relationship between pit aperture diameter (D_a) and P_{50} . In addition, no relationship between P_{50} and torus diameter or pit membrane diameter (D_m) was found. The aim of this study was to investigate these relationships for mature wood of a given species (Norway spruce). For a given cambial age, no significant correlation (data not shown) was found. It seems there are more differences within a tree than between wood of similar cambial age. Compared to the other methods, it can be summarized that pit dimensions cannot be used as a proxy for P_{50} . Other traits are much more easily to assess and show differences at similar cambial age. The method takes a lot of time, since individual bordered pits have to be measured manually. It is also a destructive method. Two of the five criteria were not fulfilled; this method was thus classified as not suitable as an alternative for classical methods. Therefore, the results are not further discussed in this thesis. Table 2 provides a short overview of the pit anatomy testing.

Table 2: Short overview about pit anatomy testing

Parameters of interest	Bordered pits (membrane diameter, D_m), the pit aperture diameter (D_a); the ratio of the pit aperture diameter to the pit diameter (PP , pit aperture percentage)
Used equipment	Hardware Leica DM4000 M microscope equipped with a Leica DFC320 R2 digital camera (Figure 19) Software Leica IM 500 Image Manager image analysing software (Leica, Wetzlar, Germany) (Figure 20)
Picture of the equipment during the measurement	 <p>Figure 19: Microscope</p>
Generic measurement output	 <p>Figure 20: Image of the bordered pits and the manual measurement</p>
Advantage	– Well established method
Disadvantage	– Slow because manual analysis – each pit has to be measured by hand – Not efficient

1.6 Thesis outline

The present thesis consists of four chapters. Chapter 1 includes a general introduction to the topic and research performed. Chapter 2 and 3 are research publications covering the two main parts of the thesis, respectively, before the general conclusions are compiled, completing the thesis. Finally, the general conclusions are summarized in Chapter 4.

Chapter 2 has been published in the Canadian Journal of Forest Research with the title “Hydraulic traits of Norway spruce sapwood estimated by Fourier transform near infrared spectroscopy (FT-NIR)”. Classical methods to determine hydraulic traits like P_{50} (applied air pressure causing 50% loss of hydraulic conductivity) and RWL_{50} (applied air pressure causing 50% relative water loss) are time consuming, labor intensive, and prone to errors. The potential of Fourier transform near-infrared (FT-NIR) spectroscopy to predict P_{50} and RWL_{50} on 24-year-old Norway spruce (*Picea abies* (L.) Karst.) sapwood samples was evaluated. FT-NIR spectra were collected from axial (transverse) and radial surface of the wood samples. By using the partial least squares regression (PLS-R) models with cross validation, there was an attempt to establish relationships between the FT-NIR spectra and the reference data from classical methods. The impact of the wavenumber range and the different pre-treatments during the PLS-R model development and the difference between the axial and radial surface were shown. For P_{50} and RWL_{50} , the models of the axial surface showed better results than for the radial. The first approach with FT-NIR to predict hydraulic traits was successful and it was concluded that this method has a high potential to be put into practice as an alternative to classical methods.

Chapter 3, titled “Within-ring variability of wood structure and its relationship to drought sensitivity in Norway spruce trunks,” has been published in the International Association of Wood Anatomists (IAWA Journal). The focus of this publication lies on wood density and other anatomical parameters like conduit wall reinforcement ($(t/b)^2$), double wall thickness (t), and lumen widths (b) as proxies for P_{50} . Xylem specimens from Norway spruce trunk wood were analysed with a SilviScan instrument for high-resolution information on spatial variations in wood anatomy and wood density, from which further parameters were derived. Properties of interest were calculated for each specimen, annual ring and its part of earlywood (EW), transition wood (TW) and latewood (LW), in order to study influences of the different sections. Also, influences of different anatomical features were compared, such as radial versus tangential lumen size. Wood density is, so far, one of the best available proxies for P_{50} , judged from correlation and that it is easy to use, but it does not necessarily reflect the mechanisms behind resistance to cavitation. New traits calculated from SilviScan data, based on estimation of conductivity loss as a dynamic process, provided even stronger correlations. This approach to find good proxies for P_{50} was successful, and the method has a high potential to replace classical methods.

2. Hydraulic traits of Norway spruce sapwood estimated by Fourier transform near-infrared spectroscopy (FT-NIR)

Saskia Luss, Manfred Schwanninger, and Sabine Rosner

Published in Canadian Journal of Forest Research

Hydraulic traits of Norway spruce sapwood estimated by Fourier transform near-infrared spectroscopy (FT-NIR)

Saskia Luss, Manfred Schwanninger, and Sabine Rosner

Abstract: The potential of Fourier transform near-infrared (FT-NIR) spectroscopy to predict hydraulic traits in Norway spruce (*Picea abies* (L.) Karst.) sapwood was evaluated. Hydraulic traits tested were P_{50} (applied air pressure causing 50% loss of hydraulic conductivity) and RWL_{50} (applied air pressure causing 50% relative water loss). Samples came from 24-year-old spruce clones. FT-NIR spectra were collected from the axial (transverse) and radial surface of each solid wood sample for the prediction of P_{50} and RWL_{50} . Partial least squares regression (PLS-R) models with cross validation were used to establish relationships between the FT-NIR spectra and the reference data from hydraulic properties analysis. The impact of the wavenumber range and the pretreatment during the PLS-R model development and the differences between the axial and radial surfaces were shown. Based on the values of the coefficient of determination (r^2) and the root mean square error of cross validation, predicted results were evaluated as acceptable. The models from the axial surface gave better results than the models from the radial surface for P_{50} ($r^2 = 0.65$), as well as for RWL_{50} ($r^2 = 0.77$). The first approach to predict hydraulic properties such as P_{50} and RWL_{50} by FT-NIR spectroscopy can be regarded as successful. We conclude that the method has high potential to be put into practice as a rapid, reliable, and nondestructive method to determine P_{50} and RWL_{50} .

Key words: Fourier transform near-infrared spectroscopy, Norway spruce, partial least squares regression, *Picea abies*, relative water loss, vulnerability to cavitation.

Résumé : Le potentiel de la spectroscopie dans le proche infrarouge à transformée de Fourier (PIR-TF) pour prédire les traits hydrauliques du bois d'aubier d'épicéa commun (*Picea abies* (L.) Karst.) a été évalué. Les traits hydrauliques qui ont été testés sont P_{50} (la pression d'air qui cause une perte de conductivité hydraulique de 50 %) et RWL_{50} (la pression d'air nécessaire pour causer une perte relative d'eau de 50 %). Les échantillons provenaient de clones d'épicéa âgés de 24 ans. Les spectres PIR-TF ont été collectés à partir de la face axiale (transverse) et de la face radiale de chaque échantillon solide de bois pour prédire P_{50} et RWL_{50} . L'analyse de régression partielle par les moindres carrés avec validation croisée a été utilisée pour établir les relations entre les spectres PIR-TF et les données de référence obtenues par l'analyse des propriétés hydrauliques. L'impact de la plage de nombres d'ondes et du prétraitement durant l'élaboration du modèle de régression ainsi que les différences entre les faces axiale et radiale ont été démontrés. Sur la base des valeurs du coefficient de détermination (r^2) et de l'écart moyen quadratique de la validation croisée, les résultats prédits ont été jugés acceptables. Les modèles élaborés à partir de la face axiale ont produit de meilleurs résultats que ceux qui ont été élaborés à partir de la face radiale tant dans le cas de P_{50} ($r^2 = 0,65$) et que de RWL_{50} ($r^2 = 0,77$). La première tentative de prédire les propriétés hydrauliques telles que P_{50} et RWL_{50} en utilisant la spectroscopie PIR-TF peut être considérée comme un succès. Nous concluons que cette méthode présente un fort potentiel d'utilisation comme méthode rapide, fiable et non destructrice pour déterminer les valeurs de P_{50} et RWL_{50} . [Traduit par la Rédaction]

Mots-clés : spectroscopie dans le proche infrarouge à transformée de Fourier, épicéa commun, régression partielle par les moindres carrés, *Picea abies*, pertes relatives en eau, vulnérabilité à la cavitation.

Introduction

Forest dieback due to drought and heat waves has been frequently observed during the last years (Allen et al. 2010; Rosner et al. 2014). Drought is one of the main climate risks determining survival in coniferous species (Bréda and Badeau 2008; Solberg 2004). As a consequence of climate change, drought and heat waves will occur more frequently and could be more extreme in the future (Intergovernmental Panel on Climate Change (IPCC) 2012). The effect of climate change, e.g., drought incidence, differs among tree species and individuals (Bréda and Badeau 2008). For Norway spruce, aberrant dry and warm weather is the main stress

factor and is related to defoliation, cone formation, and mortality (Solberg 2004). Drought stress can affect the hydraulic efficiency by cavitation of the water columns in the tracheids. Conductivity loss leads to an impairment of the water supply of the crown. Norway spruce (*Picea abies* (L.) Karst.) trees are designed to survive in northern regions (Solberg 2004) and at the alpine timberline (Mayr et al. 2002). Sectorial radial architecture in which almost completely isolated hydraulic pathways to particular stem and crown regions are present can be a possible survival strategy under harsh environmental conditions at the timberline (Larson et al. 1993, 1994). Economical losses due to top dieback after heat

Received 23 October 2014. Accepted 19 December 2014.

S. Luss. Institute of Wood Science and Technology, University of Natural Resources and Life Sciences, BOKU, Vienna, Peter-Jordan-Straße 82, A-1190 Vienna, Austria; Institute of Botany, University of Natural Resources and Life Sciences, BOKU, Vienna, Gregor-Mendel-Straße 33, A-1180 Vienna, Austria.

M. Schwanninger.* Department of Chemistry, University of Natural Resources and Life Sciences, BOKU, Vienna, Muthgasse 18, A-1190 Vienna, Austria.

S. Rosner. Institute of Botany, University of Natural Resources and Life Sciences, BOKU, Vienna, Gregor-Mendel-Straße 33, A-1180 Vienna, Austria.

Corresponding author: Saskia Luss (e-mail: saskia.luss@boku.ac.at).

*Deceased.

Can. J. For. Res. 45: 1–7 (2015) dx.doi.org/10.1139/cjfr-2014-0452

Published at www.nrcresearchpress.com/cjfr on 8 January 2015.

and drought waves (Solberg 2004; Rosner et al. 2014) might be related to weak adaptation of Norway spruce to lowland regions.

Embolism caused by drought stress occurs when xylem pressure becomes negative enough to induce cavitation (Choat et al. 2012; Hietz et al. 2008; Tyree and Zimmermann 2002). The physiological mechanisms behind dieback due to drought sensitivity are, however, not well understood yet (McDowell et al. 2008). A key factor to estimating the drought tolerance of trees is knowledge of the cavitation resistance in the sapwood (Tyree and Zimmermann 2002). Vulnerability to cavitation can be assessed by a vulnerability curve (VC), i.e., a plot that shows how the conductivity loss in a xylem tissue varies with xylem pressure (Cochard et al. 2013). The most widely used hydraulic vulnerability parameter is P_{50} , which is defined as the water potential that causes a 50% loss in hydraulic conductivity (Choat et al. 2012). Depending on the research question, the overpressure resulting in 50% relative water loss (RWL) can give additional information on the hydraulic performance of a tree (Hietz et al. 2008; Rosner et al. 2008). The RWL (%) is the amount of water loss relative to the amount of water in never-dried sapwood at full saturation, i.e., when all tracheids are filled with free water. The parameter RWL_{50} , defined as the applied air pressure necessary to cause 50% of RWL, has been reported to be strongly related to basic density (Rosner et al. 2008) and gives important information on the water storage capacity (i.e., capacitance) rather than the water transport capacity (Cochard et al. 2013). Capacitance correlates highly not only with density, but also with P_{50} or other VC parameters (McCulloh et al. 2014). Recent studies show that in woody species, the hydraulic functioning relies on both capacitance and vulnerability to cavitation (Choat et al. 2012; McCulloh et al. 2014; Meinzer et al. 2009). Many studies still mainly focus on P_{50} and embolism avoidance, whereas the dynamic influence of capacitance and refilling is widely ignored, even though it is important to understand that xylem is an active and responsive tissue (McCulloh et al. 2014). The need of more time- and cost-efficient methodology for hydraulic analysis is increasing. There is a great demand for rapid and predictive data of capacitance and vulnerability parameters to be used for predicting survival under severe drought (Cochard et al. 2013). For this reason, Fourier transform near-infrared (FT-NIR) spectroscopy is considered as an alternative to complement or even replace conventional analytical methods.

FT-NIR spectroscopy has rapidly developed to become a fast and nondestructive analytical method for many physical and chemical properties of woody materials (Leblon et al. 2013; Schimleck et al. 2000; Smith 1999; So et al. 2004; Tsuchikawa 2007; Tsuchikawa and Schwanninger 2013; Workman 1999). This nondestructive technique records the interaction of infrared light with matter (Smith 1999), operating in the range from 12 820 to 4000 cm^{-1} wavenumber (or from 780 to 2500 nm wavelength) (Blanco and Villarroya 2002; Schwanninger et al. 2011). In the FT-NIR region, the radiation is absorbed by the different chemical bonds, e.g., C–H, N–H, S–H, C=O, and O–H, of any chemical compounds present in the sample. Furthermore, the radiation is absorbed in accordance with the concentration of these compounds. As a consequence, FT-NIR spectra basically contain information about the organic composition of a wood sample (Nicolai et al. 2007; Viscarra Rossel et al. 2006). Therefore, the constituents of the material determine the characteristics and number of chemical bonds present and thus the wavenumbers and amount of NIR light that is absorbed (Foley et al. 1998; Shenk et al. 2008). However, the obtained FT-NIR spectrum contains information not only on the chemical (molecular absorbance) but also on the physical (scattering or reflective) properties of an organic material (Blanco and Villarroya 2002; Foley et al. 1998; Shenk et al. 2008). FT-NIR information cannot be directly interpreted from obtained spectra. Thus, to extract this information, multivariate statistical models such as the partial least squares regression (PLS-R) models are developed to describe the relationship between the FT-NIR spec-

Table 1. Statistics of the reference values calculated from raw data published in Rosner et al. (2008).

Trait	<i>n</i>	Mean (MPa)	SD (MPa)	SE (MPa)	Minimum (MPa)	Maximum (MPa)
P_{50}	59	-2.45	0.23	0.03	-3.00	-2.01
RWL_{50}	59	-3.12	0.34	0.04	-4.24	-2.60

Note: *n*, number of samples; SD, standard deviation; SE, standard error.

tral absorbance and the chemical components or properties of interest assessed by reference methods. Compared with linear regressions in which the quality is determined only by the coefficient of determination, many steps of validation and evaluations are necessary for PLS-R models to ensure a reliable model. The final developed PLS-R model can then be used for the fast and reliable prediction of physical or chemical properties of new samples of the same origin from which only FT-NIR spectra were collected (Foley et al. 1998; Workman 2008).

Quality parameters of wood such as modulus of elasticity (Lestander et al. 2008), fibre length, mechanical strength and stiffness (Schimleck et al. 2005; Xu et al. 2011), compression wood (McLean et al. 2014), wood density (Galleguillos-Hart et al. 2010; Hans et al. 2013; Hein et al. 2009; Hoffmeyer and Pedersen 1995; Inagaki et al. 2008, 2012; Mora et al. 2011; Rodrigues et al. 2013; Stirling et al. 2007), and natural durability (Gierlinger et al. 2003) have already been successfully predicted by PLS-R models (reviewed in Tsuchikawa (2007) and Tsuchikawa and Schwanninger (2013)). Hydraulic traits of conifer sapwood have been shown to correlate strongly with wood quality attributes such as tracheid length and wall thickness (Rosner et al. 2007), modulus of elasticity, and wood density (Domec and Gartner 2002; Rosner et al. 2008). Therefore, it is hypothesized that FT-NIR spectroscopy could have a high potential to predict hydraulic properties as well. PLS-R models could be used for quasi-nondestructive fast prediction of hydraulic characteristics of small sapwood specimen, e.g., wood cores, and would thus allow for screening of less drought-sensitive individuals.

The objective of this study is to explore the potential of models using FT-NIR spectroscopy to estimate different hydraulic properties on Norway spruce samples. P_{50} and RWL_{50} reference data were available from a previous study (Rosner et al. 2008).

Materials and methods

Reference data (Table 1) and FT-NIR spectra were used to develop PLS-R models based on FT-NIR for the prediction of P_{50} and RWL_{50} . Complex PLS-R models are often not reliable, because they are influenced by numerous chemical and structural parameters. For this reason, in this first approach to predict hydraulic parameters, only one species was used.

Plant material

Norway spruce trees grown on two sites in southern Sweden were harvested at the age of 24 years. The sites are located at an altitude of 60–120 m, and precipitation during the growth period was between 350 and 600 mm. On both sites, the soil is sandy loam till. The mean height of the trees was between 9.3 and 10.8 m, and the mean diameter at breast height (1.3 m) was from 10.6 to 11.8 cm. More details about the sampling sites and trees are described in Rosner et al. (2008).

Hydraulic reference dataset

For this study, we used hydraulic raw data obtained from previous research (Rosner et al. 2008). For the calculation of P_{50} and RWL_{50} , the fresh mass and flow was determined on small wood beams (6 mm × 6 mm × 120 mm) that were produced on a sliding microtome after stepwise application of air pressure (0.5 MPa) in a double-ended pressure chamber (PMS Instrument Company, Corvallis, Oregon). The reading accuracy of the display of the

double-ended pressure chamber was 0.05 MPa. The first flow measurement performed at full saturation was used as a reference value to calculate the loss of hydraulic conductivity after sequential application of positive pressure in the double-ended pressure chamber. Rosner et al. (2008) calculated P_{50} and RWL_{50} values for each tree from pooled data on conductivity loss or RWL data and pressure application of at least three sapwood beam specimens. Spectra were collected only from the samples that had enough data points available to construct whole VCs. Thus, the reference data for the FT-NIR models were first calculated for each wood beam and afterwards were averaged per tree. Reliable P_{50} and RWL_{50} values could be calculated for 147 samples. The mean values of our new sample set (Table 1) differ slightly from the dataset presented in Rosner et al. (2008), because for a pooled analysis (VC per tree), it is also possible to include single-point measurements of conductivity loss and applied pressure. In addition, samples with compression wood were excluded from analyses. P_{50} was calculated as described in Pammenter et al. (1998), in which the percent loss of conductivity is related to the negative of the applied pressure with a sigmoid function. The relationship between RWL and the negative of the applied pressure was fitted by means of a cubic curve and RWL_{50} was calculated (Rosner et al. 2008).

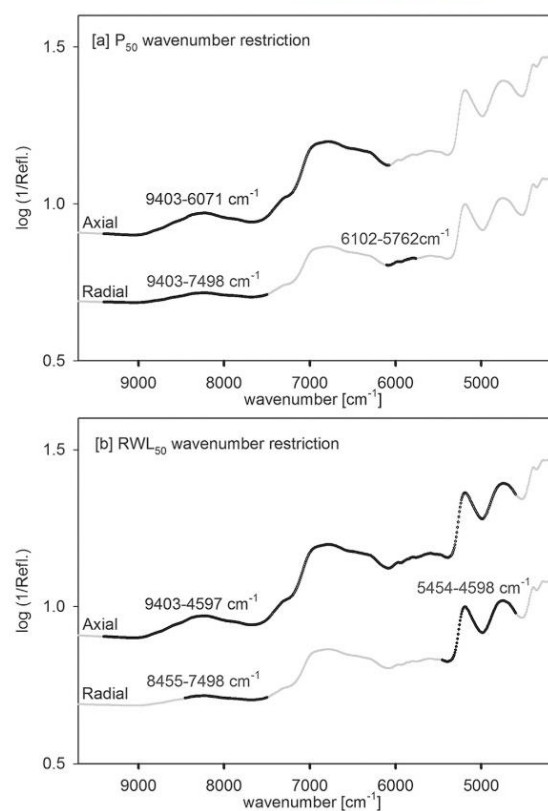
FT-NIR spectroscopy

After the flow experiments and the determination of dry mass, the wood beams were stored at $-18\text{ }^{\circ}\text{C}$. For FT-NIR spectroscopy, 5–11 specimens with a size of $6\text{ mm} \times 6\text{ mm} \times 6\text{ mm}$ were sawn from the middle part of 2–4 replicate wood beams per tree. In total, 1126 specimens from 147 samples of 59 trees were equilibrated at $21\text{ }^{\circ}\text{C}$ and 60% relative humidity for 1 week to guarantee a uniform wood moisture content of about 11% for acquisition of FT-NIR spectra. Not only are FT-NIR spectra influenced by variation in moisture content, but the surface of solid wood samples also has to be planed for the measurements. The radial sides of the small wood cubes had a planed surface, because wood beams for hydraulic measurements were produced on a sliding microtome and the axial surfaces were carefully sanded and cleaned with compressed air after sawing. The surface characteristics between samples should be similar, because the roughness can affect the NIR spectra (Cooper et al. 2011). From each solid wood sample, two FT-NIR spectra were collected from the radial ($n = 2252$) and the axial ($n = 2252$) surfaces with a multipurpose FT-NIR analyzer (MPA; Bruker, Germany). By using an integrating sphere, spectra of the whole surface were acquired in diffuse reflection from $12\,000$ to 3600 cm^{-1} , with zero filling 2 (i.e., spectrum size is doubled), 16 cm^{-1} spectral resolution, and 50 scans per spectrum. For data analysis, the spectra of each specimen and tree were averaged, resulting in 59 spectra per radial and axial surface, respectively.

Data analysis

The PLS-R method was used to establish a mathematical correlation between the FT-NIR spectra and the hydraulic parameters. Using OPUS 7.0 Quant 2 software (Bruker, Germany), PLS-R models based on the 59 averaged spectra from the axial and radial surfaces were established to predict P_{50} and RWL_{50} , respectively. First, the whole range of the spectrum was analyzed. Second, we focused on wavenumber regions for the band assignment of lignin and cellulose (reviewed in Schwanninger et al. (2011)), because both chemical traits could be related to wood density (Leblon et al. 2013; Tsuchikawa and Schwanninger 2013). To date, wood density is the best predictive trait for P_{50} and RWL_{50} in Norway spruce (Rosner et al. 2014). Different wavenumber ranges (Fig. 1) and spectral pretreatments (multiplicative scatter correction, vector normalization, and first and second derivatives) were tested. The spectral pretreatment was used to minimize the irrelevant information in the spectra to develop robust models (Blanco and Villarroya 2002). The optimum number of PLS vectors was

Fig. 1. Averaged FT-NIR spectra from the axial and radial surfaces. (a) P_{50} (applied air pressure causing 50% loss of hydraulic conductivity) and (b) RWL_{50} (applied air pressure causing 50% relative water loss) restricted wavenumber ranges (dark) for both surfaces. $\log(1/\text{Refl})$, “absorbance” (Schwanninger et al. 2011).



determined during cross validation (CV) and test set validation (TS) according to the software and is described in detail elsewhere (e.g., Gierlinger et al. 2002). The coefficient of determination for calibration (R^2 ; data not shown) and for CV and TS (r^2), the root mean square error of cross validation (RMSECV) and test set validation (RMSEP), and the ratio of the standard deviation of validation set to RMSECV (RPD) were used to evaluate the quality of the established model. To find the best wavenumber restriction and spectral pretreatment, all samples were validated by the leave-one-out CV. In a second step, the sample set was divided in half to perform CV and TS validation. Each set was used for CV and TS and the other way around to evaluate if the model statistic is similar; this shows if the number of PLS vectors is the same (Gierlinger et al. 2002; Santos et al. 2012).

Results and discussion

The PLS-R models

The ability of FT-NIR spectroscopy to predict the hydraulic properties (P_{50} and RWL_{50}) is summarized in Table 2, and r^2 , RMSECV, and RPD are given. Preprocessing methods were chosen as those that provided the best models for each property (lowest RMSECV values and highest r^2 values).

PLS-R calibration models were developed for P_{50} and RWL_{50} with spectra acquired from the axial and radial surfaces, respectively.

Table 2. Results of the cross-validated predictions for P_{50} and RWL_{50} using partial least squares (PLS) regression.

	P_{50}			RWL_{50}						
	Axial			Radial						
Wavenumber (cm ⁻¹)	9700–4100	9700–4100	9403–6071	9700–4100	9700–4100	9403–4597	9700–4100	9700–4100	9700–4100	8455–7498, 5454–4598
Pretreatment	None	1.Der, MSC	1.Der, MSC	None	None	6102–5762	None	None	2.Der	2.Der
r^2	0.34	0.42	0.65	0.34	0.43	0.53	0.64	0.6	0.66	0.68
RMSECV (MPa)	0.18	0.16	0.09	0.17	0.16	0.14	0.18	0.19	0.18	0.19
RPD	1.23	1.31	1.69	1.23	1.33	1.47	1.67	1.58	1.71	1.75
No. of PLS vectors	3	3	3	6	4	4	4	4	7	7
Outlier	2	2	10	1	2	2	4	1	1	0

Note: n = 59 for P_{50} and RWL_{50} ; n, number of samples; r^2 , coefficient of determination; RMSECV, root mean square error of cross validation; RPD, ratio of the standard deviation of analyzed data to RMSECV; 1.Der, first derivative; MSC, multiplicative scatter correction; VN, vector normalization; 2.Der, second derivative.

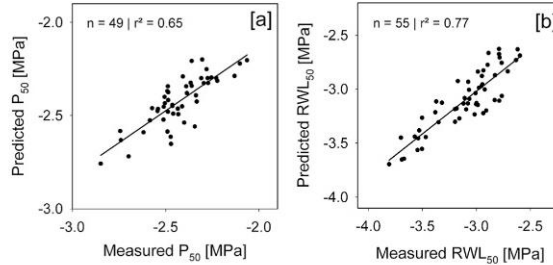


Fig. 2. Relationships between (a) P_{50} and (b) RWL_{50} measured by standard laboratory procedures and predicted by FT-NIR spectroscopy. Cross validation of P_{50} (pressure that induces 50% loss of hydraulic conductivity) and RWL_{50} (pressure application necessary to result in 50% relative water loss).

Typical FT-NIR spectra are shown in Fig. 1. Axial and radial spectra exhibited the same $\log(1/R)$ bands (hereafter termed “absorbance”; see Schwanninger et al. (2011)) but with different intensities. Four main peaks were present at 8230, 6790, 5190, and 4740 cm^{-1} . The axial surface had a higher absorbance than the radial surface (Fig. 1), as light probably passed deeper into the cross section due to the presence of tracheids that were cut open (Defo et al. 2007; Schimleck et al. 2003).

The influence of data pretreatment and the wavenumber restriction on P_{50} models is shown in Table 2. Scatterplots of predicted versus measured values for P_{50} and RWL_{50} are shown in Fig. 2. The axial calibration models for P_{50} showed r^2 values of up to 0.65, RMSECV values of more than 0.09 MPa, and a RPD value of 1.69 with three PLS vectors. Compared with the axial calibration models, the optimum number of PLS vectors were higher (4–6) for the radial models, whereas r^2 and RMSECV showed similar values for both models. There was a slight improvement in the model with restriction of the wavenumber.

The relatively strong relationship between the measured P_{50} reference data and the FT-NIR predicted spectra with the first derivative, with the multiplicative scatter correction as pretreatment and the restricted wavenumber (9403–6071 cm^{-1}), is displayed in Fig. 2a. Notably, the best model statistics ($r^2 = 0.65$, RMSECV = 0.09) were achieved after detecting and removing 10 samples as outliers during the validation (Table 2). These outliers could be removed, because either the samples had traumatic resin canals or the radial faces of the small cubes were not rectangularly aligned to the annual rings. These anatomical and textural (alignment along the grain) characteristics presumably influenced the hydraulic flow measurements and thus estimation of P_{50} , but they did not necessarily influence measurements of the moisture loss and thus estimation of RWL_{50} .

The model established for RWL_{50} (Table 2) led to better statistical results (higher r^2 and lower RMSECV) than that for P_{50} , especially with spectra acquired from the axial surface. The RWL_{50} axial calibration models showed r^2 values up to 0.77, RMSECV values below 0.18 MPa, and RPD values of 2.08. The RWL_{50} radial calibration models showed slightly lower r^2 , higher RMSECV, and lower RPD values, as well as a higher optimum number of vectors. Again, the quality of the models and their suitability for the prediction could be improved by spectra preprocessing and wavenumber selection (Table 2). The vector normalization led to the best result for the axial spectra (Fig. 2b), and the second derivative led to the best result for the radial spectra. The most suitable wavenumbers were, however, different for the two investigated anatomical directions. On the axial surface, more light may pass deeper into the cross section than on the radial surface (Defo et al. 2007; Schimleck et al. 2003); therefore, we suggest analysing spectra from the axial surface for predicting hydraulic traits. Using the

same wavenumber range (Fig. 1) resulted in much weaker models for the radial side (results not shown), whereas the exclusion of the wavenumber range of 7000–6000 cm^{-1} (Fig. 1) led to improved models. Within this wavenumber range, range bands can be assigned to water and cellulose (Schwanninger et al. 2011). The influence of this wavenumber range is not yet clear. Further work will focus on the relationship between the cutting direction (axial or radial), physical parameters, and chemical features.

PLS-R models for prediction of RWL_{50} were stronger than those for P_{50} (Fig. 2; see Supplementary Table S1¹). Coates (2002) concludes in his column entitled “Is near infrared spectroscopy only as good as the laboratory reference values?” that “the more accurate the reference values, the more accurate will be the predictions”. There is no doubt that practical assessment of P_{50} is more prone to errors compared with RWL_{50} in which only the mass has to be determined after each pressure application. Potential sources of error in the determination of P_{50} are the repeated flow measurements after pressure application performed on the same specimen. Cavitation fatigue due to damage on the bordered pits can lead to an underestimation of P_{50} in Norway spruce sapwood when repeated pressure applications are performed (Rosner et al. 2010). It is, however, quite difficult to assess possible sources of error of the reference method, because there are not two exactly equal samples, and it is not possible to resaturate and repeat the flow measurement procedure on the same specimen. The measurements to predict the hydraulic performance under drought stress are complex, and standard protocols for estimating the hydraulic function are still missing (Rosner 2014). The discussion on and the search for the most reliable method to estimate P_{50} is ongoing (Cochard et al. 2013); in this regard, the FT-NIR technique could be used as a valuable tool to compare the reliability of different methods.

Structural and chemical traits determining hydraulics: can they be reflected by NIR?

Stronger PLS-R models for RWL_{50} than those for P_{50} raises another question: to which amount can structural and chemical traits that determine hydraulics be reflected by NIR spectroscopy?

Wood density is a reliable indirect trait to estimate P_{50} of Norway spruce sapwood across cambial ages (Rosner et al. 2014). In specimens of similar cambial age, the relationship is, however, much weaker (Rosner et al. 2008). The relationship between density and RWL_{50} ($r^2 = 0.57$) was found to be stronger than the relationship between density and P_{50} ($r^2 = 0.34$) in the specimens from which spectra were collected. Moreover, within the same density range, RWL_{50} had a wider data range than P_{50} , which should, in general, be a better precondition for constructing empirical models. For Norway spruce, PLS-R models for density were successfully developed (Hauksson et al. 2001; Hoffmeyer and Pedersen 1995; Thygesen 1994). Hoffmeyer and Pedersen (1995) evaluated the density and the strength of Norway spruce cross sections by FT-NIR spectroscopy and a four-factor model was obtained ($r^2 = 0.77$). PLS-R models for density were, however, found to be stronger in other conifer species (Tsuchikawa and Schwanninger 2013) such as black spruce (*Picea mariana* (Mill.) Britton, Sterns & Poggenb.) and balsam fir (*Abies balsamea* (L.) Mill.) ($r^2 = 0.88$) (Xu et al. 2011). In Japanese larch (*Larix kaempferi* (Lam.) Carrière), a four-factor PLS-R density model was developed ($r^2 = 0.98$) (Rodrigues et al. 2013). The better model statistics obtained for RWL_{50} compared with P_{50} might be explained by the stronger correlation between density and RWL_{50} than between density and P_{50} . However, prediction of P_{50} by the FT-NIR models gave much better results ($r^2 = 0.65$) than prediction by wood density ($r^2 = 0.34$). The variability in P_{50} should be strongly related to the characteristics of bordered pits (Lens et al. 2011). It is not yet known which pit properties exactly deter-

mine P_{50} in Norway spruce wood and if these properties can be assessed by FT-NIR at all. Hot candidates are pit frequency (Domec et al. 2006), pit diameter (Mayr et al. 2002), and the characteristics of the pit membrane, e.g., its rigidity (Hacke et al. 2004; Domec et al. 2006). There is correlation between the hydraulic vulnerability and pit aperture size factors (Mayr et al. 2002; Rosner et al. 2007). It remains to be tested to what extent the spectra can reflect the pit frequency, the pit aperture diameter, and their anatomical and mechanical properties, e.g., the size of the pores in the fibrillose margo or the stiffness of the torus.

This study suggests that the hydraulically relevant properties should be better reflected by spectra from the axial surface. However, bordered pits are more frequently found in the radial cell wall and are more numerous at the ends of the tracheids than in the middle parts (Meier 1962; Sirviö and Kärenlampi 1998). Also, pit frequency and diameter should be more reliably assessed on the radial wood surface. However, these pit properties can be measured only on exact radial splits, which would result in a rather rough surface that is not suitable for performing flow experiments (tightening into the tubing system) and for collecting reliable spectra. Further anatomical and chemical analyses can provide more information about the differences between the axial and radial surfaces.

NIR is suitable to predict chemical constituents such as extractives, lignin, and cellulose in conifer wood (reviewed in Tsuchikawa and Schwanninger (2013)). However, little is known about the chemistry of pit membranes and their role in hydraulic functions, especially in resistance to cavitation. The effect of commercial chemicals on vulnerability to cavitation was recently tested in two angiosperm species by Dusotoit-Coucaud et al. (2014). Against a background of ongoing debate over the presence of pectins in pit membranes, they found evidence that cellulose and pectins are critical components for vulnerability to cavitation and that they likely have distinct roles in the efficiency and safety of xylem hydraulics. For the final P_{50} model, the wavenumber ranges between 9403 and 6071 cm^{-1} were chosen (Fig. 1); the peak at 6790 cm^{-1} can be assigned to cellulose (bond vibration, first overtone at the O–H structure) (Schwanninger et al. 2011). Bauch and Berndt (1973) investigated about 100 coniferous species by histochemical methods and some by spectrophotometrical methods to determine the chemical composites of their pit membranes. It was found that for many species in sapwood, the pit membranes consist mainly of pectins accompanied by cellulose and hemicellulose without any phenolic compounds. The substances in the membranes can differ between neighbouring tracheids and likewise even between neighbouring pits. It remains to be tested if pit membrane chemistry affects hydraulic vulnerability of Norway spruce and if hydraulically relevant variations between tracheids or neighboring pits can be reflected by FT-NIR spectra of the entire solid wood specimen.

Conclusions

The first approach to predict hydraulic properties such as P_{50} and RWL_{50} by FT-NIR spectroscopy can be regarded as successful; the PLS-R models were stronger than the relationship between wood density and these hydraulic parameters. However, the PLS-R models gave better results for RWL_{50} than for P_{50} , which might be explained by the stronger relationship between RWL_{50} and wood density, and due to the strong influence of the characteristics of the bordered pits on P_{50} , their properties might not be assessed by FT-NIR spectra. Application of the technique on specimens with a wider P_{50} and RWL_{50} data range might lead to a further improvement of the models. This implies development of techniques to collect FT-NIR spectra from smaller surface areas, e.g., from

¹Supplementary table is available with the article through the journal Web site at <http://nrcresearchpress.com/doi/suppl/10.1139/cjfr-2014-0452>.

branches. Thereafter, the calibration could be put into practice as a rapid, reliable, and nondestructive method to determine P_{50} and RWL_{50} . Furthermore, applications of FT-NIR on other species or in conjunction with other reference methods, e.g., the centrifuge technique, are suggested. Relating FT-NIR spectra to different hydraulic methods to assess P_{50} could be an important contribution to the ongoing discussion about the different methods that are currently used to determine hydraulic traits.

Acknowledgements

This article is in memoriam to Manfred Schwanninger (passed away 25 December 2013). We thank him for his scientific input. We thank Notburga Gierlinger for providing the project idea, the valuable scientific input, and helpful discussions. We also thank to the two anonymous reviewers for their valuable scientific comments and linguistic corrections. This study was funded by Commission of the European Communities (Rue de la Loi, Brussels, Belgium, European Union) within the framework of the project Designing Trees for the Future.

References

- Allen, C.D., Macalady, A.K., Chenchouni, H., Bachelet, D., McDowell, N., Vennetier, M., Kitzberger, T., Rigling, A., Breshears, D.D., Hogg, E.H., Gonzalez, P., Fensham, R., Zhang, Z., Castro, J., Demidova, N., Lim, J.H., Allard, G., Running, S.W., Semerci, A., and Cobb, N. 2010. A global overview of drought and heat-induced tree mortality reveals emerging climate change risks for forests. *For. Ecol. Manage.* **259**(4): 660–684. doi:10.1016/j.foreco.2009.09.001.
- Bauch, J., and Berndt, H. 1973. Variability of the chemical composition of pit membranes in bordered pits of gymnosperms. *Wood Sci. Technol.* **7**(1): 6–19. doi:10.1007/BF00353374.
- Blanco, M., and Villarroya, I. 2002. NIR spectroscopy: a rapid-response analytical tool. *Trends Anal. Chem.* **21**(4): 240–250. doi:10.1016/S0165-9936(02)00404-1.
- Bréda, N., and Badaeu, V. 2008. Forest tree responses to extreme drought and some biotic events: towards a selection according to hazard tolerance? *C. R. Geosci.* **340**(9–10): 651–662. doi:10.1016/j.crte.2008.08.003.
- Choat, B., Jansen, S., Brodribb, T.J., Cochard, H., Delzon, S., Bhaskar, R., Bucci, S.J., Field, T.S., Gleason, S.M., Hacke, U.G., Jacobsen, A. L., Lens, F., Maherali, H., Martínez-Vilalta, J., Mayr, S., Mencuccini, M., Mitchell, P.J., Nardini, A., Pittermann, J., Pratt, R.B., Sperry, J.S., Westoby, M., Wright, I.J., and Zanne, A.E. 2012. Global convergence in the vulnerability of forests to drought. *Nature*, **491**(7426): 752–755. doi:10.1038/nature11688.
- Coates, D. 2002. "Is near infrared spectroscopy only as good as the laboratory reference values?" An empirical approach. *Spectrosc. Eur.* **14**(4): 24–26.
- Cochard, H., Badel, E., Herbette, S., Delzon, S., Choat, B., and Jansen, S. 2013. Methods for measuring plant vulnerability to cavitation: a critical review. *J. Exp. Bot.* **64**(15): 4779–4791. doi:10.1093/jxb/ert193.
- Cooper, P.A., Jeremic, D., Radivojevic, S., Ung, Y.T., and Leblon, B. 2011. Potential of near-infrared spectroscopy to characterize wood products. *Can. J. For. Res.* **41**: 2150–2157. doi:10.1139/x11-088.
- Defo, M., Taylor, A.M., and Bond, B. 2007. Determination of moisture content and density of fresh-sawn red oak lumber by near infrared spectroscopy. *For. Prod. J.* **57**: 68–72.
- Domec, J.C., and Gartner, B.L. 2002. Age- and position-related changes in hydraulic versus mechanical dysfunction of xylem: inferring the design criteria for Douglas-fir wood structure. *Tree Physiol.* **22**(2–3): 91–104. doi:10.1093/treephys/22.2-3.91.
- Domec, J., Lachenbruch, B., and Meinzer, F. 2006. Bordered pit structure and function determine spatial patterns of air-seeding thresholds in xylem of Douglas-fir (*Pseudotsuga menziesii*; Pinaceae) trees. *Am. J. Bot.* **93**(11): 1588–1600. doi:10.3732/ajb.93.11.1588.
- Dusotoit-Coucaud, A., Brunel, N., Tixier, A., Cochard, H., and Herbette, S. 2014. Hydrolase treatments help unravel the function of intervessel pits in xylem hydraulics. *Physiol. Plant.* **150**(3): 388–396. doi:10.1111/ppl.12092.
- Foley, W.J., McIwee, A., Lawler, I., Aragones, L., Woolnough, A.P., and Berding, N. 1998. Ecological applications of near infrared reflectance spectroscopy — a tool for rapid, cost-effective prediction of the composition of plant and animal tissues and aspects of animal performance. *Oecologia*, **116**(3): 293–305. doi:10.1007/s004420050591.
- Galleguillos-Hart, C., Fernández, M., and Guesalaga, A. 2010. A portable method to estimate wood basic density from increment cores using spectroscopic techniques. *J. Near Infrared Spectrosc.* **18**(1): 465–472. doi:10.1255/jnirs.899.
- Gierlinger, N., Schwanninger, M., Hinterstoisser, B., and Wimmer, R. 2002. Rapid determination of heartwood extractives in *Larix* sp. by means of Fourier transform near infrared spectroscopy. *J. Near Infrared Spectrosc.* **10**(3): 203–214. doi:10.1255/jnirs.336.
- Gierlinger, N., Jacques, D., Schwanninger, M., Wimmer, R., Hinterstoisser, B., and Pâques, L.E. 2003. Rapid prediction of natural durability of larch heartwood using Fourier transform near-infrared spectroscopy. *Can. J. For. Res.* **33**(9): 1727–1736. doi:10.1139/x03-092.
- Hacke, U.G., Sperry, J.S., and Pittermann, J. 2004. Analysis of circular bordered pit function II. Gymnosperm tracheids with torus-margo pit membranes. *Am. J. Bot.* **91**(3): 386–400. doi:10.3732/ajb.91.3.386.
- Hans, G., Leblon, B., Stirling, R., Nader, J., La Rocque, A., and Cooper, P. 2013. Monitoring of moisture content and basic specific gravity in black spruce logs using a hand-held MEMS-based near-infrared spectrometer. *For. Chron.* **89**(5): 607–620. doi:10.5558/tfc2013-112.
- Hauksson, J.B., Bergqvist, G., Bergsten, U., Sjöström, M., and Edlund, U. 2001. Prediction of basic wood properties for Norway spruce. Interpretation of near infrared spectroscopy data using partial least squares regression. *Wood Sci. Technol.* **35**(6): 475–485. doi:10.1007/s00226-001-0123-3.
- Hein, P.R.G., Campos, A.C.M., Trugilho, P.F., Lima, J.T., and Chaix, G. 2009. Near infrared spectroscopy for estimating wood basic density in *Eucalyptus urophylla* and *Eucalyptus grandis*. *Cerne*, **15**: 133–141. Available from http://www.dcf.ufla.br/cerne/artigos/24-07-20094097v15_n2_artigo%2002.pdf [accessed 15 December 2014].
- Hietz, P., Rosner, S., Sorz, J., and Mayr, S. 2008. Comparison of methods to quantify loss of hydraulic conductivity in Norway spruce. *Ann. For. Sci.* **65**(5): 1. doi:10.1051/forest:2008023.
- Hoffmeyer, P., and Pedersen, J. 1995. Evaluation of density and strength of Norway spruce wood by near infrared reflectance spectroscopy. *Holz. Roh-Werkst.* **53**(3): 165–170. doi:10.1007/BF02716418.
- Inagaki, T., Yonenobu, H., and Tsuchikawa, S. 2008. Near-infrared spectroscopic monitoring of the water adsorption/desorption process in modern and archaeological wood. *Appl. Spectrosc.* **62**(8): 860–865. doi:10.1366/000370208785284312.
- Inagaki, T., Schwanninger, M., Kato, R., Kurata, Y., Thanapase, W., Puthson, P., and Tsuchikawa, S. 2012. *Eucalyptus camaldulensis* density and fiber length estimated by near-infrared spectroscopy. *Wood Sci. Technol.* **46**: 143–155. doi:10.1007/s00226-010-0379-6.
- Intergovernmental Panel on Climate Change (IPCC). 2012. Managing the risks of extreme events and disasters to advance climate change adaptation. A special report of Working Groups I and II of the Intergovernmental Panel on Climate Change. Edited by C.B. Field, V. Barros, T.F. Stocker, D. Qin, D.J. Dokken, K.L. Ebi, M.D. Mastrandrea, K.J. Mach, G.K. Plattner, S.K. Allen, M. Tignor, and P.M. Midgley. Cambridge University Press, Cambridge, UK. pp. 1–19. doi:10.1017/CBO9781139177245.
- Larson, D.W., Matthes-Sears, U., and Kelly, P.E. 1993. Cambial dieback and partial shoot mortality in cliff-face *Thuja occidentalis*: evidence for sectorial radial architecture. *Int. J. Plant Sci.* **154**(4): 496–505. doi:10.1086/297133.
- Larson, D.W., Doubt, J., and Matthes-Sears, U. 1994. Radially sectorial hydraulic pathways in the xylem of *Thuja occidentalis* as revealed by the use of dyes. *Int. J. Plant Sci.* **155**(5): 569–582. doi:10.1086/297195.
- Leblon, B., Adedipe, O., Hans, G., Haddadi, A., Tsuchikawa, S., Burger, J., Stirling, R., Pirouz, Z., Groves, K., Nader, J., and LaRocque, A. 2013. A review of near-infrared spectroscopy for monitoring moisture content and density of soil wood. *For. Chron.* **89**(5): 595–606. doi:10.5558/tfc2013-111.
- Lens, F., Sperry, J.S., Christman, M.A., Choat, B., Rabae, D., and Jansen, S. 2011. Testing hypotheses that link wood anatomy to cavitation resistance and hydraulic conductivity in the genus *Acer*. *New Phytol.* **190**(3): 709–723. doi:10.1111/j.1469-8137.2010.03518.x.
- Lestander, T.A., Lindeberg, J., Eriksson, D., and Bergsten, U. 2008. Prediction of *Pinus sylvestris* clear-wood properties using NIR spectroscopy and biorthogonal partial least squares regression. *Can. J. For. Res.* **38**(7): 2052–2062. doi:10.1139/X08-047.
- Mayr, S., Wolfswenger, M., and Bauer, H. 2002. Winter-drought induced embolism in Norway spruce (*Picea abies*) at the alpine timberline. *Physiol. Plant.* **115**(1): 74–80. doi:10.1034/j.1399-3054.2002.1150108.x.
- McCulloh, K.A., Johnson, D.M., Meinzer, F.C., and Woodruff, D.R. 2014. The dynamic pipeline: hydraulic capacitance and xylem hydraulic safety in four tall conifer species. *Plant Cell Environ.* **37**(5): 1171–1183. doi:10.1111/pce.12225.
- McDowell, N., Pockman, W.T., Allen, C.D., Breshears, D.D., Cobb, N., Kolb, T., Plaut, J., Sperry, J., West, A., Williams, D.G., and Yezze, E.A. 2008. Mechanisms of plant survival and mortality during drought: why do some plants survive while others succumb to drought? *New Phytol.* **178**(4): 719–739. doi:10.1111/j.1469-8137.2008.02436.x.
- McLean, J.P., Jin, G., Brennan, M., Nieuwoudt, M.K., and Harris, P.J. 2014. Using NIR and ATR-FTIR spectroscopy to rapidly detect compression wood in *Pinus radiata*. *Can. J. For. Res.* **44**(7): 820–830. doi:10.1139/cjfr-2013-0329.
- Meier, H. 1962. Chemical and morphological aspects of the fine structure of wood. *Pure Appl. Chem.* **5**: 37–52. doi:10.1351/pac196205010037.
- Meinzer, F.C., Johnson, D.M., Lachenbruch, B., McCulloh, K.A., and Woodruff, D.R. 2009. Xylem hydraulic safety margins in woody plants: coordination of stomatal control of xylem tension with hydraulic capacitance. *Funct. Ecol.* **23**: 922–930. doi:10.1111/j.1365-2435.2009.01577.x.
- Mora, C.R., Schimleck, L.R., Clark, A., and Daniels, R.F. 2011. Determination of basic density and moisture content of merchantable loblolly pine logs by near infrared spectroscopy. *J. Near Infrared Spectrosc.* **19**: 391–399. doi:10.1255/jnirs.947.
- Nicolai, B.M., Beullens, K., Bobelyn, E., Peirs, A., Saeys, W., Theron, K.L., and Lammertyn, J. 2007. Nondestructive measurement of fruit and vegetable

- quality by means of NIR spectroscopy: a review. *Postharvest Biol. Technol.* **46**(2): 99–118. doi:10.1016/j.postharvbio.2007.06.024.
- Pammenter, N.W., and Van der Willigen, C. 1998. A mathematical and statistical analysis of the curves illustrating vulnerability of xylem to cavitation. *Tree Physiol.* **18**(8–9): 589–593. doi:10.1093/treephys/18.8-9.589.
- Rodrigues, J.C., Fujimoto, T., Schwanninger, M., and Tsuchikawa, S. 2013. Prediction of wood density using near infrared-based partial least squares regression models calibrated with x-ray microdensity. *NIR News*, **24**(2): 4–8. doi:10.1255/nirn.1352.
- Rosner, S. 2014. A new type of vulnerability curve: is there truth in vine? *Tree Physiol.* doi:10.1093/treephys/tpu080.
- Rosner, S., Klein, A., Müller, U., and Karlsson, B. 2007. Hydraulic and mechanical properties of young Norway spruce clones related to growth and wood structure. *Tree Physiol.* **27**(8): 1165–1178. doi:10.1093/treephys/27.8.1165.
- Rosner, S., Klein, A., Müller, U., and Karlsson, B. 2008. Tradeoffs between hydraulic and mechanical stress responses of mature Norway spruce trunk wood. *Tree Physiol.* **28**(8): 1179–1188. doi:10.1093/treephys/28.8.1179.
- Rosner, S., Konnerth, J., Plank, B., Salaberger, D., and Hansmann, C. 2010. Radial shrinkage and ultrasound acoustic emissions of fresh versus pre-dried Norway spruce sapwood. *Trees*, **24**(5): 931–940. doi:10.1007/s00468-010-0464-3.
- Rosner, S., Svetlik, J., Andreassen, K., Borja, I., Dalsgaard, L., Evans, R., Karlsson, B., Tollesrud, M.M., and Solberg, S. 2014. Wood density as a screening trait for drought sensitivity in Norway spruce. *Can. J. For. Res.* **44**(2): 154–161. doi:10.1139/cjfr-2013-0209.
- Santos, A.J., Alves, A., Simões, R.M., Pereira, H., Rodrigues, J., and Schwanninger, M. 2012. Estimation of wood basic density of *Acacia melanoxylon* (R. Br.) by near infrared spectroscopy. *J. Near Infrared Spectrosc.* **20**(2): 267–274. doi:10.1255/jnirs.986.
- Schimleck, L.R., Raymond, C.A., Beadle, C.L., Downes, G.M., Kube, P.D., and French, J. 2000. Applications of NIR spectroscopy to forest research. *Appita J.* **53**: 458–464.
- Schimleck, L.R., Mora, C., and Daniels, R.F. 2003. Estimation of the physical wood properties of green *Pinus taeda* radial samples by near infrared spectroscopy. *Can. J. For. Res.* **33**(12): 2297–2305. doi:10.1139/x03-173.
- Schimleck, L.R., Evans, R., Jones, P.D., Daniels, R.F., Peter, G.F., and Clark, A., III. 2005. Estimation of microfibril angle and stiffness by near infrared spectroscopy using sample sets having limited wood density variation. *IAWA J.* **26**(2): 175–187. doi:10.1163/22941932-90000109.
- Schwanninger, M., Rodrigues, J., and Fackler, K. 2011. A review of band assignments in near infrared spectra of wood and wood components. *J. Near Infrared Spectrosc.* **19**(5): 287–308. doi:10.1255/jnirs.955.
- Shenk, J.S., Workman, J.J., Jr., and Westerhaus, M.O. 2008. Application of NIR spectroscopy to agricultural products. *In Handbook of near-infrared analysis.* Edited by D. Burns and E. Ciurczak. CRC Press, Boca Raton, Florida. pp. 347–386.
- Sirviö, J., and Kärenlampi, P. 1998. Pits as natural irregularities in softwood fibers. *Wood Fiber Sci.* **30**(1): 27–39.
- Smith, B. 1999. Infrared spectral interpretation: a systematic approach. CRC Press, Boca Raton, Florida.
- So, C.-L., Via, B.K., Groom, L.H., Schimleck, L.R., Shupe, T.F., Kelley, S.S., and Rials, T.G. 2004. Near infrared spectroscopy in the forest products industry. *For. Prod. J.* **54**: 6–16.
- Solberg, S. 2004. Summer drought: a driver for crown condition and mortality of Norway spruce in Norway. *For. Pathol.* **34**(2): 93–104. doi:10.1111/j.1439-0329.2004.00351.x.
- Stirling, R., Trung, T., Breuil, C., and Bicho, P. 2007. Predicting wood decay and density using NIR spectroscopy. *Wood Fiber Sci.* **39**: 414–423.
- Thygesen, L.G. 1994. Determination of dry matter content and basic density of Norway spruce by near infrared reflectance and transmittance spectroscopy. *J. Near Infrared Spectrosc.* **2**: 127–135. doi:10.1255/jnirs.39.
- Tsuchikawa, S. 2007. A review of recent near infrared research for wood and paper. *Appl. Spectrosc. Rev.* **42**(1): 43–71. doi:10.1080/05704920601036707.
- Tsuchikawa, S., and Schwanninger, M. 2013. A review of recent near-infrared research for wood and paper (part 2). *Appl. Spectrosc. Rev.* **48**(7): 560–587. doi:10.1080/05704928.2011.621079.
- Tyree, M.T., and Zimmermann, M.H. 2002. Xylem structure and the ascent of sap. Springer, Berlin.
- Viscarra Rossel, R.A., Walvoort, D.J.J., McBratney, A.B., Janik, L.J., and Skjemstad, J.O. 2006. Visible, near infrared, mid infrared or combined diffuse reflectance spectroscopy for simultaneous assessment of various soil properties. *Geoderma*, **131**: 59–75. doi:10.1016/j.geoderma.2005.03.007.
- Workman, J.J., Jr. 1999. Review of process and noninvasive near-infrared and infrared spectroscopy: 1993–1999. *Appl. Spectrosc. Rev.* **34**(1–2): 1–89. doi:10.1081/ASR-100100839.
- Workman, J.J., Jr. 2008. NIR spectroscopy calibration basics. *In Handbook of near-infrared analysis.* Edited by D.A. Burns and E.W. Ciurczak. CRC Press, Boca Raton, Florida. pp. 123–150.
- Xu, Q., Qjin, M., Ni, Y., Defo, M., Dalpke, B., and Sherson, G. 2011. Predictions of wood density and module of elasticity of balsam fir (*Abies balsamea*) and black spruce (*Picea mariana*) from near infrared spectral analyses. *Can. J. For. Res.* **41**(2): 352–358. doi:10.1139/X10-215.

3. Within-ring variability of wood structure and its relationship to drought sensitivity in Norway spruce trunks

Saskia Luss, Sven-Olof Lundqvist, Robert Evans, Thomas Grahn, Lars Olsson, Gai Petit and Sabine Rosner

Published in IAWA Journal



BRILL

Within-ring variability of wood structure and its relationship to drought sensitivity in Norway spruce trunks

Saskia Luss^{1,*}, Sven-Olof Lundqvist², Robert Evans³, Thomas Grahn²,
Lars Olsson², Giau Petit⁴, and Sabine Rosner¹

¹Institute of Botany, University of Natural Resources and Life Sciences, BOKU Vienna,
Gregor Mendel Straße 33, A-1180 Vienna, Austria

²IIC Industrins Internationaliserings Cent. AB, Rosenlundsgatan 48B, SE-118 63, Stockholm,
Sweden

³SilviScan Pty Ltd, 8 Dobell Place, Doncaster East, Victoria 3109, Australia

⁴Dipartimento Territorio e Sistemi Agro-Forestali, Università degli Studi di Padova,
Viale dell'Università 16, 35020 Legnaro PD, Italy

*Corresponding author: e-mail: saskia.luss@boku.ac.at

Accepted for publication: 30 July 2018 – Available online: September 2018

ABSTRACT

Relationships between hydraulic vulnerability expressed as P_{50} (the air pressure causing 50% loss of hydraulic conductivity) and within-ring differences in wood density (WD) and anatomical features were investigated with the aim to find efficient proxies for P_{50} relating to functional aspects. WD and tracheid dimensions were measured with SilviScan on Norway spruce (*Picea abies* (L.) Karst.) trunk wood.

P_{50} was strongly related to mean WD ($r = -0.64$) and conduit wall reinforcement ($(t/b)^2$), the square of the ratio between the tracheid double wall thickness (t) and the lumen width (b), where use of tangential lumen width ($(t/b_t)^2$) gave better results ($r = -0.54$) than radial lumen width ($r = -0.31$). The correlations of P_{50} with earlywood (EW), transition wood (TW) and latewood (LW) traits were lower than with the specimen averages, both for WD ($r = -0.60$ for WD_{EW} , $r = -0.56$ for WD_{TW} , $r = -0.23$ for WD_{LW}) and all anatomical traits. The loss of hydraulic conductivity was addressed as a dynamic process and was simulated by defining consecutive phases of 5% theoretical conductivity loss. WD and tracheid traits were calculated and correlated with P_{50} values of each specimen. Tightest correlations were found for $(t/b_t)^2$, at relative cumulated theoretical conductivities until 45 to 50% ($r = -0.75$).

We conclude that WD is one of the best available proxies for P_{50} , but does not necessarily reflect the mechanism behind resistance to cavitation. The new trait, based on estimation of conductivity loss as a dynamic process, provided even stronger correlations.

Keywords: Vulnerability to cavitation, percent loss of conductivity, wood density, wood anatomy, wall thickness, tracheid dimensions, conduit wall reinforcement.

INTRODUCTION

List of abbreviations:

b	tracheid lumen width, arithmetic mean of b_t and b_r
b_r	radial lumen width
B_R	radial tracheid width from one middle lamella to the next
b_t	tangential lumen width
B_T	tangential tracheid width from one middle lamella to the next
EW	earlywood
LW	latewood
P_{50}	hydraulic vulnerability
t	tracheid double wall thickness
$(t/b)^2$	conduit wall reinforcement
$(t/b_r)^2$	radial conduit wall reinforcement
$(t/b_t)^2$	tangential conduit wall reinforcement
$(t/b_h)^2$	conduit wall reinforcement of $\pm 10\%$ of mean hydraulic lumen diameter
$(t/b_{hr})^2$	radial conduit wall reinforcement of $\pm 10\%$ of radial hydraulic lumen diameter
$(t/b_{ht})^2$	tangential conduit wall reinforcement of $\pm 10\%$ of tangential hydraulic lumen diameter
TW	transition wood
WD	wood density
WD_{EW}	earlywood wood density
WD_{TW}	transition wood wood density
WD_{LW}	latewood wood density

During the past years forest dieback due to drought and heat waves has been frequently observed (Allen *et al.* 2010; Sargent *et al.* 2014; Rosner *et al.* 2014). For the future it is predicted that climate change will bring more extreme and frequent drought and heat waves (Schär *et al.* 2004; IPCC 2012; IPCC 2014). For coniferous species such as Norway spruce drought is one of the main climate risks (Solberg 2004; Bréda & Badeau 2008; Sargent *et al.* 2014). Still, the knowledge about the physiological mechanisms behind dieback due to drought sensitivity are not yet well understood (McDowell *et al.* 2008). More knowledge on relationships between anatomical structure and hydraulic functioning within tree trunks may allow the development of screening methods to determine the vulnerability to drought, for selection of more suitable provenances or individuals (Rosner 2013). The most widely used hydraulic vulnerability parameter is P_{50} , defined as the water potential that causes 50% loss in hydraulic conductivity (Choat *et al.* 2012). There are also other techniques to measure xylem hydraulics, but all available methods, P_{50} included, are delicate, labour intensive and can be performed only on samples of fresh wood. Therefore, there is a need for more rapid methods to measure vulnerability to cavitation (Cochard *et al.* 2013; Luss *et al.* 2014), and preferably methods which can be applied on larger samples more representative for the tree. An alternative approach is to find proxies for adaptive traits related to drought resistance (Ruiz Diaz Britez *et al.* 2014).

Vulnerability to cavitation is linked to xylem structure (Hacke *et al.* 2001; Domec & Gartner 2002b; Dalla-Salda *et al.* 2009). Pittermann *et al.* (2010) concluded that, among structural parameters in conifers, the ratio of the torus to aperture diameter shows the strongest direct relationship with P_{50} across species. For conifers, relationships have been found also with wood attributes such as tracheid double wall thickness, tracheid length (Rosner *et al.* 2007) and wood density (Domec & Gartner 2002a; Rosner *et al.* 2008; Dalla-Salda *et al.* 2009). In that regard, wood density is one of the most promising candidates (Rosner *et al.* 2008) in the search for proxies of hydraulic vulnerability in mature Norway spruce wood. Density as a proxy has also the advantage that it correlates strongly with a variety of hydraulic and biomechanical performance measures, a lot of density data are available and it is relatively simple to assess. Density of wood results from anatomical and to some extent also from chemical properties, which define how much mass there is in a given volume (Rathgeber *et al.* 2006; Lachenbruch & McCulloh 2014; Cuny *et al.* 2014). Intensive research on the relationship between vulnerability to cavitation and density within tree trunks has been carried out for Norway spruce (Rosner *et al.* 2007, 2008, 2014) and Douglas-fir (Domec & Gartner 2002a; Dalla-Salda *et al.* 2009, 2014). Dalla-Salda *et al.* (2014) showed that also within-ring wood density variations are related to vulnerability to cavitation in Douglas-fir. There are several patterns of variation of wood properties within trees (Zobel & van Buijtenen 1989), on different levels of scale. One pattern is the variation within an annual ring that in conifers is characterised by a transition from wide and thin-walled cells formed at the beginning of the growing season to narrow and thick-walled cells formed at the end. Traditionally, tree rings are described as of two parts: earlywood (EW) and latewood (LW) (Mork 1928). But often the transition from EW to LW extends over a considerable part of the ring. For more descriptive information on within-ring variations, a third compartment, termed transition wood (TW), has been introduced between EW and LW (Olsson *et al.* 1998; Park & Spiecker 2005; Dalla-Salda *et al.* 2014; Hong *et al.* 2015). Dalla-Salda *et al.* (2014) found that TW has a major impact on the between-tree variation of vulnerability to cavitation. In Norway spruce, P_{50} is strongly related to mean ring wood density (Rosner *et al.* 2014). Wood density influences also the mechanical properties of the tracheids, including their resistance to collapse. Thus, the question arises: can a detailed analysis of the variability of anatomical traits within annual rings bring further understanding of hydraulic vulnerability?

Several methods to determine wood density and anatomical traits exist and they undergo a continuous development and refinement (Lehmann & Evans 2010). SilviScan is a quasi-non-destructive method, since it can be applied on material from wood cores. It has been developed for rapid analysis of radial variations in many wood and fibre properties on the annual ring and within-ring level, using automated and integrated X-ray and microscopy measurements, combined with image and data analyses. Among the properties measured are wood density (wood moisture in equilibrium with the conditioned laboratory atmosphere), tracheid widths radially and tangentially in the wood matrix, and tracheid wall thickness (Evans 1994). These traits show differences across the annual ring and with tree height (reviewed in Lachenbruch *et al.* 2011; Carrer *et al.* 2015), which can be described on an aggregated level as EW, TW and LW.

Across species, Hacke *et al.* (2001) found a tight relationship between cavitation resistance and $(t/b)^2$, the conduit wall reinforcement, where t is the tracheid double cell wall thickness and b the tracheid lumen width. Also in *Picea abies*, mean $(t/b)^2$ proved as a good proxy for P_{50} (Rosner *et al.* 2016b). However, cavitation normally occurs or is at least initiated locally in wood, at vulnerable locations within rings. Therefore, it is important to investigate how P_{50} of the whole annual ring relates also to the anatomical variability within annual rings. A recent study by Nardini *et al.* (2017) showed by means of *in vivo* imaging with micro computed tomography that there is a progressive embolisation from wider to narrower conduits with increasing xylem tension.

The aim of this study was to investigate how P_{50} of Norway spruce (*Picea abies* (L.) Karst.) sapwood specimens is related to the within-ring variability in wood density and anatomical traits, in order to learn more about the influence of wood design on vulnerability to cavitation. We hypothesised that anatomical features corresponding to 50% of the cumulated theoretical hydraulic conductivity of a given wood sample are stronger related to P_{50} than a mean value calculated for the whole sample span. In order to test this hypothesis, we analysed SilviScan datasets from 50 Norway spruce specimens originating from different sites in southern Sweden and Norway and correlated potential functional traits such as wood density and $(t/b)^2$ with P_{50} .

MATERIALS AND METHODS

Plant material

The specimens ($n = 50$) came from Norway spruce (*Picea abies* (L.) Karst.) trees grown on two sites in southern Sweden (Tönnersjöheden and Vissefjärda) and two sites in southern Norway (Sande and Hoxmark). These were harvested at the age of 24 years on the Swedish sites and at 40–50 years on the Norwegian sites. The trees from Sweden were located at altitudes of 60 and 120 m, respectively, on sites with soil of sandy loam till. Their mean height was 10.1 ± 1.5 m and the mean diameter at breast height was 11.2 ± 2.5 cm. The sites in Norway had rather shallow soils of clay mixed with a mineral soil layer and sand fractions (Hentschel *et al.* 2014). The trees of these sites had mean height 21.4 ± 1.6 m and mean diameter at breast height of 29.1 ± 4.8 cm. Wood boles from trees of the Swedish site were taken at breast height, from trees of the Norwegian site from the living crown (10th whorl from top). More details of the Swedish sampling sites and trees can be found in Rosner *et al.* (2008) and of the Norwegian sites in Rosner *et al.* (2014).

Wood boles were debarked and split along the grain out in the field. The samples had a length of 200 mm when they were put in plastic bags with fresh water and 0.01% Micropur Classic (Katadyn Products Inc., Wallisellen, Switzerland). Within 48 hours, the samples were sent to BOKU Vienna (Austria) where they were stored at -18°C until further preparation steps.

Vulnerability to cavitation

A core in studies of sensitivity to drought is the vulnerability curve (VC), the decrease in hydraulic conductivity plotted against the stress applied, causing these con-

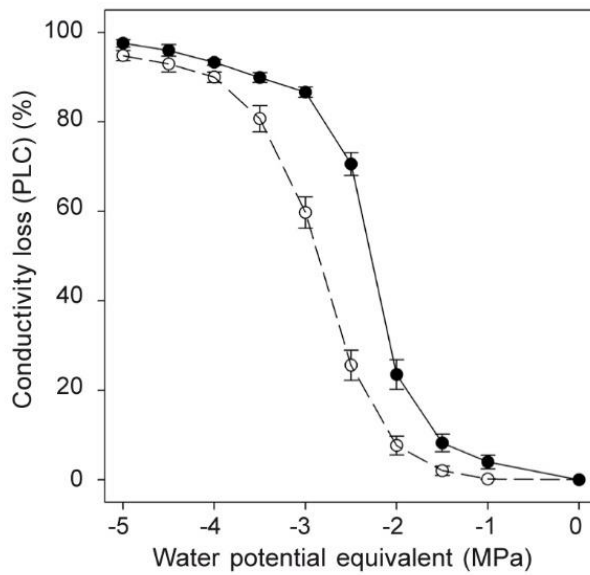


Figure 1. Hydraulic vulnerability curves for two sample clusters; cluster one (open symbols) comprises specimens with $P_{50} < -2.5$ MPa (-2.88 ± 0.19 MPa, $n = 19$), cluster two (closed symbols), specimens with $P_{50} \geq -2.5$ MPa (-2.29 ± 0.18 MPa, $n = 31$). Whiskers denote the standard errors.

ductivity losses (Fig. 1). In our case, the stress was induced by the application of compressed air in a pressure collar; the positive pressure applied is an equivalent for the water potential (Cochard *et al.* 2013). The water potential has a negative algebraic sign and describes the tension that develops during water transport in small conduits.

The method used in this study for the assessment of VCs is described in detail in Rosner *et al.* (2008). The most important parameter derived from VC is the P_{50} (Choat *et al.* 2012), defined as the pressure (*i.e.* water potential) that induces 50% loss of the initial hydraulic conductivity. For the calculation of P_{50} , the flow through small wood beams ($6 \times 6 \times 120$ mm, produced from the 200-mm-long samples) was determined on stepwise air pressure application in a double ended pressure chamber (PMS Instrument, Corvallis, OR). In Rosner *et al.* (2008), such calculated P_{50} values were presented for each tree from pooled data of at least three sapwood beam specimens. In the current study, we recalculated P_{50} for the single wood beams and SilviScan analyses were performed on all samples for which enough data points were available to construct whole VCs (Luss *et al.* 2014). This resulted in data on P_{50} and anatomical features from 50 wood beam samples originating from the sapwood of 38 trees. The 50 samples were then divided into two groups, one with $P_{50} < -2.5$ MPa ($n = 19$) and one group with $P_{50} > -2.5$ MPa ($n = 31$), representing low and high hydraulic vulnerability. Average curves for each cluster are presented in Figure 1.

SilviScan measurements

For the SilviScan measurements, specimens with a length of 1 cm were sawn from the wood beams used for hydraulic testing. 35 samples originating from 28 of the trees harvested in Sweden were analysed by Innventia (Sweden) with its SilviScan instrument. Fifteen specimens originating from 10 trees harvested at the sites in southern Norway were analysed with the SilviScan instrument at CSIRO (Australia). These analyses provided detailed data on the spatial variations in WD and anatomy. The data were compiled in the form of averages for consecutive 50 μm wide intervals across the 6 mm of the specimens. These data showed large differences in growth among the samples:

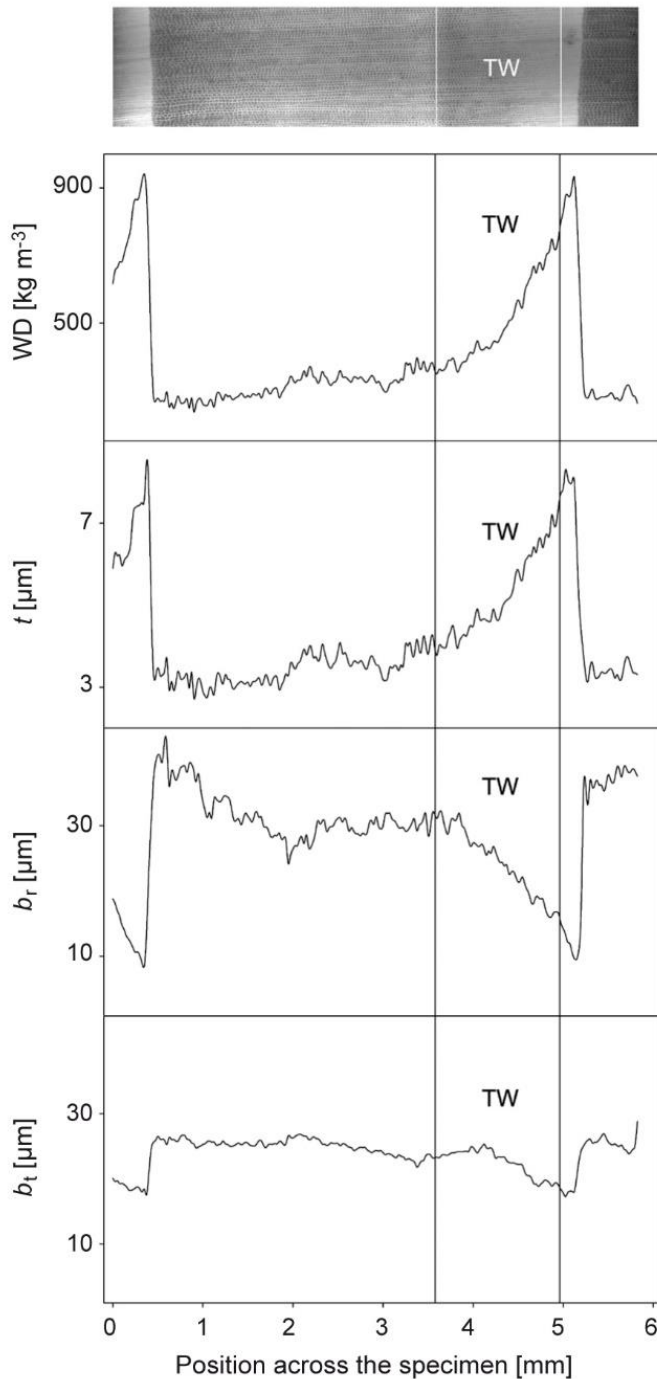


Figure 2. Examples of SilviScan datasets for radial variations in one of the 6 mm broad specimens of Norway spruce, showing wood density (WD), tracheid double wall thickness (t), radial lumen width (b_r) and tangential lumen width (b_t). On the top of the four graphs, the X-ray microdensity profile of the same sample is shown. Note that denser compartments such as the latewood are lighter than the less dense parts (*i.e.* earlywood) in an X-ray micrograph. TW shows the transition wood part. Adjacent to TW is on the left side earlywood (EW) and on the right side latewood (LW). This specimen belongs to the cluster with the higher vulnerability with fast-grown wood (Fig. 1).

from fast-grown wood with one complete annual ring with small parts of other rings at the edges, to slow-grown wood with three complete rings. Figure 2 shows an example for wood density (WD), tracheid double wall thickness (t), radial (b_r) and tangential lumen (b_t) widths for a specimen with one complete annual ring.

Discrimination of earlywood, transition wood, and latewood

The individual rings and their intra-ring compartments of EW, TW and LW were identified based on the density variations across the analysed wood specimens. As

mentioned above, the intra-ring variations have traditionally been described with two parts only, EW and LW, most often using the definition of Mork (1928), setting a transition point where the tracheid double wall thickness equals the lumen diameter. Several other definitions of a transition point between two compartments of rings have been suggested and their benefits discussed (Denne 1988; Koubaa *et al.* 2002; Park & Spiecker 2005; Cuny *et al.* 2014). The intra-ring variations are, however, normally characterised by relatively stable property levels at the innermost and outermost parts of the rings with a transition zone in between, constituting a considerable part of the ring. This transition may be very different in character and is often strongly influenced by annual weather and other factors. The definition of a transition wood compartment used in this study, the “20-80” method (Kostiainen *et al.* 2009; Franceschini *et al.* 2012; Chen *et al.* 2014; 2016; Hong *et al.* 2015), was introduced by Olsson *et al.* 1998) to obtain less weather-dependent data on these inner and outer parts of each ring, and a better description of the statistical distributions of wood and tracheid (“fibre”) properties for industrial applications. The method was first applied on brightness data from wood images, and was then introduced on density data from SilviScan. For each ring, the span from minimum to maximum density (or brightness) is determined. The part from 0 to 20 % of the span is defined as EW, the part from 80 to 100 % as LW, and the part in between as TW.

Potential hydraulic proxies for P_{50}

Hydraulic proxies tested in this study were: wood density (WD), tracheid double wall thickness (t), mean lumen width (b), radial lumen width (b_r), and tangential lumen width (b_t), as well as conduit wall reinforcement $(t/b)^2$ (Hacke *et al.* 2001; Hacke & Jansen 2009). Conduit wall reinforcement traits were calculated using mean lumen widths (average of radial and tangential width) $(t/b)^2$, radial lumen widths $(t/b_r)^2$ and tangential lumen widths $(t/b_t)^2$. Arithmetic mean values were calculated of WD, t , b , b_r , b_t , $(t/b)^2$, $(t/b_r)^2$, $(t/b_t)^2$ for the whole radial spans of the specimens and for EW, TW and LW of complete annual rings.

As the hydraulic conductivity of lumens with different widths are not proportional to these widths but rather to their fourth power, the arithmetic averages for the conduit wall reinforcements were complemented with average hydraulic lumen diameters. These were calculated as $\Sigma d^5 / \Sigma d^4$ (Kolb & Sperry 1999; Rosner *et al.* 2016b), where d represents the averages of the different types of lumen widths for the 50 μm intervals provided by the SilviScan dataset, resulting in hydraulically weighted averages for mean (b_h), radial (b_{hr}) and tangential (b_{ht}) lumen widths. Hydraulic lumen widths were then used to calculate the corresponding hydraulically adjusted conduit wall reinforcements (Hacke *et al.* 2001; Hacke & Jansen 2009); $(t/b_h)^2$ was calculated for $\pm 10\%$ (*i.e.* 90–110 %) of b_h ($(t/b_h)^2$), for $\pm 10\%$ of b_{hr} ($(t/b_{hr})^2$) and for $\pm 10\%$ of b_{ht} ($(t/b_{ht})^2$) according to Domec *et al.* (2009) and Rosner *et al.* (2016b).

According to Hagen-Poiseuille’s law, the volumetric flow in a pipe increases with the fourth power of its radius. In order to analyse the variability of the within-ring variation in lumen diameter for each P_{50} cluster (see chapter *Vulnerability to cavitation*), data for the 50 μm intervals were sorted into 1 μm broad categories of mean lumen diameters (b),

from 11 to 33 μm . The data for mean lumen diameter widths were cumulated to 1 μm categories, starting with the intervals of the largest lumen diameters (typically part of EW) to the smallest lumens (typically from LW), followed by normalisation to 100 % for the total sum. Then, the series representing the two clusters were plotted *versus* lumen diameters.

Further, the hydraulic conductivity (K) was calculated as an average for every 50 μm radial section across the samples from the corresponding SilviScan data on widths of tracheids and lumens. It is assumed, that the hydraulic conductivity is fully controlled by the lumen size. The Hagen-Poiseuille law has been used to calculate a theoretical hydraulic conductivity of water conducting elements in the (secondary) xylem (Tyree & Zimmermann 2002). The following equation was used to calculate K :

$$K [m^2 MPa^{-1} s^{-1}] = \frac{b_r^3 b_t^3}{8\eta B_R B_T (b_r + b_t)^2} \quad \text{Equation 1}$$

where B_R is the radial tracheid width, b_r the radial lumen width, B_T the tangential tracheid width and b_t the tangential lumen width.

The vulnerability curves for the clusters of specimens with high and low vulnerability presented in Figure 1 illustrate the dynamic character of loss in conductivity. In order to investigate how wood with different anatomical characteristics is involved in loss of conductivity during various phases, the 50 μm wide intervals of each specimen were sorted according to WD, from the interval with lowest WD (presumably with high vulnerability and K) to the highest WD (with low vulnerability and K). The K values of the intervals were successively added, ending with the total theoretical hydraulic conductivity of the specimen. The curve was normalised with this value, resulting in a curve from 0 % to 100 %, expressing the proportions in which wood of different WDs (or hydraulic vulnerabilities) contributed to the total hydraulic conductivity of the specimen. The cumulated hydraulic conductivity was then divided into 20 phases, representing each a theoretical stepwise increase in 5 % conductivity. WD and anatomical traits were calculated for each stepwise cumulated K phase.

Statistical analyses

Statistical analyses were carried out for all traits with IBM SPSS Statistics 21. Pearson correlation coefficient was used to test relationships between traits. Mean values were tested for significant differences by the Student's t test. P_{50} values and calculated traits that were related to P_{50} followed a normal distribution. Correlations or differences were accepted as significant if $P < 0.05$.

RESULTS

P₅₀ related to wood density and anatomical traits across the whole specimen

Strongest relationships with P_{50} and averages for other traits across the full specimen were found for mean WD ($r = -0.64$) and $(t/b_{ht})^2$, *i.e.* conduit wall reinforcement calculated from $\pm 10\%$ of the tangential hydraulic lumen diameter ($r = -0.64$). All other anatomical traits had correlation coefficients below 0.6 (Table 1). The weakest correlation was obtained for $(t/b_r)^2$ ($r = -0.31$, $P < 0.05$), while $(t/b_t)^2$ showed a much better result ($r = -0.54$, $P < 0.001$).

Table 1.

Pearson correlation coefficients for the whole span of the specimen and the compartments of earlywood (EW), transition wood (TW), and latewood (LW) for the correlation of P_{50} with means of wood density (WD), double wall thickness (t), lumen widths as average between radial and tangential widths (b), radial lumen width (b_r), tangential lumen width (b_t), conduit wall reinforcement calculated from lumen diameters ($(t/b)^2$), from radial lumen width ($(t/b_r)^2$) and from tangential lumen width ($(t/b_t)^2$). For averages across the whole specimens, correlations are given also with conduit wall reinforcement calculated from $\pm 10\%$ of the mean hydraulic lumen diameter ($(t/b_h)^2$), from $\pm 10\%$ of the radial hydraulic lumen diameter ($(t/b_{hr})^2$) and from $\pm 10\%$ of the tangential hydraulic lumen diameter ($(t/b_{ht})^2$). The significance level of the correlation coefficients are indicated by asterisks: ***, $P < 0.001$; **, $P < 0.01$; *, $P < 0.05$.

	WD	t	b	b_r	b_t	$(t/b)^2$	$(t/b_r)^2$	$(t/b_t)^2$	$(t/b_h)^2$	$(t/b_{hr})^2$	$(t/b_{ht})^2$
Whole span	-0.64***	-0.57***	0.55***	0.44**	0.59***	-0.48***	-0.31*	-0.54***	-0.53***	-0.45**	-0.64***
EW	-0.60***	-0.36**	0.42**	0.24	0.43**	-0.59***	-0.51***	-0.55***			
TW	-0.56***	-0.39**	0.56***	0.48***	0.55***	-0.45**	-0.37**	-0.49***			
LW	-0.23	-0.14	0.28	0.20	0.28	-0.13	-0.05	-0.14			

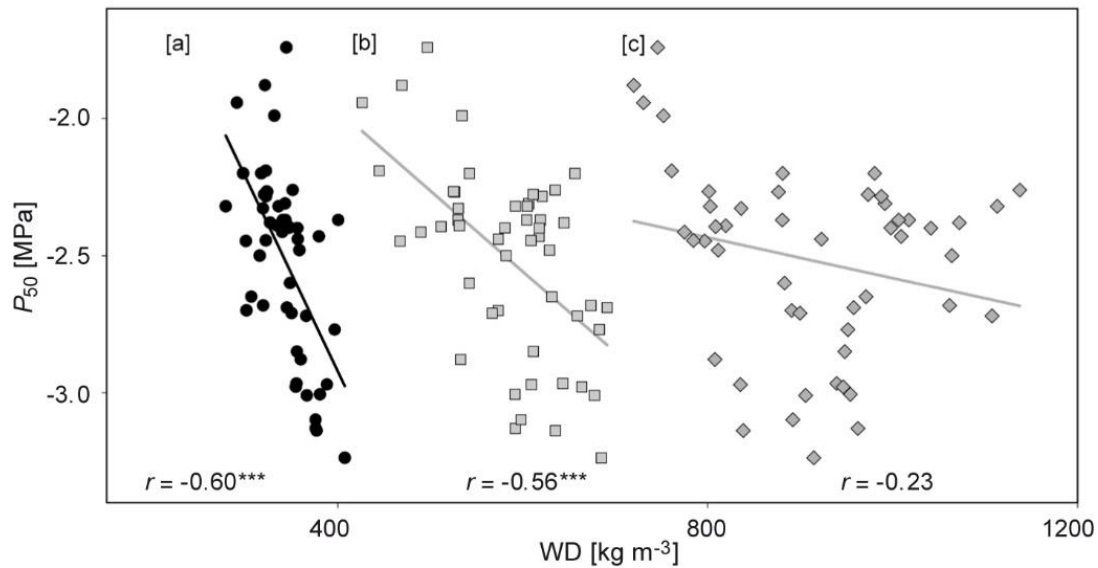


Figure 3. Hydraulic vulnerability (P_{50}) plotted against mean values of WD for the (a) earlywood (EW), (b) transition wood (TW) and (c) latewood (LW) parts of the specimens, resulting in three data points for the P_{50} value of each specimen. Filled black circles denote EW, gray squares denote TW and dark gray diamonds denote LW. Linear relationships are indicated by regression lines for each part separately; “***” indicates $P < 0.001$.

Structure-function relationships for earlywood, transition wood, and latewood

The strongest correlations were found with WD_{EW} ($r = -0.60$) and with WD_{TW} ($r = -0.56$), while no significant relationship was found with WD_{LW} (Table 1, Fig. 3). Nor were significant relationships found between P_{50} and any other anatomical trait of LW (Table 1). All lumen traits of TW (b , b_r and b_t) showed stronger correlations with P_{50} than those of EW. In contrast, all $(t/b)^2$ traits of EW showed tighter relationships with P_{50} than those of TW (Table 1). Figure 3 also shows that the range of WD values in EW among the specimens investigated is much narrower, compared to those in TW and LW.

Within-ring variability of wood density and anatomy traits of the clusters with high and low P_{50}

In Figure 1, the concept of vulnerability curves (VC) was illustrated for two clusters of samples: samples with P_{50} values < -2.5 MPa (min = -3.24 MPa, max = -2.60 MPa, mean = -2.88 ± 0.19 MPa, $n = 19$), and samples ≥ -2.5 MPa (min = -2.50 MPa, max = -1.74 MPa, mean = -2.29 ± 0.18 MPa, $n = 31$). Figure 4 visualises the differences in intra-ring variations of wood density and anatomical traits between the specimens of high and low hydraulic vulnerability, with plots of averages for successive 5% intervals within the complete annual rings for WD, tracheid double wall thickness (t), radial lumen width (b_r), tangential lumen width (b_t), $(t/b_r)^2$ and $(t/b_t)^2$. Differences in the mean values of WD, t , $(t/b_r)^2$ and $(t/b_t)^2$ between P_{50} clusters were statistically significant for all 5% segments, except in the LW of the annual rings (Fig. 4). Above 95%, *i.e.* in the latest formed LW part, no traits investigated showed significant differences, except $(t/b)^2$ traits. Significant differences in b_t were found after 25% of the annual ring, and

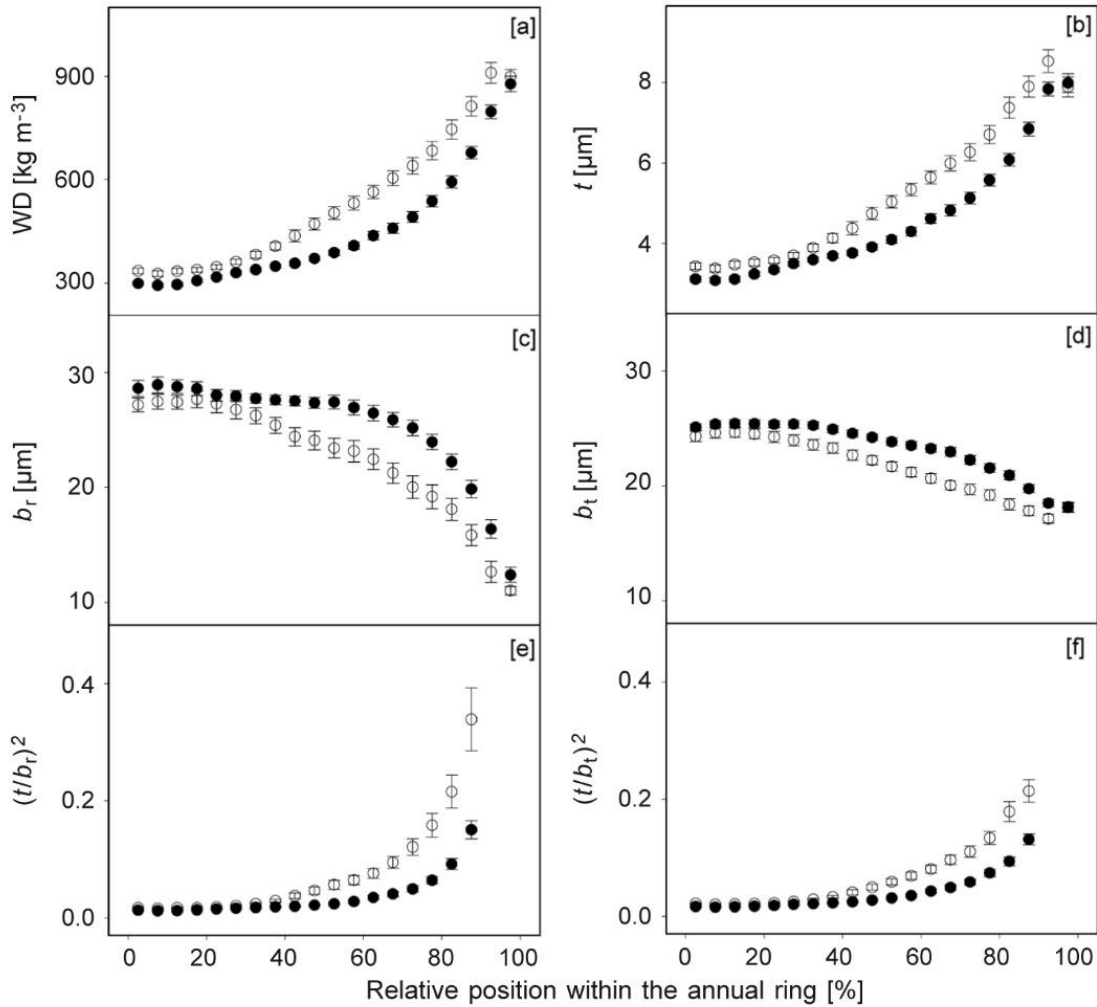


Figure 4. Mean values and standard errors of wood density (WD) (a), double tracheid wall thickness (t) (b), radial lumen width (b_r) (c), tangential lumen width (b_t) (d), radial conduit wall reinforcement $(t/b_r)^2$ (e) and tangential conduit wall reinforcement $(t/b_t)^2$ (f) of 5% radial segments of annual ring for P_{50} below -2.5 MPa (open symbols, *i.e.* less vulnerable to cavitation) and above P_{50} -2.5 MPa (closed symbols, *i.e.* more vulnerable to cavitation).

in b_r after 35% of the annual ring. Even though there were statistically significant differences between the two P_{50} categories in WD and $(t/b)^2$ traits, differences in the mean values were not much until 35% of the annual ring compared to the absolute differences from 40% until 80% of the annual ring (Fig. 4). In order to compare both clusters, it was necessary to relate the traits to a relative radial position within the tree ring. The cluster with low P_{50} values and low vulnerability included specimens with narrower rings and thus lower contents of EW, while the specimens with a high EW content were found in the more vulnerable cluster. Thus, the less vulnerable wood had generally higher WD. The differences were, however, small at the innermost part of the rings where EW dominated and in the very outermost part where LW dominated in both P_{50} categories, respectively. But the differences were pronounced from the mid- to the 2/3-part where TW dominated in the less vulnerable category and EW in the other.

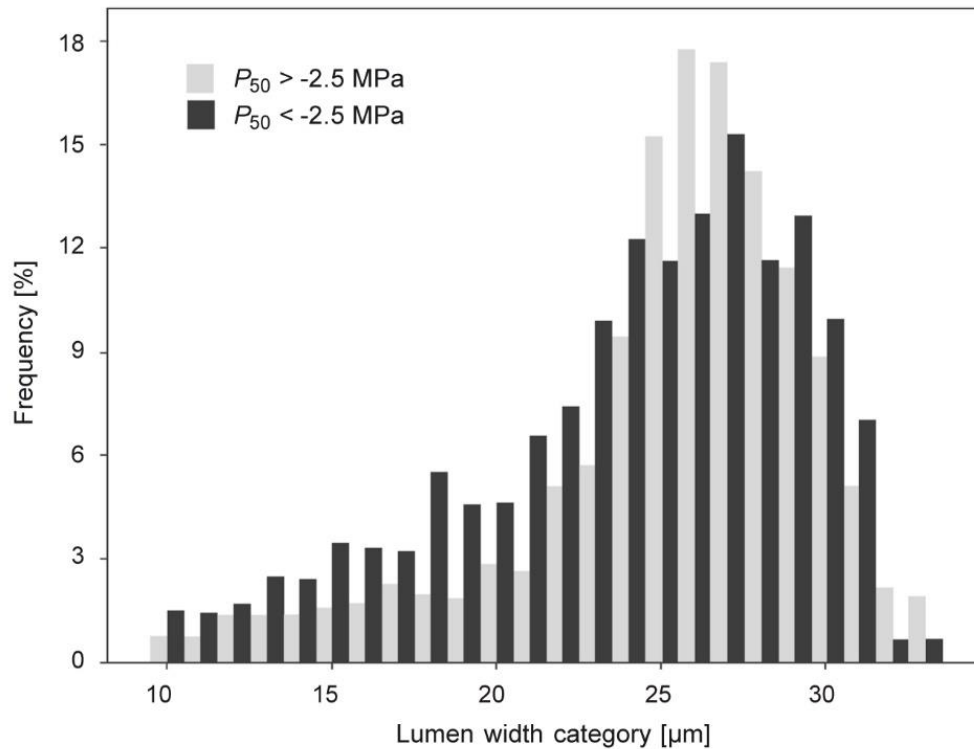


Figure 5. Histograms of the mean tracheid lumen width for P_{50} below -2.5 MPa (black bars, $n = 19$ specimens) and above -2.5 MPa (grey bars, $n = 31$ specimens).

Significant differences between lumen clusters were found in the range between 16 – 25 μm , where the relative cumulated lumen widths were significantly higher in more hydraulically vulnerable samples (Fig. 6a). Histograms of the frequency distributions of lumen diameter for the two clusters showed that more vulnerable wood specimens had a much higher fraction of larger lumen widths than the less vulnerable specimens (Fig. 5). In Figure 6b and 6c the average WD and $(t/b_t)^2$ are plotted *versus* the lumen categories. No significant differences between the two vulnerability groups were found when compared at the same lumen size categories.

A novel approach to predict P_{50}

In search for more structural-functional related proxies for P_{50} , we calculated the theoretical hydraulic conductivity (K) and added it cumulatively in 5% steps, starting with the lowest WD. Based on our findings described above, it was hypothesised that parts of the specimens with wood of different anatomical features will lose their conductive capacity in the same order as this accumulation, starting with wood of lowest WD and large lumen sizes, successively followed by wood of higher density, meaning that the 5% parts would correspond to different phases of the successive loss of conductivity of the specimen. The averages for WD and anatomical traits contributing to each 5% step were then calculated and correlated to the P_{50} values. This way, we were able to investigate not only different traits as proxies for P_{50} , but also to estimate critical levels of such functional traits of each specimen, providing even sharper proxies.

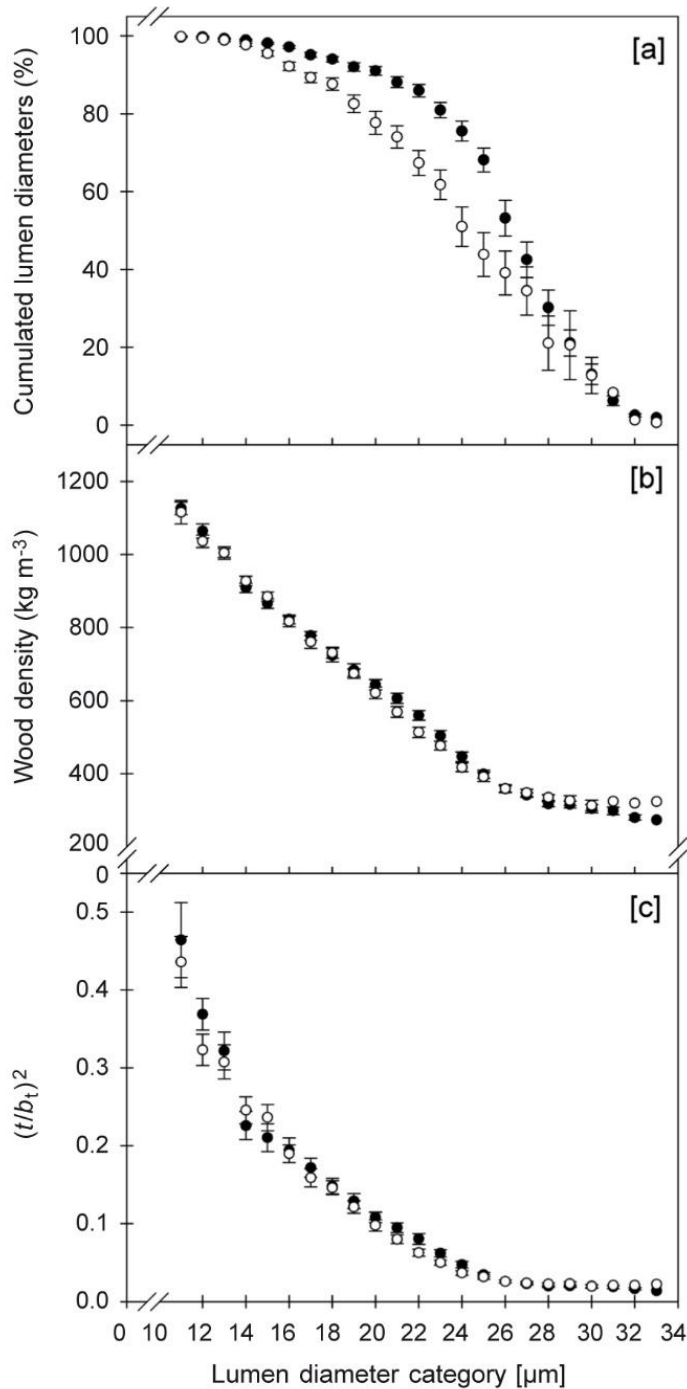


Figure 6. Mean values and standard errors of cumulated lumen diameter, wood density and tangential conduit wall reinforcement $(t/b_t)^2$, calculated from the largest to the smallest diameters and plotted against lumen diameter categories ($1 \mu\text{m}$ steps) for the clusters of specimen with $P_{50} < -2.5$ MPa (open symbols) and $P_{50} \geq -2.5$ MPa (closed symbols).

The correlation coefficients for the relationship between these potential functional traits and P_{50} are listed in Table 2. P_{50} was tightest correlated with the mean WD of the specimens calculated until 40 to 45% of the cumulated K ($r = -0.72$, $P < 0.0001$) and with the mean $(t/b_t)^2$ calculated until 45 to 50% ($r = -0.75$, $P < 0.0001$) (Fig. 7). Much weaker relationships were found between P_{50} and b , b_r , b_t as well as $(t/b_r)^2$; also the mean of the double wall thickness as well as $(t/b)^2$ were more weakly related to P_{50} .

Table 2.

Pearson correlation coefficients for wood density (WD), double wall thickness (t), lumen equivalent diameter (b), radial lumen width (b_r), tangential lumen width (b_t), conduit wall reinforcement (t/b)², radial conduit wall reinforcement (t/b_r)² and tangential conduit wall reinforcement (t/b_t)² at cumulated hydraulic conductivity (K) in consecutive 5% steps for the whole sample span. The significance level of the correlation coefficients of the linear equations are indicated by asterisks: ***, $P < 0.001$; **, $P < 0.01$; *, $P < 0.05$.

Cumulated K [%]	WD	t	b	b_r	b_t	$(t/b)^2$	$(t/b_r)^2$	$(t/b_t)^2$
≤ 05	-0.47**	-0.35*	0.14	0.01	0.35*	-0.54***	-0.40**	0.54***
≤ 10	-0.62***	-0.45**	0.20	0.06	0.37**	-0.65***	-0.50***	0.60***
≤ 15	-0.68***	-0.50***	0.23	0.07	0.44**	-0.68***	-0.51***	-0.67***
≤ 20	-0.71***	-0.52***	0.27	0.10	0.45**	-0.70***	-0.53***	-0.69***
≤ 25	-0.71***	-0.53***	0.29*	0.13	0.46**	-0.69***	-0.53***	-0.70***
≤ 30	-0.71***	-0.52***	0.32*	0.15	0.46**	-0.68***	-0.53***	-0.71***
≤ 35	-0.71***	-0.53***	0.34*	0.17	0.47**	-0.68***	-0.52***	-0.73***
≤ 40	-0.72***	-0.53***	0.36*	0.19	0.48***	-0.69***	-0.53***	-0.74***
≤ 45	-0.72***	-0.54***	0.37**	0.20	0.49***	-0.69***	-0.53***	-0.75***
≤ 50	-0.71***	-0.54***	0.38**	0.21	0.49***	-0.68***	-0.53***	-0.75***
≤ 55	-0.71***	-0.55***	0.38**	0.22	0.48***	-0.67***	-0.53***	-0.74***
≤ 60	-0.70***	-0.56***	0.39**	0.23	0.49***	-0.66***	-0.53***	-0.73***
≤ 65	-0.70***	-0.57***	0.40**	0.24	0.49***	-0.66***	-0.54***	-0.72***
≤ 70	-0.65***	-0.60***	0.43**	0.27	0.49***	-0.66***	-0.57***	-0.71***
≤ 75	-0.69***	-0.61***	0.45**	0.29*	0.51***	-0.65***	-0.57***	-0.70***
≤ 80	-0.70***	-0.63***	0.47**	0.31*	0.53***	-0.65***	-0.58***	-0.70***
≤ 85	-0.70***	-0.64***	0.50***	0.34*	0.55***	-0.65***	-0.59***	-0.69***
≤ 90	-0.70***	-0.64***	0.51***	0.37**	0.57***	-0.64***	-0.60***	-0.67***
≤ 95	-0.69***	-0.65***	0.53***	0.40**	0.58***	-0.64***	-0.59***	-0.67***
≤ 100	-0.64***	-0.57***	0.55***	0.45**	0.59***	-0.48***	-0.32*	-0.54***

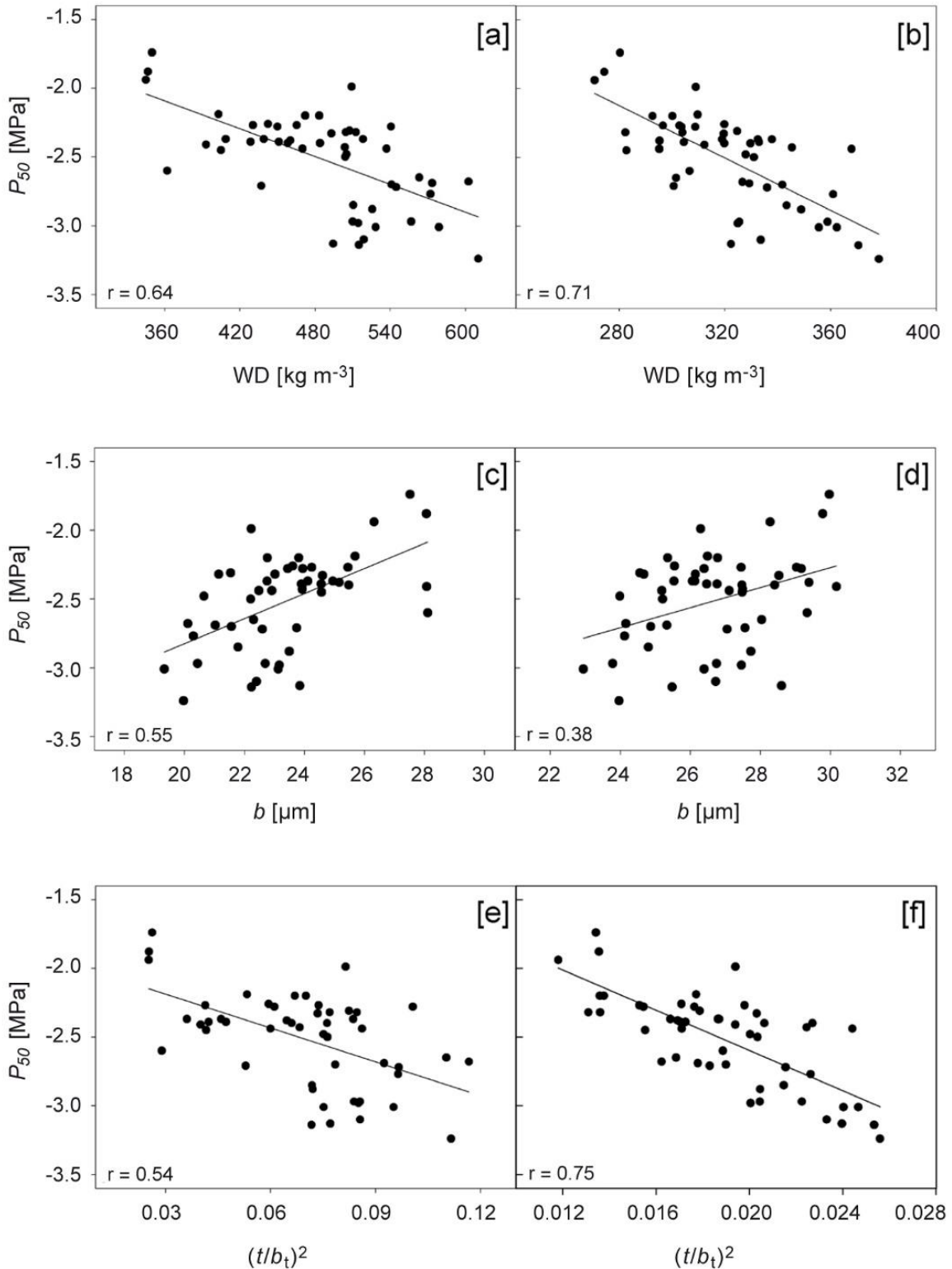


Figure 7. Hydraulic vulnerability (P_{50}) plotted against the mean wood density (WD) lumen widths and conduit wall reinforcement calculated from tangential lumen diameters $(t/b_t)^2$ for the whole wood sample [a, c, e] and for the cumulated theoretical hydraulic conductivity (K) range until 50% [b, d, f].

DISCUSSION

Predictive power of wood density and anatomical traits for hydraulic vulnerability

Classical methods to determine P_{50} values are destructive, time consuming, labour intensive and prone to errors (Cochard *et al.* 2013). There is thus a strong need for easily assessable proxies. Research on relationships between wood structure and its effect on multiple aspects of performance enable a better management and selection of plant material (Lachenbruch & McCulloh 2014). Rapid and easy prediction of P_{50} would be useful in tree improvement to screen for individuals or provenances with higher hydraulic safety (Dalla-Salda *et al.* 2009; Rosner *et al.* 2016a).

Wood density (WD) has a high potential as a proxy for hydraulic vulnerability (Dalla-Salda *et al.* 2011; Rosner *et al.* 2014). Also the present study showed a significant correlation between mean ring WD and P_{50} . WD can thus be used as a proxy for P_{50} , but there is no direct causal relationship. The statistical correlation exists because anatomical traits interact so that they adversely influence hydraulic vulnerability and WD (Hacke *et al.* 2001; Lachenbruch & McCulloh 2014; Bouche *et al.* 2014; Zwieniecki & Secchi 2015). WD is largely defined by the cross-sectional area and wall thickness of the tracheids, which also define the cross-sectional extension of the lumens, influencing P_{50} . Hacke *et al.* (2001) were first to find a strong relationship between P_{50} and mechanical proxies such as $(t/b)^2$. Their results were thereafter confirmed by many other studies (*e.g.* Domec *et al.* 2009; Bouche *et al.* 2014; Rosner *et al.* 2016a, b). Relationships within a species between P_{50} and $(t/b)^2$ were found to be stronger (Domec *et al.* 2009; Rosner *et al.* 2016a) than across conifer species (Bouche *et al.* 2014; Rosner *et al.* 2016a).

Recently, Rosner *et al.* (2016b) found that detangling tracheid lumen width in radial and tangential lumen diameters results in a higher predictive quality of $(t/b)^2$ for P_{50} . In the present study, we confirm that $(t/b_{ht})^2$, derived from tangential hydraulic lumen diameters, showed a stronger correlation with P_{50} than $(t/b_{hr})^2$, derived from radial hydraulic lumen diameters.

Radial lumen diameters are very variable within an annual ring and are strongly influenced by climate, annual weather and other site conditions than tangential lumen diameters (*e.g.* Vysotskaya & Vaganov 1989; Larson 1994). In many conifer species bordered pits are generally located in the radial-longitudinal walls (Domec *et al.* 2006) but they can be found in tangential cell walls, too (Kitin *et al.* 2009; Rosner 2013). In Norway spruce, EW tracheids are the most effective water-conducting pipes and there are higher numbers of pits per conduit length unit in EW than in LW (Rosner *et al.* 2007).

To sum up, WD is an easy-to-use proxy for P_{50} and there are also some other anatomically oriented proxies which are easier to assess than the classical labour-intensive methods. An ambition of the study was, however, to learn more about the intra-ring variation of WD and wood anatomy and their relationship to P_{50} . Therefore, we also investigated (a) influences of the individual compartments of EW, TW, and LW, (b) of the anatomical variability within rings, and (c) a new approach introducing dynamic aspects of conductivity loss through the analysis of 5% steps in the cumulated hydraulic conductivity (K).

Contribution of earlywood, transition wood, and latewood to variations in P_{50}

Where cavitation initiates and where it ceases within a tree ring and how it distributes to P_{50} is poorly understood (“*who is the lord of the ring*” (Dalla-Salda et al. 2014)). For Douglas-fir, Dalla-Salda et al. (2014) found that LW tracheids of the main trunk are more vulnerable to cavitation compared to EW tracheids. The hypothesis that EW transports water more efficiently and is less vulnerable to embolism than some parts of LW was supported by Domec et al. (2002b) and Rosner (2013). In many studies on structure-function relationships, annual rings are separated into two parts (EW and LW) (Koubaa et al. 2002; Domec & Gartner 2002b). In other studies, annual rings were however divided into three parts (Kostiainen et al. 2009; Rozenberg et al. 2004; Franceschini et al. 2013; Dalla-Salda et al. 2014), including also a transition part. This is preferable for wood in which the transition from earlywood to latewood constitutes a considerable part of the rings, such as in Norway spruce (Fig. 2). Our comparison of correlations of P_{50} with averages for full specimens and *versus* averages for the compartments showed generally higher correlations for the former type. The highest correlation among compartment types was found for WD_{EW} , generally the largest compartment, and almost as high for WD_{TW} , but no significant correlation between P_{50} and WD in the latewood, which constitute a minor part of the annual rings. Dalla-Salda et al. (2014) observed the dynamics of embolism propagation in EW, TW, and LW of Douglas-fir. They describe that the initiation and the distribution of the cavitation follows a discrete development in two steps. When a water-deficit episode has started, the cavitation occurs and distributes in the LW. LW tracheids lose free moisture earlier than EW tracheids. This was also shown for Norway spruce branch compression wood, which is more vulnerable than opposite wood (Mayr et al. 2003) and distinct latewood parts as visualised by means of neutron transmission profiles of dehydrating mature Norway spruce wood beams (Rosner 2013). Dalla-Salda et al. (2014) report that, after the water deficit further increases, embolism spreads in the EW and finally reaches the TW. In Douglas-fir, TW is thus the last conductive part within an annual ring before full cavitation occurs. We found slightly stronger relationships between EW density and P_{50} than between TW density and P_{50} and no correlation between LW density and P_{50} . This may at first sight seem contradictory, but shall not be a surprise, as P_{50} does not relate to the local initiation of cavitation, but how vulnerable the wood of the specimen is, when cavitation already has happened in LW and been distributed to various extents, influenced by the anatomy of the wood, where relatively more conductivity is lost when the tracheids with large lumens are affected. Accordingly, no anatomical traits of LW investigated showed any significant relationship with P_{50} .

A new approach for predicting P_{50} based on cumulated estimated hydraulic conductivity

Lumen and double wall dimensions play a major role in the resistance to cavitation (Pittermann et al. 2010; Delzon et al. 2010; Dalla-Salda et al. 2014; Bouche et al. 2014). According to Hacke et al. (2001), tracheids with lumen widths (b) close to the hydraulic lumen diameter (b_h) will cavitate at P_{50} , if air seeding progresses from wide to narrow tracheids. The parameter $(t/b_h)^2$, the second power of the ratio between the

double wall thickness (t) and lumen width (b) ratio of tracheids which deviate only slightly from the hydraulic lumen diameter, was introduced as an estimate for P_{50} by Hacke *et al.* (2001). Use of hydraulic lumen diameter as a basis for calculating conduit wall reinforcement proxies for P_{50} has the disadvantage that all lumen diameters in a radial file have to be assessed before a $(t/b)^2$ for tracheids with *e.g.* $\pm 10\%$ of the hydraulic lumen diameters (Domec *et al.* 2009) can be calculated. We overcame that by analysing the specimens with SilviScan, providing datasets which can be used to calculate hydraulic diameters. When using this approach, the best anatomical proxy in this study for P_{50} was $(t/b_{ht})^2$, calculated from tracheids with $\pm 10\%$ of the tangential hydraulic diameter (Rosner *et al.* 2016b).

The new approach presented in this study, relating P_{50} to WD and anatomical traits in the perspective of different phases in the loss of hydraulic conductivity (K), provided potential proxies with higher correlations to P_{50} than averages of the traits across specimens or their parts of EW, TW, or LW. P_{50} is not a static trait but is calculated from a dynamic dataset (Fig. 1), which implies the need of a screening approach that addresses the stepwise loss of conductivity within different regions of an annual ring. The novelty of this study compared to earlier approaches (*e.g.* Dalla-Salda *et al.* 2009; Rosner 2013; Rosner *et al.* 2016b) was to introduce a dynamic aspect to relate to the vulnerability curve used when determining proxies for P_{50} , rather than a static use of trait data. This was made possible by the analysis of wood- and tracheid traits with use of SilviScan, providing synchronised WD and anatomical data from the same locations across the specimens. The results obtained with the new approach are considered to be particularly sound, as the tightest correlations with P_{50} , the pressure at which 50% of the conductivity has been lost, were obtained with the tangential conduit wall reinforcement ($(t/b_t)^2$) until 45–50% of the estimated K ($r = -0.75$) and with WD until 40–45% of the estimated K ($r = -0.72$).

Thus, the correlations with P_{50} obtained when introducing the dynamic perspective were stronger than found using static averages ($r = -0.64$ for $(t/b_{ht})^2$, $r = -0.54$ for $(t/b_t)^2$ and $r = -0.64$ for WD). It should however be considered that the consistency of these relationships across species and locations within the trees (different positions in trunks, branches and roots) is yet to be investigated. For example, Willson *et al.* (2008) found a correlation between the hydraulically weighted conduit diameter (d_h) and K for stems, but not for roots. It would be of particular interest to see if the new approach can be applied to investigate differences in P_{50} and K between juvenile and mature wood and the considerable variations among clones, which have been shown for juvenile wood of Norway spruce (Rosner *et al.* 2007). Differences may also occur due to tradeoffs between hydraulic and mechanical demands of plant organs, which may mask relationships between hydraulics and quantitative anatomical traits (Baas 1983; Lachenbruch *et al.* 2011; Rosner 2013).

CONCLUSIONS

The aim of this study was the search for a proxy that reflects the wood-functional aspects of resistance to cavitation and that is applicable on Norway spruce wood originating from different sites. The study confirmed that WD data from micro X-ray transmission

has a high potential as a proxy for P_{50} . Also the conduit wall reinforcement is a hot candidate as a hydraulic vulnerability proxy, where the best correlations were obtained by using the tangential width of the lumen. Analysis of anatomical traits may provide a much deeper understanding of the mechanisms behind vulnerability to cavitation than analysis of wood density. SilviScan can provide such data for radial variations in both wood density and all anatomic traits involved from measurements on the same sample, produced for instance from increment cores. In this study, it can thus be put into practice for efficient and non-destructive estimation of several proxies for hydraulic vulnerability (P_{50}) based on wood density and anatomical traits. The most important result of this study is that such data can be used to introduce a dynamic perspective on vulnerability to cavitation by estimating successive loss of hydraulic conductivity for individual specimens. From this we could determine phases of conductivity maintenance and related trait values, new candidate proxies, which provided clearly higher correlations with P_{50} than earlier studied proxies based on static averages.

We conclude that analysis of anatomical variability is useful to increase our understanding of structure-function relationships and can help to increase the predictive quality of anatomical traits for drought sensitivity. Similar studies shall be performed on other woody species in order to learn more about nature's designs to cope with drought stress.

ACKNOWLEDGEMENTS

The research has received funding from the European Union's Seventh Framework Programme for research, technological development and demonstration under grant agreement n° 284181 ("Trees4Future"), from the Swedish strategic research program Bio4Energy and from the European Union's Horizon 2020 research and innovation program under the Marie Skłodowska-Curie grant agreement n° 645654 (Topwood). The contents of this publication reflect only the authors' views and the European Union is not liable for any use that may be made of the information contained therein.

REFERENCES

- Allen CD, Macalady AK, Chenchouni H, Bachelet D, McDowell N, Vennetier M, Kitzberger T, Rigling A, Breshears DD, Hogg EH, Gonzalez P, Fensham R, Zhang Z, Castro J, Demidova N, Lim J-H, Allard G, Running SW, Semerci A, Cobb N. 2010. A global overview of drought and heat-induced tree mortality reveals emerging climate change risks for forests. *Forest Ecol. Managem.* 259: 660–684. <https://doi.org/10.1016/j.foreco.2009.09.001>.
- Baas P. 1983. Ecological patterns in xylem anatomy. In: Givnish TJ (ed.), *On the economy of plant form and function*: 327–352. Cambridge University Press, London, New York, New Rochelle, Melbourne, Sydney
- Bouche PS, Larter M, Domec JC, Burlett R, Gasson P, Jansen S, Delzon S. 2014. A broad survey of hydraulic and mechanical safety in the xylem of conifers. *J. Exp. Bot.* 65 (15): 4419–4431. <https://doi.org/10.1093/jxb/eru218>.
- Bréda N, Badeau V. 2008. Forest tree responses to extreme drought and some biotic events: towards a selection according to hazard tolerance? *Comptes Rendus Geoscience* 340 (9-10): 651–662. <https://doi.org/10.1016/j.crte.2008.08.003>.
- Carrer M, von Arx G, Castagneri D, Petit G. 2015. Distilling allometric and environmental information from time series of conduit size: the standardization issue and its relationship to tree hydraulic architecture. *Tree Physiol.* 35: 27–33. DOI: 10.1093/treephys/tpu108.

- Chen Z-Q, Gil MRG, Karlsson B, Lundqvist S-O, Olsson L, Wu HX. 2014. Inheritance of growth and solid wood quality traits in a large Norway spruce population tested at two locations in southern Sweden. *Tree Genetics & Genomes* 10: 1291–1303. <https://doi.org/10.1007/s11295-014-0761-x>.
- Chen Z-Q, Karlsson B, Mörling T, Olsson L, Mellerowicz EJ, Wu HX, Lundqvist S-O, Gil MRG. 2016. Genetic analysis of fiber dimensions and their correlation with stem diameter and solid-wood properties in Norway spruce. *Tree Genetics & Genomes* 12: 123. <https://doi.org/10.1007/s11295-016-1065-0>.
- Choat B, Jansen S, Brodribb TJ, Cochard H, Delzon S, Bhaskar R, Bucci SJ, Feild TS, Gleason SM, Hacke UG, Jacobsen AL, Lens F, Maherali H, Martínez-Vilalta J, Mayr S, Mencuccini M, Mitchell PJ, Nardini A, Pitterman J, Pratt RB, Sperry JS, Westoby M, Wright IJ, Zanne AE. 2012. Global convergence in the vulnerability of forests to drought. *Nature* 491: 752–755. <https://doi.org/10.1038/nature11688>.
- Cochard H, Badel E, Herbette S, Delzon S, Choat B, Jansen S. 2013. Methods for measuring plant vulnerability to cavitation: a critical review. *J. Exp. Bot.* 64 (15): 4779–4791. <https://doi.org/10.1093/jxb/ert193>.
- Cuny HE, Rathgeber CBK, Frank D, Fonti P, Fournier M. 2014. Kinetics of tracheid development explain conifer tree-ring structure. *New Phytol.* 203: 1231–1241. <https://doi.org/10.1111/nph.12871>.
- Dalla-Salda G, Fernández ME, Sergent AS, Rozenberg P, Badel E, Martinez Meier A. 2014. Dynamics of cavitation in a Douglas-fir tree-ring: transition-wood, the lord of the ring? *J. Plant Hydraul.* 1. <https://doi.org/10.20870/jph.2014.e005>.
- Dalla-Salda G, Martinez-Meier A, Cochard H, Rozenberg P. 2009. Variation of wood density and hydraulic properties of Douglas-fir (*Pseudotsuga menziesii* (Mirb.) Franco) clones related to a heat and drought wave in France. *For. Ecol. Managem.* 257: 182–189. <https://doi.org/10.1016/j.foreco.2008.08.019>.
- Dalla-Salda G, Martinez-Meier A, Cochard H, Rozenberg P. 2011. Genetic variation of xylem hydraulic properties shows that wood density is involved in adaptation to drought in Douglas-fir (*Pseudotsuga menziesii* (Mirb.) Franco). *Ann. For. Sci.* 68: 747–757. <https://doi.org/10.1007/s13595-011-0091-1>.
- Delzon S, Douthe C, Sala A, Cochard H. 2010. Mechanism of water-stress induced cavitation in conifers: bordered pit structure and function support the hypothesis of seal capillary-seeding. *Plant Cell Environm.* 33: 2101–2111. <https://doi.org/10.1111/j.1365-3040.2010.02208.x>.
- Denne MP. 1988. Definition of latewood according to Mork (1928). *IAWA J.* 10: 59–62.
- Domec J-C, Gartner BL. 2002a. How do water transport and water storage differ in coniferous earlywood and latewood? *J. Exp. Bot.* 53: 2369–2379. <https://doi.org/10.1093/jxb/erf100>.
- Domec J-C, Gartner BL. 2002b. Age- and position-related changes in hydraulic versus mechanical dysfunction of xylem: inferring the design criteria for Douglas-fir wood structure. *Tree Physiol.* 22: 91–104. <https://doi.org/10.1093/treephys/22.2-3.91>.
- Domec J-C, Lachenbruch BL, Meinzer FC. 2006. Bordered pit structure and function determine spatial patterns of air-seeding thresholds in xylem of Douglas-fir (*Pseudotsuga menziesii*; Pinaceae) trees. *Am. J. Bot.* 93: 1600–1610. <https://doi.org/10.3732/ajb.93.11.1588>.
- Domec J-C, Warren JM, Meinzer FC, Lachenbruch BL. 2009. Safety for xylem failure by implosion and air-seeding within roots, trunks and branches of young and old conifer trees. *IAWA J.* 30: 101–120. <https://doi.org/10.1163/22941932-90000207>.

- Evans R. 1994. Rapid measurement of the transverse Dimensions of Tracheids in radial wood sections from *Pinus radiata*. *Holzforschung* 48: 168–172. <https://doi.org/10.1515/hfsg.1994.48.2.168>.
- Franceschini T, Lundqvist S-O, Bontemps J-D, Grahn T, Olsson L, Evans R, Leban J-M. 2012. Empirical models for radial and tangential fibre width in tree rings of Norway spruce in north-western Europe. *Holzforschung* 66: 219–230. <https://doi.org/10.1515/HF.2011.150>.
- Franceschini T, Longuetaud F, Bontemps J-D, Bouriaud O, Caritey B-D, Leban J-M. 2013. Effect of ring width, cambial age, and climatic variables on the within-ring wood density profile of Norway spruce *Picea abies* (L.) Karst. *Trees* 27: 913–925. <https://doi.org/10.1007/s00468-013-0844-6>.
- Hacke UG, Jansen S. 2009. Embolism resistance of three boreal conifer species varies with pit structure. *New Phytol.* 182: 675–686. <https://doi.org/10.1111/j.1469-8137.2009.02783.x>.
- Hacke UG, Sperry JS, Pockman WT, Davis SD, McCulloh K. 2001. Trends in wood density and structure are linked to prevention of xylem implosion by negative pressure. *Oecologia* 126: 457–461. <https://doi.org/10.1007/s004420100628>.
- Hentschel R, Rosner S, Kayler ZE, Andreassen K, Børja I, Solberg S, Tveito OE, Priesack E, Gessler A. 2014. Norway spruce physiological and anatomical predisposition to dieback. *Forest Ecol. Managem.* 322: 27–36. <https://doi.org/10.1016/j.foreco.2014.03.007>.
- Hong Z, Fries A, Lundqvist S-O, Andersson Gull B, Wu HX. 2015. Measuring stiffness using acoustic tool for Scots pine breeding selection. *Scand. J. For. Res.* 30 : 363–372. <https://doi.org/10.1080/02827581.2014.1001783>.
- IPCC. 2012. Intergovernmental Panel on Climate Change. Managing the risks of extreme events and disasters to advance climate change adaptation. A special report of working groups I and II of the IPCC. Field CB, Barros V, Stocker TF, Qin D, Dokken DJ, Ebi KL, Mastrandrea MD, Mach KJ, Plattner G-K, Allen SK, Tignor M, Midgley PM (eds.). Cambridge University Press, Cambridge, UK, and New York, USA. 582 pp. <https://doi.org/10.1017/CBO9781139177245>.
- IPCC. 2014. Intergovernmental Panel on Climate Change. Climate Change 2014: Impacts, Adaptation, and Vulnerability. Part A: Global and Sectoral Aspects. Contribution of Working Group II to the Fifth Assessment Report of the Intergovernmental Panel on Climate Change. Field CB, Barros VR, Dokken DJ, Mach KJ, Mastrandrea MD, Bilir TE, Chatterjee M, Ebi KL, Estrada YO, Genova RC, Girma B, Kissel ES, Levy AN, MacCracken S, Mastrandrea PR, White LL (eds.). Cambridge University Press, Cambridge, UK and New York, USA, pp. 1–32. <https://doi.org/10.1017/CBO9781107415379>.
- Kitin P, Fujii T, Abe H, Takata K. 2009. Anatomical features that facilitate radial flow across growth rings and from xylem to cambium in *Cryptomeria japonica*. *Ann. Bot.* 103 (7): 1145–1157. <https://doi.org/10.1093/aob/mcp050>.
- Kolb KJ, Sperry JS. 1999. Transport constraints on water use by the Great Basin shrub, *Artemisia tridentata*. *Plant Cell Environm.* 22: 925–935. <https://doi.org/10.1046/j.1365-3040.1999.00458.x>.
- Kostiainen K, Kaakinen S, Saranpää P, Sigurdsson BD, Lundqvist S-O, Linder S, Vapaavuori E. 2009. Stem wood properties of mature Norway spruce after 3 years of continuous exposure to elevated CO₂ and temperature. *Glob. Chang. Biol.* 15: 368–379. <https://doi.org/10.1111/j.1365-2486.2008.01755.x>.
- Koubaa A, Zhang S, Makni S. 2002. Defining the transition from earlywood to latewood in black spruce based on intra-ring wood density profiles from X-ray densitometry. *Ann. Forest Sci.* 59: 511–518. <https://doi.org/10.1051/forest:2002035>.
- Lachenbruch B, McCulloh KA. 2014. Traits, properties, and performance: How woody plants combine hydraulic and mechanical functions in a cell, tissue, or whole plant. *New Phytol.* 204: 747–764. <https://doi.org/10.1111/nph.13035>.

- Lachenbruch B, Moore J, Evans R. 2011. Radial variation in wood structure and function in woody plants, and hypotheses for its occurrence. In: Meinzer FC, Lachenbruch B, Dawson TE (eds.), Size and age-related changes in tree structure and function: 121–164. Springer, Dordrecht. <https://doi.org/10.1007/978-94-007-1242-3>.
- Larson PR. 1994. The vascular cambium: development and structure. Springer Series in Wood Science. Springer Verlag, Berlin. <https://doi.org/10.1007/978-3-642-78466-8>.
- Lehmann E, Evans R. 2010. SilviScan vs. neutron imaging to generate radial softwood density profiles. Wood Research 55: 49–60.
- Luss S, Schwanninger M, Rosner S. 2014. Hydraulic traits of Norway spruce sapwood estimated by Fourier Transform Near Infrared Spectroscopy (FT-NIR). Can. J. For. Res. 45: 625–631. <https://doi.org/10.1139/cjfr-2014-0452>.
- Mayr S, Schwienbacher F, Bauer H. 2003. Winter at the alpine timberline. Why does embolism occur in Norway spruce but not in stone pine? Plant Physiol. 131: 780–792. <https://doi.org/10.1104/pp.011452>.
- McDowell N, Pockman WT, Allen CD, Breshears DD, Cobb N, Kolb T, Plaut J, Sperry J, West A, Williams DG, Ypez EA. 2008. Mechanisms of plant survival and mortality during drought: why do some plants survive while others succumb to drought? New Phytol. 178: 719–739. <https://doi.org/10.1111/j.1469-8137.2008.02436.x>.
- Mork E. 1928. Die Qualität des Fichtenholzes unter besonderer Rücksichtnahme auf Schleif- und Papierholz. Der Papier-Fabrikant 26: 741–747.
- Nardini A, Savi T, Losso A, Petit G, Pacilè S, Tromba G, Mayr S, Trifilò P, Lo Gullo MA, Salleo S. 2017. X-ray microtomography observations of xylem embolism in stems of *Laurus nobilis* are consistent with hydraulic measurements of percentage loss of conductance. New Phytol. 213: 1068–1075. DOI: 10.1111/nph.14245.
- Olsson L, Hedenberg Ö, Lundqvist S-O. 1998. Measurements of growth ring patterns – comparisons of methods. STFI- Rapport TF111. Stockholm.
- Park Y-I, Spiecker H. 2005. Variations in the tree-ring structure of Norway spruce (*Picea abies*) under contrasting climates. Dendrochronologia 23: 93–104. <https://doi.org/10.1016/j.dendro.2005.09.002>.
- Pittermann J, Choat B, Jansen S, Stuart SA, Lynn L, Dawson TE. 2010. The relationships between xylem safety and hydraulic efficiency in the Cupressaceae: the evolution of pit membrane form and function. Plant Physiol. 153: 1919–1931. <https://doi.org/10.1104/pp.110.158824>.
- Rathgeber C, Decoux V, Leban J. 2006. Linking intra-tree-ring wood density variations and tracheid anatomical characteristics in Douglas fir (*Pseudotsuga menziesii* (Mirb.) Franco). Ann. Forest Sci. 63: 699–706. <https://doi.org/10.1051/forest:2006050>.
- Rosner S. 2013. Hydraulic and biomechanical optimization in Norway spruce trunkwood – a review. IAWA J. 34: 365–390. <https://doi.org/10.1163/22941932-00000031>.
- Rosner S, Klein A, Müller U, Karlsson B. 2007. Hydraulic and mechanical properties of young Norway spruce clones related to growth and wood structure. Tree Physiol. 27: 1165–1178. <https://doi.org/10.1093/treephys/27.8.1165>.
- Rosner S, Klein A, Müller U, Karlsson B. 2008. Tradeoffs between hydraulic and mechanical stress response of mature Norway spruce trunkwood. Tree Physiol. 28: 1179–1188. <https://doi.org/10.1093/treephys/28.8.1179>.
- Rosner S, Luss S, Světlík J, Andreassen K, Børja I, Evans R, Tveito OE, Solberg S. 2016a. Chronology of hydraulic vulnerability in trunkwood of conifer trees with and without symptoms of top dieback. J. Plant Hydraul. 3 (e-001): 1–5. <https://doi.org/10.20870/jph.2016.e001>.
- Rosner S, Světlík J, Andreassen K, Børja I, Dalsgaard I, Evans R, Karlsson B, Tollefsrud MM, Solberg S. 2014. Wood density as a screening trait for drought sensitivity in Norway spruce. Can. J. For. Res. 44: 154–161. <https://doi.org/10.1139/cjfr-2013-0209>.

- Rosner S, Svetlik J, Andreassen K, Borja I, Dalsgaard L, Evans R, Luss S, Tveito OE, Solberg S. 2016b. Novel hydraulic vulnerability proxies for a boreal conifer species reveal that opportunists may have lower survival prospects under extreme climatic events. *Front Plant Sci.* 7: 831. <https://doi.org/10.3389/fpls.2016.00831>.
- Rozenberg P, Schüte G, Ivkovich M, Bastien C, Bastien JC. 2004. Clonal variation of indirect cambium reaction to within-growing season temperature changes in Douglas-fir. *Forestry* 77: 257–268. <https://doi.org/10.1093/forestry/77.4.257>.
- Ruiz Diaz Britez M, Sergent A-S, Martinez Meier A, Bréda N, Rozenberg P. 2014. Wood density proxies of adaptive traits linked with resistance to drought in Douglas fir (*Pseudotsuga menziesii* (Mirb.) Franco). *Trees* 28: 1289–1304. <https://doi.org/10.1007/s00468-014-1003-4>.
- Schär C, Vidale PL, Lüthi D, Frei C, Häberli C, Mark A, Lindinger MA, Appenzeller C. 2004. The role of increasing temperature variability in European summer heatwaves. *Nature* 427: 332–336. <https://doi.org/10.1038/nature02230.1>.
- Sergent A-S, Rozenberg P, Bréda N. 2014. Douglas-fir is vulnerable to exceptional and recurrent drought episodes and recovers less well on less fertile sites. *Ann. For. Sci.* 71: 697–708. <https://doi.org/10.1007/s13595-012-0220-5>.
- Solberg S. 2004. Summer drought: a driver for crown condition and mortality of Norway spruce in Norway. *Forest Pathology* 34: 93–104. <https://doi.org/10.1111/j.1439-0329.2004.00351.x>.
- Tyree MT, Zimmermann MH. 2002. Xylem structure and the ascent of sap. Springer Verlag, Berlin.
- Vysotskaya LG, Vaganov TA. 1989. Components of the variability of radial cell size in tree rings of conifers. *IAWA J.* 10: 417–426. <https://doi.org/S>.
- Willson CJ, Manos PS, Jackson RB. 2008. Hydraulic traits are influenced by phylogenetic history in the drought-resistant, invasive genus *Juniperus* (Cupressaceae). *Am. J. Bot.* 95: 299–314. <https://doi.org/10.3732/ajb.95.3.299>.
- Zobel BJ, van Buijtenen JP. 1989. Wood variation: its causes and control. Springer Verlag, Berlin.
- Zwieniecki MA, Secchi F. 2015. Threats to xylem hydraulic function of trees under ‘new climate normal’ conditions. *Plant Cell Environm.* 38: 1713–1724. <https://doi.org/10.1111/pce.12412>.

4. General Conclusions

Conclusions

Methods for efficient characterization of hydraulic properties of trees and their vulnerability to drought are increasingly important in our time of climate change. Such methods would be very useful in tree improvement for more resilient trees, for selection of trees suitable for different sites, and in research. The aim of this study was to test the potential of more efficient alternative methods for determining the hydraulic vulnerability (P_{50}) in order to replace classical methods. Two different approaches based on well-established techniques were tested.

The following criteria were defined for the selection of the methods to test: (I) non-destructive, (II) efficient, (III) easy to assess, (IV) well established, and (V) limited sample preparation required. The study was performed on samples from Norway spruce. To ensure that the comparison of the methods was sound, the same set of samples in the form of wood microbeams was used for the measurements with all instruments.

The first approach (see chapter 2) shows how Fourier transform near infrared spectroscopy (FT-NIR) and prediction models (partial least square regression (PLS-R) models) can be used to determine the desired parameter P_{50} . The second approach, described in chapter 3, uses data from a SilviScan instrument on between and within annual ring variations in wood density and anatomical properties to calculate good proxies for the hydraulic vulnerability (P_{50}).

FT-NIR technology is widely used in various fields and is described as a non-destructive, fast, and simple method. All these characteristics could be confirmed. One advantage is that this technique does not require advanced sample preparation, which speeds up measurements in comparison to the classical and most other methods. PLS-R modeling and interpretation of the results requires a lot of expertise and takes more time at the beginning. But compared to the classical method, the search for suitable prediction models is very fast. With routine and experience, time can be saved. Models that have already been created allow a prediction to be made within a few seconds. This makes this method very attractive.

The models developed and presented in this thesis are promising and have already inspired other authors to concentrate on this topic (Savi et al. 2019). A large pool of prediction models for different tree species and parameters would be a great enrichment for the determination of the hydraulic parameter in practice. It is recommended that the models are developed based on large sample size representing large spans of P_{50} variation, as FT-NIR is super sensitive and e.g. compression wood or other anatomical or chemical variations can influence the results.

All samples used on this modelling were from the same species. It cannot be taken for granted that it is possible to use the models across conifers. Bordered pits or other anatomical structures may also have an influence on the results, so it is important to note that the direction (axial, radial, tangential) of the measured sample must also be carefully considered. Moreover, the age of the trees must be taken into account. For example, the models developed were not tested for very young or old trees. The results of this thesis provide strong and positive indications. This could be very interesting for forestry and tree breeders as a method to detect more suitable provenances and clones for propagation. But for use in practice, further work is recommended. It would be preferable that European or world-wide networks work together to establish different models for the praxis.

SilviScan is a well-established instrument for efficient measurements of radial variations in a large number of wood and fiber properties from the same sample, through the integration of microscopy and X-ray techniques. In this study, high resolution data on within and between ring variations of wood density (WD) and cross-sectional tracheid dimensions were used to

calculate for instance conduit wall reinforcement $((t/b)^2)$ from tracheid lumen width (b) and tracheid double wall thickness (t) were used to find proxies for P_{50} . WD had previously been observed as a potential proxy for P_{50} , and significant correlation between WD and P_{50} was confirmed, but there is no direct causal relationship between the two parameters. A new approach was developed, introducing dynamic aspects of conductivity loss through the analysis of 5% steps in the cumulated hydraulic conductivity (K), producing even stronger correlations. It would be desirable to test this approach for other tree species in order to better assess its potential.

Normally, samples analysed with SilviScan originate from increment cores taken from standing trees, which is common practice in forestry. The cores are then sawn into radial strips and polished on one side for microscopy, using machinery designed for this, and the strips are kept some days in the conditioned lab of the instrument to reach a stable controlled moisture content before the measurements are performed, routines which by now have been applied on at least 100 000 samples. Analogous procedures should be possible to develop also for the sample preparation before FT-NIR measurements for the method described above, including production of samples of suitable dimensions and to secure same the surface properties between samples.

Another benefit of the Silviscan alternative is that it provides spatially matched information on many growth-, wood- and fibre related properties from the same sample, and many of those are also of interest for tree improvement, research and industry. This is an advantage over FT-NIR spectroscopy, even though it is theoretically possible to predict different parameters with FT-NIR spectroscopy, but only with previously created PLS-R models the specific parameter and type of material. When choosing the method, it should also be considered that SilviScan is currently available solely at three locations in the world (Melbourne, Stockholm, and Vancouver). This factor makes this measurement method more exclusive than for example FT-NIR.

Both methods investigated have advantages, and it is not possible to generally state which method is preferred to the classical methods. Using SilviScan, data are obtained which relate to identifiable features in wood, data which can be used to sharpen proxies. Regarding FT-NIR measurements: when routines for sample preparation are available and reliable prediction models in place for the types of trees of interest, this method should be more efficient and have the potential to approach applications in the field. However, with the expectation that successive updates of the models will be needed. It is safe to assume that FT-NIR and SilviScan both have high potential to replace classical methods.

In conclusion, this thesis tested two different methods to replace classical methods to determine P_{50} . Both methods, FT-NIR spectroscopy and SilviScan, showed promising results. The results shall be seen as a basis for further tests and development. They have already inspired other projects to continue research in this field and hopefully this will be continued in the future.

5. References

- Allen, C.D., Macalady, A.K., Chenchouni, H., Bachelet, D., McDowell, N., Vennetier, M., Kitzberger, T., Rigling, A., Breshears, D.D., Hogg, E.H. (Ted), Gonzalez, P., Fensham, R., Zhang, Z., Castro, J., Demidova, N., Lim, J.-H., Allard, G., Running, S.W., Semerci, A., and Cobb, N. 2010. A global overview of drought and heat-induced tree mortality reveals emerging climate change risks for forests. *For. Ecol. Manage.* **259**(4): 660–684. doi:10.1016/j.foreco.2009.09.001.
- Auty, D., Gardiner, B.A., Achim, A., Moore, J.R., and Cameron, A.D. 2013. Models for predicting microfibril angle variation in Scots pine. *Ann. For. Sci.* **70**: 209–218. doi:10.1007/s13595-012-0248-6.
- Böhm, J. 1893. Capillarität und Saftsteigen. *Dtsch. Bot. Gesellschaft* **11**: 203–212.
- Bouche, P.S., Larter, M., Domec, J.-C., Burlett, R., Gasson, P., Jansen, S., and Delzon, S. 2014. A broad survey of hydraulic and mechanical safety in the xylem of conifers. *J. Exp. Bot.* **65**(15): 4419–4431. doi:10.1093/jxb/eru218.
- Bréda, N., and Badeau, V. 2008. Forest tree responses to extreme drought and some biotic events: Towards a selection according to hazard tolerance? *Comptes Rendus Geosci.* **340**(9–10): 651–662. doi:10.1016/j.crte.2008.08.003.
- Bruker Optik GmbH. 2012. MPA Benutzerhandbuch. Ettlingen, Deutschland.
- Buksnowitz, C., Müller, U., Evans, R., Teischinger, A., and Grabner, M. 2008. The potential of SilviScan's X-ray diffractometry method for the rapid assessment of spiral grain in softwood, evaluated by goniometric measurements. *Wood Sci. Technol.* **42**: 95–102. doi:10.1007/s00226-007-0153-6.
- Chen, F.F., and Evans, R. 2010. Automated measurement of vessel properties in birch and poplar wood. *Holzforschung* **64**: 369–374. doi:10.1515/HF.2010.057.
- Chen, Z.Q., Gil, M.R.G., Karlsson, B., Lundqvist, S.-O., Olsson, L., and Wu, H.X. 2014. Inheritance of growth and solid wood quality traits in a large Norway spruce population tested at two locations in southern Sweden. *Tree Genet. Genomes* **10**: 1291–1303. doi:10.1007/s11295-014-0761-x.
- Choat, B., Jansen, S., Brodribb, T.J., Cochard, H., Delzon, S., Bhaskar, R., Bucci, S.J., Feild, T.S., Gleason, S.M., Hacke, U.G., Jacobsen, A.L., Lens, F., Maherali, H., Martínez-Vilalta, J., Mayr, S., Mencuccini, M., Mitchell, P.J., Nardini, A., Pittermann, J., Pratt, R.B., Sperry, J.S., Westoby, M., Wright, I.J., and Zanne, A.E. 2012. Global convergence in the vulnerability of forests to drought. *Nature* **491**: 752–755. doi:10.1038/nature11688.
- Chung, H.-H., and Kramer, P.J. 1975. Absorption of water and ³²P through suberized and unsuberized roots of loblolly pine. *Can. J. For. Res.* **5**: 229–235. doi:10.1139/x75-031.
- Cochard, H. 2014. The basics of plant hydraulics. *J. Plant Hydraul.* **1**: e-0001. doi:10.20870/jph.2014.e001.
- Cochard, H., Badel, E., Herbette, S., Delzon, S., Choat, B., and Jansen, S. 2013. Methods for measuring plant vulnerability to cavitation: a critical review. *J. Exp. Bot.* **64**(15): 4779–4791. doi:10.1093/jxb/ert193.
- Cooper, P.A., Jeremic, D., Radivojevic, S., Ung, Y.T., and Leblon, B. 2011. Potential of near-infrared spectroscopy to characterize wood products. *Can. J. For. Res.* **41**: 2150–2157. doi:10.1139/X11-088.
- Dalla-Salda, G., Fernández, M.E., Sergent, A.-S., Rozenberg, P., Badel, E., and Martinez-Meier, A. 2014. Dynamics of cavitation in a Douglas-fir tree-ring: transition-wood, the lord of the ring? *J. Plant Hydraul.* **1**: e-0005. doi:10.20870/jph.2014.e005.

- Defo, M. 2008. SilviScan-3. A revolutionary technology for high-speed wood microstructure and properties analysis. Available from <http://chaireafd.uqat.ca/midiForesterie/pdf/20080422PresentationMauriceDefo.pdf> [accessed 20 September 2019].
- Doshi, G.N. 1998. Analysis and applications of FT-IR Systems. Faculty of New Jersey Institute of Technology. Available from <http://archives.njit.edu/vol01/etd/1990s/1998/njit-etd1998-018/njit-etd1998-018.pdf>.
- Downes, G.M., Evans, R., Schimleck, L.R., and Fritts, H.C. 2000. The commercial cambium: understanding the origin of wood property variation. *In* Cell and Molecular Biology of Wood Formation. *Edited by* R.A. Savidge, J.R. Barnett, and R. Napier. Garland Science, London, U.K. pp. 325–336.
- Downes, G.M., Nyakuengama, J.G., Evans, R., Northway, R., Blakemore, P., Dickson, R.L., and Lausberg, M. 2002. Relationship between wood density, microfibril angle and stiffness in thinned and fertilized *Pinus radiata*. *IAWA J.* **23**: 253–265. doi:10.1163/22941932-90000302.
- Evans, R. 1994. Rapid measurement of the transverse dimensions of tracheids in radial wood sections from *Pinus radiata*. *Holzforschung* **48**: 168–172.
- Evans, R. 2006. Wood stiffness by x-ray diffractometry. *In* Characterization of the Cellulosic Cell Wall, Proceeding. *Edited by* D. Stokke and L. Groom. Blackwell Publishing, Grand Lake, Colorado, USA. pp. 138–146. doi:10.1002/9780470999714.ch11.
- Evans, R., Downes, G., Menz, D., and Stringer, S. 1995. Rapid measurement of variation in tracheid transverse dimensions in a radiata pine tree. *Appita J.* **48**: 134–138.
- Farjon, A. 2017. *Picea abies*. The IUCN Red List of Threatened Species 2017: e.T42318A71233492. *In* Red List of Threatened Species: *Picea abies*. Available from <http://dx.doi.org/10.2305/IUCN.UK.2017-2.RLTS.T42318A71233492.en>.
- Foley, W.J., McIlwee, A., Lawler, I., Aragones, L., Woolnough, A.P., and Berding, N. 1998. Ecological applications of near infrared reflectance spectroscopy - a tool for rapid, cost-effective prediction of the composition of plant and animal tissues and aspects of animal performance. *Oecologia* **116**: 293–305.
- Franceschini, T., Lundqvist, S.-O., Bontemps, J.D., Grahn, T., Olsson, L., Evans, R., and Leban, J.M. 2012. Empirical models for radial and tangential fibre width in tree rings of Norway spruce in north-western Europe. *Holzforschung* **66**: 219–230. doi:10.1515/HF.2011.150.
- Fries, A., Ulvcróna, T., Wu, H.X., and Kroon, J. 2014. Stem damage of lodgepole pine clonal cuttings in relation to wood and fiber traits, acoustic velocity, and spiral grain. *Scand. J. For. Res.* **29**(8): 764–776. doi:10.1080/02827581.2014.978886.
- Hacke, U.G., Stiller, V., Sperry, J.S., Pittermann, J., and McCulloh, K.A. 2001. Cavitation fatigue. Embolism and refilling cycles can weaken the cavitation resistance of xylem. *Plant Physiol.* **125**(2): 779–786. Available from <http://www.pubmedcentral.nih.gov/articlerender.fcgi?artid=64879&tool=pmcentrez&rendertype=abstract>.
- Hammond, W.M., Yu, K., Wilson, L.A., Will, R.E., Anderegg, W.R.L., and Adams, H.D. 2019. Dead or dying? Quantifying the point of no return from hydraulic failure in drought-induced tree mortality. *New Phytol.* **223**: 1834–1843. doi:10.1111/nph.15922.
- Hentschel, R., Rosner, S., Kayler, Z.E., Andreassen, K., Børja, I., Solberg, S., Tveito, O.E., Priesack, E., and Gessler, A. 2014. Norway spruce physiological and anatomical predisposition to dieback. *For. Ecol. Manage.* **322**: 27–36. doi:10.1016/j.foreco.2014.03.007.
- Hietz, P., Rosner, S., Sorz, J., and Mayr, S. 2008. Comparison of methods to quantify loss of hydraulic conductivity in Norway spruce. *Ann. For. Sci.* **65**: 502–508. doi:10.1051/forest:2008023 Available.

- Hindle, P.H. 2001. Historical Development. *In Handbook of near-infrared analysis*, 3rd edition. *Edited by* D.A. Burns and E.W. Ciurczak. CRC Press, Boca Raton, FL, USA. pp. 3–6.
- Hong, Z., Fries, A., Lundqvist, S.-O., Andersson Gull, B., and Wu, H.X. 2015. Measuring stiffness using acoustic tool for Scots pine breeding selection. *Scand. J. For. Res.* **30**: 363–372. doi:10.1080/02827581.2014.1001783.
- IPCC. 2012. Summary for Policymakers. *In Managing the risks of extreme events and disasters to advance climate change adaptation.* *Edited by* C.B. Field, V. Barros, T.F. Stocker, Q. Dahe, D.J. Dokken, K.L. Ebi, M.D. Mastrandrea, K.J. Mach, G.-K. Plattner, S.K. Allen, M. Tignor, and P.M. Midgley. A Special Report of Working Groups I and II of the Intergovernmental Panel on Climate Change. Cambridge University Press, Cambridge, UK, and New York, NY, USA. pp. 1–19. doi:10.1017/CBO9781139177245.
- IPCC. 2014. Summary for policymakers. *In Climate Change 2014: Impacts, Adaptation, and Vulnerability. Part A: Global and Sectoral Aspects. Contribution of Working Group II to the Fifth Assessment Report of the Intergovernmental Panel on Climate Change.* *Edited by* C.B. Field, V.R. Barros, D.J. Dokken, K.J. Mach, M.D. Mastrandrea, T.E. Bilir, M. Chatterjee, K.L. Ebi, Y.O. Estrada, R.C. Genova, B. Girma, E.S. Kissel, A.N. Levy, S. MacCracken, P.R. Mastrandrea, and L.L. White. Cambridge University Press, Cambridge, United Kingdom and New York, NY, USA. pp. 1–32. doi:10.1017/CBO9781107415379.
- Klein, T., Zeppel, M.J.B., Anderegg, W.R.L., Bloemen, J., De Kauwe, M.G., Hudson, P., Ruehr, N.K., Powell, T.L., von Arx, G., and Nardini, A. 2018. Xylem embolism refilling and resilience against drought-induced mortality in woody plants: processes and trade-offs. *Ecol. Res.* **33**(5): 839–855. Springer Japan. doi:10.1007/s11284-018-1588-y.
- Knapic, S., Grahn, T., Lundqvist, S.-O., and Pereira, H. 2018. Juvenile wood characterization of *Eucalyptus botryoides* and *E. maculata* by using SilviScan. *BioResources* **13**(2): 2342–2355. doi:10.15376/biores.13.2.2342-2355.
- Kostiainen, K., Kaakinen, S., Saranpää, P., Sigurdsson, B.D., Lundqvist, S.-O., Linder, S., and Vapaavuori, E. 2009. Stem wood properties of mature Norway spruce after 3 years of continuous exposure to elevated [CO₂] and temperature. *Glob. Chang. Biol.* **15**(2): 368–379. doi:10.1111/j.1365-2486.2008.01755.x.
- Kramer, P.J., and Bullock, H.C. 1966. Seasonal variations in the proportions of suberized and unsuberized roots of trees in relation to the absorption of water. *Am. J. Bot.* **53**(2): 200–204. doi:10.2307/2440089.
- Larson, D.W., Doubt, J., and Matthes-Sears, U. 1994. Radially sectorized hydraulic pathways in the xylem of *Thuja occidentalis* as revealed by the use of dyes. *Int. J. Plant Sci.* **155**(5): 569–582. doi:10.1086/297195.
- Larson, D.W., Matthes-Sears, U., and Kelly, P.E. 1993. Cambial dieback and partial shoot mortality in cliff-face *Thuja occidentalis*: evidence for sectorized radial architecture. *Int. J. Plant Sci.* **154**(4): 496–505. doi:10.1086/297133.
- Leblon, B., Adedipe, O., Hans, G., Haddadi, A., Tsuchikawa, S., Burger, J., Stirling, R., Pirouz, Z., Groves, K., Nader, J., and LaRocque, A. 2013. A review of near-infrared spectroscopy for monitoring moisture content and density of soil wood. *For. Chronicles* **89**(5): 595–606.
- Linder, H., and Knodel, H. 2012. Linder Biologie. Sekundarstufe 2. Gesamtband. *In* 24th edition. *Edited By* H. Bayerhuber, W. Hauber, and U. Kull. Bildungshaus Schulbuchverlage Westermann Schroedel Diesterweg Schöningh Winklers GmbH, Braunschweig.
- Lindström, H., Evans, J.W., and Verrill, S.P. 1998. Influence of cambial age and growth conditions on microfibril angle in young Norway Spruce (*Picea abies* [L.] Karst.). *Holzforschung* **52**: 573–581. doi:10.1515/hfsg.1998.52.6.573.

- Lipták, B.G. 2006. Advantages of Fourier-Transform Near-Infrared Spectroscopy. *In* Analysis and Analyzers. doi:10.4324/9781315370323.
- Lundgren, C. 2004. Cell wall thickness and tangential and radial cell diameter of fertilized and irrigated Norway spruce. *Silva Fenn.* **38**(1): 95–106. doi:http://dx.doi.org/10.14214/sf.438.
- Lundqvist, S.-O., Grahn, T., and Hedenberg, Ö. 2005. Models for fibre dimensions in different softwood species. Simulation and comparison of within and between tree variations for Norway and Sitka spruce, Scots and Loblolly pine. *In* Proceedings IUFRO Conference. Auckland, New Zealand.
- Lundqvist, S.-O., Hansson, Å., and Olsson, L. 2007. SilviScan measurements on Maritime pine. French samples cut perpendicular to the fibres. STFI-Packforsk Report No. 326. Sweden.
- Lundqvist, S.-O., Olsson, L., Evans, R., Chen, F.F., and Vapaavuori, E. 2010. Variations in properties of hardwood analysed with SilviScan – Examples of wood, fibre and vessel properties of birch (*Betula*). *In* „Hardwood Science and Technology” The 4th Conference on Hardwood Research and Utilisation in Europe 2010 Variations. Sopron, Hungary.
- Lundqvist, S.-O., Seifert, S., Grahn, T., Olsson, L., García-Gil, M.R., Karlsson, B., and Seifert, T. 2018. Age and weather effects on between and within ring variations of number, width and coarseness of tracheids and radial growth of young Norway spruce. *Eur. J. For. Res.* **137**(5): 719–743. doi:10.1007/s10342-018-1136-x.
- Luss, S., Lundqvist, S.-O., Evans, R., Grahn, T., Olsson, L., Petit, G., and Rosner, S. 2019. Within-ring variability of wood structure and its relationship to drought sensitivity in Norway spruce trunks. *IAWA J.* **40**(2): 288–310. doi:10.1163/22941932-40190216.
- Luss, S., Schwanninger, M., and Rosner, S. 2015. Hydraulic traits of Norway spruce sapwood estimated by Fourier transform near-infrared spectroscopy (FT-NIR). *Can. J. For. Res.* **45**(6): 625–631. doi:10.1139/cjfr-2014-0452.
- Macfall, J.S., Johnson, G.A., and Kramer, P.J. 1990. Observation of a water-depletion region surrounding loblolly pine roots by magnetic resonance imaging. *Proc. Natl. Acad. Sci. U. S. A.* **87**: 1203–1207. doi:10.1073/pnas.87.3.1203.
- Martin-StPaul, N.K., Longepierre, D., Huc, R., Delzon, S., Burrell, R., Joffre, R., Rambal, S., and Cochard, H. 2014. How reliable are methods to assess xylem vulnerability to cavitation? The issue of “open vessel” artifact in oaks. *Tree Physiol.* **34**: 894–905. doi:10.1093/treephys/tpu059.
- Mayr, S. 2002. Eine modifizierte Sperry-Apparatur zur Messung des Emboliegrades im Xylem von Bäumen. *Berichte des naturwissenschaftlich-medizinischen Vereins in Innsbruck* 2002 Folge 89: 99-110.
- Mayr, S., Schmid, P., Laur, J., Rosner, S., Charra-Vaskou, K., Dämon, B., and Hacke, U.G. 2014. Uptake of water via branches helps timberline conifers refill embolized xylem in late winter. *Plant Physiol.* **164**: 1731–1740. doi:10.1104/pp.114.236646.
- Mayr, S., Wolfschwenger, M., and Bauer, H. 2002. Winter-drought induced embolism in Norway spruce (*Picea abies*) at the Alpine timberline. *Physiol. Plant.* **115**: 74–80. doi:10.1034/j.1399-3054.2002.1150108.x.
- McDowell, N., Pockman, W.T., Allen, C.D., Breshears, D.D., Cobb, N., Kolb, T., Plaut, J., Sperry, J., West, A., Williams, D.G., and Yezzer, E.A. 2008. Mechanisms of plant survival and mortality during drought: why do some plants survive while others succumb to drought? *New Phytol.* **178**(4): 719–739. doi:10.1111/j.1469-8137.2008.02436.x.
- McElrone, A.J., Choat, B., Gambetta, G.A., and Brodersen, C.R. 2013. Water Uptake and Transport in Vascular Plants. *Nat. Educ. Knowl.* **4**(5): 6.
- Mork, E. 1928. Die Qualität des Fichtenholzes unter besonderer Rücksichtnahme auf Schleif- und Papierholz. *Der Pap.* **26**: 741.

- Müller, U., Gindl, W., and Teischinger, A. 2003. Effects of cell anatomy on the plastic and elastic behaviour of different wood species loaded perpendicular to grain. *IAWA J.* **24**(2): 117–128. doi:10.1163/22941932-90000325.
- Nicolaï, B.M., Beullens, K., Bobelyn, E., Peirs, A., Saeys, W., Theron, K.I., and Lammertyn, J. 2007. Nondestructive measurement of fruit and vegetable quality by means of NIR spectroscopy: A review. *Postharvest Biol. Technol.* **46**: 99–118. doi:10.1016/j.postharvbio.2007.06.024.
- Olsson, L., Hedenberg, Ö., and Lundqvist, S.-O. 1998. Measurements of growth ring patterns—comparisons of methods. STFI- Rapport TF111. Stockholm. 23pp.
- Owen-Reece, H., Smith, M., Elwell, C.E., and Goldstone, J.C. 1999. Near infrared spectroscopy. *Br. J. Anaesth.* **82**(3): 418–426.
- Pammenter, N.W., and Vander Willigen, C. 1998. A mathematical and statistical analysis of the curves illustrating vulnerability of xylem to cavitation. *Tree Physiol.* **18**: 589–593. doi:10.1093/treephys/18.8-9.589.
- Piispänen, R., Heinonen, J., Valkonen, S., Mäkinen, H., Lundqvist, S.-O., and Saranpää, P. 2014. Wood density of Norway spruce in uneven-aged stands. *Can. J. For. Res.* **44**: 136–144. doi:10.1139/cjfr-2013-0201.
- Pittermann, J., Sperry, J., Hacke, U.G., Wheeler, J.K., and Sikkema, E.H. 2006. Inter-tracheid pitting and the hydraulic efficiency of conifer wood: the role of tracheid allometry and cavitation protection. *Am. J. Bot.* **93**(9): 1265–1273. doi:10.3732/ajb.93.9.1265.
- Rosner, S. 2013. Hydraulic and biomechanical optimization in Norway spruce trunkwood – a review. *IAWA J.* **34**(4): 365–390. doi:10.1163/22941932-00000031.
- Rosner, S. 2017. Wood density as a proxy for vulnerability to cavitation: Size matters. *J. Plant Hydraul.* **4**: e-001. doi:10.20870/jph.2017.e001.
- Rosner, S., Gierlinger, N., Klepsch, M., Karlsson, B., Evans, R., Lundqvist, S.-O., Světlík, J., Børja, I., Dalsgaard, L., Andreassen, K., Solberg, S., and Jansen, S. 2018. Hydraulic and mechanical dysfunction of Norway spruce sapwood due to extreme summer drought in Scandinavia. *For. Ecol. Manage.* **409**: 527–540. doi:10.1016/j.foreco.2017.11.051.
- Rosner, S., Heinze, B., Savi, T., and Dalla-Salda, G. 2019a. Prediction of hydraulic conductivity loss from relative water loss: new insights into water storage of tree stems and branches. *Physiol. Plant.* **165**: 843–854. doi:10.1111/ppl.12790.
- Rosner, S., Johnson, D.M., Voggeneder, K., and Domec, J.-C. 2019b. The conifer-curve: fast prediction of hydraulic conductivity loss and vulnerability to cavitation. *Ann. For. Sci.* **76**: 82. doi:10.1007/s13595-019-0868-1.
- Rosner, S., and Karlsson, B. 2011. Hydraulic efficiency compromises compression strength perpendicular to the grain in Norway spruce trunkwood. *Trees* **25**(2): 289–299. doi:10.1007/s00468-010-0505-y.
- Rosner, S., Klein, A., Müller, U., and Karlsson, B. 2007. Hydraulic and mechanical properties of young Norway spruce clones related to growth and wood structure. *Tree Physiol.* **27**: 1165–1178. doi:10.1093/treephys/27.8.1165.
- Rosner, S., Klein, A., Müller, U., and Karlsson, B. 2008. Tradeoffs between hydraulic and mechanical stress responses of mature Norway spruce trunk wood. *Tree Physiol.* **28**: 1179–1188. doi:10.1093/treephys/28.8.1179.
- Rosner, S., Svetlík, J., Andreassen, K., Børja, I., Dalsgaard, I., Evans, R., Karlsson, B., M, T.M., and Solberg, S. 2014. Wood density as a screening trait for drought sensitivity in Norway spruce. *Can. J. For. Res.* **44**: 154–161. doi:10.1139/cjfr-2013-0209.
- Savi, T., Tintner, J., Da Sois, L., Grabner, M., Petit, G., and Rosner, S. 2019. The potential of Mid-Infrared spectroscopy for prediction of wood density and vulnerability to embolism in woody angiosperms. *Tree Physiol.* **39**: 503–510. doi:10.1093/treephys/tpy112.

- Scallan, A.M., and Green, H. V. 1974. A technique for determining the transverse dimensions of the fibres in wood. *Wood Fiber Sci.* **5**: 323–333.
- Schadauer, K., Niese, G., and Matzik, H. 2015. *Österreichische Waldinventur - Baumartenatlas*. Bundesforschungs- und Ausbildungszentrum für Wald. Available from https://bfw.ac.at/700/2092_1_1.html [accessed 20 September 2019].
- Schär, C., Vidale, P.L., Lüthi, D., Frei, C., Häberli, C., Liniger, M.A., and Appenzeller, C. 2004. The role of increasing temperature variability in European summer heatwaves. *Nature* **427**: 332–336. doi:10.1038/nature02230.1.
- Schimleck, L., Dahlen, J., Apiolaza, L.A., Downes, G., Emms, G., Evans, R., Moore, J., Pâques, L., Van den Bulcke, J., and Wang, X. 2019. Non-Destructive Evaluation Techniques and What They Tell Us about Wood Property Variation. *Forests* **10**(9): 728. doi:10.3390/f10090728.
- Schimleck, L.R., Mora, C.R., Peter, G.F., and Evans, R. 2010. Alternative methods for nondestructively determining modulus of elasticity in young trees. *IAWA Journal* **31**: 161–167. doi:10.1163/22941932-90000013.
- Schimleck, L.R., Raymond, C.A., Beadle, C.L., Downes, G.M., Kube, P.D., and French, J. 2000. Applications of NIR spectroscopy to forest research. *Appita J.* **53**: 458–464.
- Schmidt-Vogt, H., Liese, W., Dujesiefken, D., and Rehfuess, K.E. 1986. *Die Fichte. Ein Handbuch in zwei Bänden. Band II/1*. Verlag Paul Parey, Hamburg und Berlin.
- Schopfer Peter; Brennicke Axel. 2010. *Pflanzenphysiologie*. Spektrum Akademischer Verlag, Heidelberg. doi:10.1007/978-3-8274-2352-8.
- Schwanninger, M., Rodrigues, J., and Fackler, K. 2011. A review of band assignments in near infrared spectra of wood and wood components. *J. Near Infrared Spectrosc.* **19**: 287–308. doi:10.1255/jnirs.955.
- Sergent, A.-S., Rozenberg, P., and Bréda, N. 2012. Douglas-fir is vulnerable to exceptional and recurrent drought episodes and recovers less well on less fertile sites. *Ann. For. Sci.* **71**: 697–708. doi:10.1007/s13595-012-0220-5.
- Shenk, J.S., Workman Jr., J.J., and Westerhaus, M.O. 2008. Application of NIR Spectroscopy to Agricultural Products. *In Handbook of near-infrared analysis.*, 3rd edition. Edited by D. Burns and E. Ciurczak. CRC Press, Boca Raton, FL, USA. pp. 347–386.
- Skrøppa, T. 2003. Norway spruce (*Picea abies*). EUFORGEN Tech. Guidel. Genet. Conserv. Use: 6.
- Smith, B. 1999. *Infrared spectral interpretation: a systematic approach*. CRC Press, Boca Raton, Florida, USA.
- Smith, B.C. 2011. *Fundamentals of fourier transform infrared spectroscopy*. CRC Press, Boca Raton, Florida, USA.
- So, C.-L., Via, B.K., Groom, L.H., Schimleck, L.R., Shupe, T.F., Kelley, S.S., and Rials, T.G. 2004. Near infrared spectroscopy in the forest products industry. *For. Prod. J.* **54**: 6–16.
- Solberg, S. 2004. Summer drought: a driver for crown condition and mortality of Norway spruce in Norway. *For. Pathol.* **34**: 93–104. doi:10.1111/j.1439-0329.2004.00351.x.
- Sperry, J.S., Donnely, J.R., and Tyree, M.T. 1988. A method for measuring hydraulic conductivity and embolism in xylem. *Plant. Cell Environ.* **11**: 35–40. doi:10.1111/j.1365-3040.1988.tb01774.x.
- Strasburger, E., Noll, F., Schenck, H., and Usw. 1983. *Lehrbuch der Botanik*. doi:10.1007/BF02200303.
- Tsuchikawa, S. 2007. A review of recent near infrared research for wood and paper. *Appl. Spectrosc. Rev.* **42**: 43–71. doi:10.1080/05704920601036707.

- Tsuchikawa, S., and Schwanninger, M. 2013. A review of recent near-infrared research for wood and paper (Part 2). *Appl. Spectrosc. Rev.* **48**: 560–587. doi:10.1080/05704928.2011.621079.
- Tyree, M.T., Davis, S.D., and Cochard, H. 1994. Biophysical perspectives of xylem evolution: Is there a tradeoff of hydraulic efficiency for vulnerability to dysfunction? *IAWA J.* **15**: 335–360. doi:10.1163/22941932-90001369.
- Tyree, M.T., and Sperry, J.S. 1989. Vulnerability of xylem to cavitation and embolism. *Annu. Rev. Plant Physiol. Plant Mol. Biol.* **40**: 19–38. doi:10.1146/annurev.pp.40.060189.000315.
- Tyree, M.T., and Zimmermann, M.H. 2002. *Xylem structure and the ascent of sap*. Springer Verlag, Berlin, Heidelberg, New York. doi:10.1016/0378-1127(85)90081-7.
- Vergeynst, L.L. 2015. Investigation and application of the acoustic emission technique to measure drought-induced cavitation in woody plants. Universiteit Gent.
- Viscarra Rossel, R.A., Walvoort, D.J.J., McBratney, A.B., Janik, L.J., and Skjemstad, J.O. 2006. Visible, near infrared, mid infrared or combined diffuse reflectance spectroscopy for simultaneous assessment of various soil properties. *Geoderma* **131**: 59–75. doi:10.1016/j.geoderma.2005.03.007.
- Wilhelmsson, L., Arlinger, J., Spångberg, K., Lundqvist, S.-O., Grahn, T., Hedenberg, Ö., and Olsson, L. 2002. Models for predicting wood properties in stems of *Picea abies* and *Pinus sylvestris* in Sweden. *Scand. J. For. Res.* **17**: 330–350. doi:10.1080/02827580260138080.
- Workman Jr., J.J. 1999. Review of process and non-invasive near-infrared and infrared spectroscopy: 1993–1999. *Appl. Spectrosc. Rev.* **34**: 1–89. doi:10.1081/ASR-100100839.
- Workman Jr., J.J. 2008. NIR spectroscopy calibration basics. *In Handbook of near-infrared analysis*, 3rd edition. Edited by D.A. Burns and E.W. Ciurczak. CRC Press, Boca Raton, FL, USA. pp. 123–150.

6. Table of figures

Figure 1: <i>Picea abies</i> , Illustration by Koehler 1887	9
Figure 2: [a] Schema of the water potential in conifers according to McElrone et al. 2013; [b] transpiration draws water from the leaf; [c] cohesion and adhesion draws water up the xylem; [d] negative water potential draws water into the roots. Blue circles show the water molecules.	11
Figure 3: Schema of sampling and sample preparation according to Rosner <i>et al.</i> , 2008. [a to b] Wood boles, 20 – 30 cm in length, were taken from the main trunk of Norway spruce trees after felling; [b to c] “Plank-like” longitudinal samples were produced along a diameter at the centre of the boles by splitting along the grain [c to d]. These samples were debarked and small beams were split along the grain from their sapwood. Thereafter, these were planed on a sliding microtome; small beams of sapwood with a size of 6 mm x 6 mm x 120 mm (radial x tangential x axial), were used for the measurements	13
Figure 4: [a] Modified Sperry equipment designed by Mayr 2002 for repeated flow measurement; [b] fully saturated wood beams; [c] PMS instrument	14
Figure 5: PMS instrument and [a and b] how the small wood beams (brown scheme) have to be fixed in the double ended pressure collar. [c] Closed pressure collar; [d] Pressure is applied (green arrows)	15
Figure 6: Example of a vulnerability curve showing how the percent loss of conductivity is related to the negative of the applied pressure, starting from pressure 0 MPa to the right, moving leftward to more negative water potentials.	16
Figure 7: Example of a vulnerability curve for the determination of P_{50} and RWL_{50} . The relationship between RWL and the negative of the applied pressure was thereafter fitted by means of a cubic curve and RWL_{50} was calculated (Rosner et al. 2008).	17
Figure 8: Sample preparation. Buzzsawn pieces	19
Figure 9: Electromagnetic spectra with focus on Infrared rays (IR)	20
Figure 10: Example of a spectrum. A spectrum can be compared with a fingerprint. Due to the unique combination of atoms of each different material, it is not possible for another compound to show the exact same near infrared spectrum.	21
Figure 11: [a] FT-NIR fiber optic; [b] detail of the fiber optic with an example of a wood sample	22
Figure 12: [a] MPA; [b] Sample on an integrating sphere	23
Figure 13: Illustration of the three measurement units of the current SilviScan instruments and how they are integrated. Referring to Robert Evans illustrations.....	24
Figure 14: The three measurement units of SilviScan-3. Left to right: the densitometer (density variation), cell scanner (tree ring orientations and cross-sectional cell dimensions) and diffractometer (microfibril angle, wood stiffness), which are integrated via a server. [Photo: ©Rob Evans, CSIRO] ..	25
Figure 15: Example of a samples for measurements on SilviScan: [a] typical sample strip from pith to bark, polished at the top for measurements of cross-sectional tracheid dimensions (Lundqvist and Olsson, 2007); [b] 6 mm x 6 mm pieces from specimens analysed for P_{50} , glued onto a support, prior to its processing with SilviScan’s precision equipment into a sample similar to [a], to be followed by high resolution measurement of variations in wood density and cross-sectional tracheid dimensions from edge to edge of each specimen, as well as averages for all their annual rings and their parts of earlywood, transition wood and latewood.	26
Figure 16: X-ray densitometric images and Illustration of density thresholds for earlywood, transition wood and latewood. [Image and Illustration: Lundqvist <i>et al.</i> , 2018]	27
Figure 17: Norway spruce sample during the measurements with the Zwick/Roll Z020	29
Figure 18: Course of the stress/strain curve for radial compression perpendicular to the grain: The blue circle marks the position for acquisition of the parameter “peak force, radial compression”(σ _r).....	29
Figure 19: Microscope.....	30
Figure 20: Image of the bordered pits and the manual measurement.....	30

7. Curriculum Vitae

Persönliche Daten

Name	Saskia Luss
Geburtsdatum	08.02.1984
Geburtsort	Wien, Österreich
Staatsbürgerschaft	Österreich
Familienstand	verheiratet
Universität	Universität für Bodenkultur, Wien

Ausbildungen

2012 – bis jetzt	Doktorat Universität für Bodenkultur, Wien
2005 – 2011	Master of Science (Wildtierökologie und Wildtiermanagement) Universität für Bodenkultur, Wien
2009 – 2011	Bachelor of Education (Umweltpädagogik) Hochschule für Agrar- und Umweltpädagogik, Wien
2005 – 2009	Bachelor der technischen Naturwissenschaften (Umwelt- und Bioressourcenmanagement) Universität für Bodenkultur, Wien
1999 – 2004	Höhere Graphische Bundes-, Lehr- und Versuchsanstalt, Wien (Fotografie) Höhere Graphische Bundes-, Lehr- und Versuchsanstalt, Wien

Beruflicher Werdegang

Seit 2019	SaLu Media Geschäftsführerin
2015 – bis jetzt	Westermann Österreich, Verlage E. DORNER Lektorin und Projektmanagerin
2012 – 2015	Universität für Bodenkultur, Institut für Holztechnologie und nachwachsende Rohstoffe Wissenschaftliche Mitarbeiterin und Doktorat
2011 – 2012	z-works Werbeagentur Junior Account Manager

2011	Wiener Umweltschutzabteilung Naturführerin für Kindergärten und Schulklassen
2010/11	Höhere Graphische Bundes-, Lehr- und Versuchsanstalt Schulpraxis
2010	Bezirksbauernkammer Korneuburg Beratungspraxis
2009	Modeschule Hetzendorf Schulpraxis
2009	Österreichische Bundesforste AG - Biosphärenpark Wienerwald Unterstützung bei Waldpädagogischen Führungen
2009	Naturaktiv Zentrum Unterstützung bei Veranstaltungen
2008	Max Planck Institut – Institut für Kolloid- und Grenzflächenforschung (Potsdam-Deutschland) Praktikum
2008 - 2011	Forschungsinstitut für Wildtierkunde Projektmitarbeit
2007 - 2011	Flash Media geringfügige Beschäftigung
2007	Österreichische Bundesforste - WND Naturraummanagement / Natur- und Umweltschutz
1999 - 2007	Diverse Praktika und geringfügige Beschäftigungen

Publikationen

Luss, S., Lundqvist, S.-O., Evans, R., Grahn, T., Olsson, L., Petit, G., and Rosner, S. (2019): Within-ring variability of wood structure and its relationship to drought sensitivity in Norway spruce trunks. IAWA J. 40(2): 288–310.

Rosner, S.; Světlík, J.; Andreassen, K.; Børja, I.; Dalsgaard, L.; Evans, R.; Luss, S.; Tveito, O. E.; Solberg, S. (2017): Novel hydraulic vulnerability proxies for a boreal conifer species reveal that opportunists may have lower survival prospects under extreme climatic events. In: Bräuning, A.; Bolte, A.; Nabais, C.; Rossi, S.; Sass-Klaassen, U., Studying tree responses to extreme events, 62-75; Frontiers in Plant Science; ISBN ISBN 978-2-88945-192

Rosner, S., Svetlík, J., Andreassen, K., Børja, I., Dalsgaard, I., Evans, R., Luss, S., Tveito, O. E., Solberg, S. (2016): Novel Hydraulic Vulnerability Proxies for a Boreal Conifer Species Reveal That Opportunists May Have Lower Survival Prospects under Extreme Climatic Events. *Front Plant Sci.*; 7:831

Rosner, S; Luss, S; Světlík, J; Andreassen, K; Børja, I; Dalsgaard, L; Evans, R; Tveito, OE; Solberg, S (2016): Chronology of hydraulic vulnerability in trunk wood of conifer trees with and without symptoms of top dieback. *Journal of Plant Hydraulics*, 3.

Luss, S; Schwanninger, M; Rosner, S (2015): Hydraulic traits of Norway spruce sapwood estimated by Fourier transform near-infrared spectroscopy (FT-NIR). *CAN J FOREST RES.* 2015; 45(6): 625-631.

Luss, S. (2011): Untersuchungen zur Nahrungsökologie des Alpenschneehuhns unter Verwendung unterschiedlicher Analysemethoden. Masterarbeit an der Universität für Bodenkultur.

Luss, S. (2011): Begegnungen zwischen Mensch und Ziesel - Ein Spannungsfeld oder eine Bereicherung. Bachelorarbeit an der Hochschule für Agrar- und Umweltpädagogik.

Gierlinger, N.; Luss, S.; König, C.; Konnerth, J.; Eder, M.; Fratzl, P. (2010): Cellulose microfibril orientation of *Picea abies* and its variability at the micron-level determined by Raman imaging. *Journal of experimental botany* 61.2 (2010): 587-595.

Budweiser, L.; Heissenberger, K.; Luss, S.; Huber P., Schneider, M.; Schicker F. (2008): Eukalyptus – weltweit verbreitet. *Forstzeitung* 08/08, 10-11.

Beiträge bei wissenschaftlichen Veranstaltungen

Rosner S., Světlík J., Andreassen K., Børja I., Dalsgaard L., Evans R., Luss S., Tveito OE, Solberg S. (2016): Annual changes in hydraulic vulnerability of Norway spruce wood are triggered by climatic conditions of the previous growing season. [Poster]
[Tagung der Austrian Society of Plant Biology (ATSPB), Berchtesgaden, May 26-28]
In: Universität Salzburg, Proceedings of the 21. Tagung der Austrian Society of Plant Biology (ATSPB)

Rosner S., Luss S., Světlík J., Andreassen K., Børja I., Dalsgaard L., Evans R., Tveito O.E., Solberg S. (2015): Carbon starvation or opportunistic strategy?. [Xylem International Meeting, Bordeaux, September 7-9, 2015]

Luss, S; Schwanninger, M; Gierlinger, N; Hinterstoisser, B; Rosner, S (2014): Novel and fast estimation of hydraulic traits of Norway spruce sapwood by Fourier transform near infrared (FT-NIR) spectroscopy. [20. Tagung der Austrian Society of Plant Biology (ATSPB), Lunz am See, Austria, Juni 19-21, 2014]

Luss, S.; Rosner, S.; Gierlinger, N.; Schwanninger, M. (2013): Hydraulic properties and wood density of Norway spruce wood estimated by Fourier transform near infrared spectroscopy (FT-NIR). [Clim Tree 2013, Zürich, SCHWEIZ, SEP 1-5, 2013]

Forschungsberichte

Duscher, T.; Luss, S.; Reimoser, F. (2010): Untersuchung zur Wiederbesiedlung der rekultivierten Trasse Loop Kirchberg-Lichtenau durch Ziesel. Im Auftrag der OMV Gas GmbH, pp. 18.

Duscher, T.; Luss, S.; Duscher, A.; Habe, M.; Reimoser, F. (2009): Wissenschaftliche Untersuchung zur Umlenkung von Zieseln (*Spermophilus citellus*) und Feldhamstern (*Cricetus cricetus*) durch Maßnahmen der Habitatgestaltung. Im Auftrag der OMV Gas GmbH, pp. 41.

Lampe, T.; Reimoser, F.; Duscher, A.; Luss, S.; Kukla, P.; Meidlinger, K.; Schreiber, B. (2008):
Möglichkeiten zur Sicherung von Zieselbeständen, deren Lebensraum durch
Baumaßnahmen
verändert wird. pp. 36.

Ausstellung

2003/2004

Wanderausstellung „durcheinander – durch einander“
inklusive Fotobuch

Ich erkläre eidesstattlich, dass ich die Arbeit selbständig angefertigt habe. Es wurden keine anderen als die angegebenen Hilfsmittel benutzt. Die aus fremden Quellen direkt oder indirekt übernommenen Formulierungen und Gedanken sind als solche kenntlich gemacht. Diese schriftliche Arbeit wurde noch an keiner Stelle vorgelegt.

Wien, am 8.2.2020

A handwritten signature in black ink, appearing to be 'S. Luss', with a stylized flourish at the end.

Saskia Luss MSc BEd